2009

DETAILED SURFACE ANALYSIS OF LIP SEAL ELASTOMERS RAN AGAINST SHAFTS MANUFACTURED WITH TRIANGULAR CAVITIES

Vetrivel Kanakasabai
University of Kentucky, vetri4@gmail.com

ABSTRACT OF THESIS

DETAILED SURFACE ANALYSIS OF LIP SEAL ELASTOMERS RAN AGAINST SHAFTS MANUFACTURED WITH TRIANGULAR CAVITIES

Previous experimental and theoretical results indicate that the keys to successful radial lip seals are the surface characteristics of the shaft and the microasperity pattern that develops due to wear on the elastomer. In this study, the lip seal was tested against five different patterns of shaft surface: plain stainless steel, triangular cavities oriented towards air, triangular cavities oriented towards oil, triangular cavities leading and triangular cavities lagging. Using Zygo optical profilometer and scanning electron microscope, a thorough surface characterization of the micro-asperities and micro-cavities is done on the lip seal elastomer. Correlation coefficients were calculated between the surface parameters of the final shaft surface and elastomer. Although both the surface characteristics of the shaft and the micro-asperities that develop on the elastomer sealing zone are responsible for a successful operation of the lip seal, the deterministic triangular micro-cavity patterns created on the shaft surface dominated the pumping direction with a large variability in the pumping rate. This variability is due to the elastomer wear in. This study also finds a significant correlation between the axial position of minimum roughness on the sealing zone of the elastomer and the pumping rate of the lip seals.

KEYWORDS: Lip Seal, Surface Characterization, Wear, Microasperities and Microcavities, Surface Textured Shaft

Vetrivel Kanakasabai

25th August, 2009

(Date)

DETAILED SURFACE ANALYSIS OF LIP SEAL ELASTOMERS RAN AGAINST SHAFTS MANUFACTURED WITH TRIANGULAR CAVITIES

By

Vetrivel Kanakasabai

Dr. L. Scott Stephens

(Director of Thesis)

Dr. L. Scott Stephens

(Director of Graduate Studies)

25th August, 2009

(Date)

RULES FOR THE USE OF THESES

Unpublished theses submitted for the Master's degree and deposited in the University of Kentucky Library are as a rule open for inspection, but are to be used only with due regard to the rights of the authors. Bibliographical references may be noted, but quotations or summaries of parts may be published only with the permission of the author, and with the usual scholarly acknowledgements.

Extensive copying or publication of the thesis in whole or in part also requires the consent of the Deal of the Graduate School of the University of Kentucky.

A library that borrows this thesis for use by its patrons is expected to secure the signature of each user.

Name Date

_____

_____

_____

_____

_____

_____

_____

_____

_____

_____

_____

THESIS

Vetrivel Kanakasabai

The Graduate School

University of Kentucky

2009

DETAILED SURFACE ANALYSIS OF LIP SEAL ELASTOMERS RAN AGAINST SHAFTS MANUFACTURED WITH TRIANGULAR CAVITIES

THESIS

A thesis submitted in partial fulfillment of the
requirements for the degree of Master of Science in Mechanical Engineering in the
College of Engineering
at the University of Kentucky

By

Vetrivel Kanakasabai

Lexington, Kentucky

Director: Dr. Scott Stephens, Professor of Mechanical Engineering

Lexington, Kentucky

2009

To my loving
Parents and friends

ACKNOWLEDGMENTS

I would like to thank my advisor, Dr. L. S. Stephens for his support, constant motivation and guidance during my study and research at the University of Kentucky. It was a great privilege for me to work with him. I would like to thank my thesis committee members: Dr. Keith Rouch and Dr. Y. Charles Lu. It is a pleasure to thank Katherine H. Warren for her contribution to this research and for introducing me to the various equipments and processes in the laboratory. I would like to thank the Timken Company for their assistance in this project.

My Parents have been great source of support throughout my life and I wish to thank them for their love and encouragement. I would also like to thank my friends and members of the Bearings and Seals Laboratory who helped to make my study at the University of Kentucky a pleasant and memorable one.

TABLE OF CONTENTS

LIST OF TABLES

LIST OF FIGURES

CHAPTER 1 – INTRODUCTION

1.1 OVERVIEW OF LIP SEAL OPERATION

Radial lip seals are used to retain lubricant and to prevent external contamination. The radial lip seal assembly consists of a shaft, lip seal elastomer, garter spring and sealed fluid. Because of intricate sealing, wear and leakage mechanisms involved in the operation of a lip seal, it is difficult to predict its performance accurately. The components in the lip seal assembly are manufactured by different industries, which further adds complexity. Figure 1 shows the cross sectional view of the lip seal geometry.

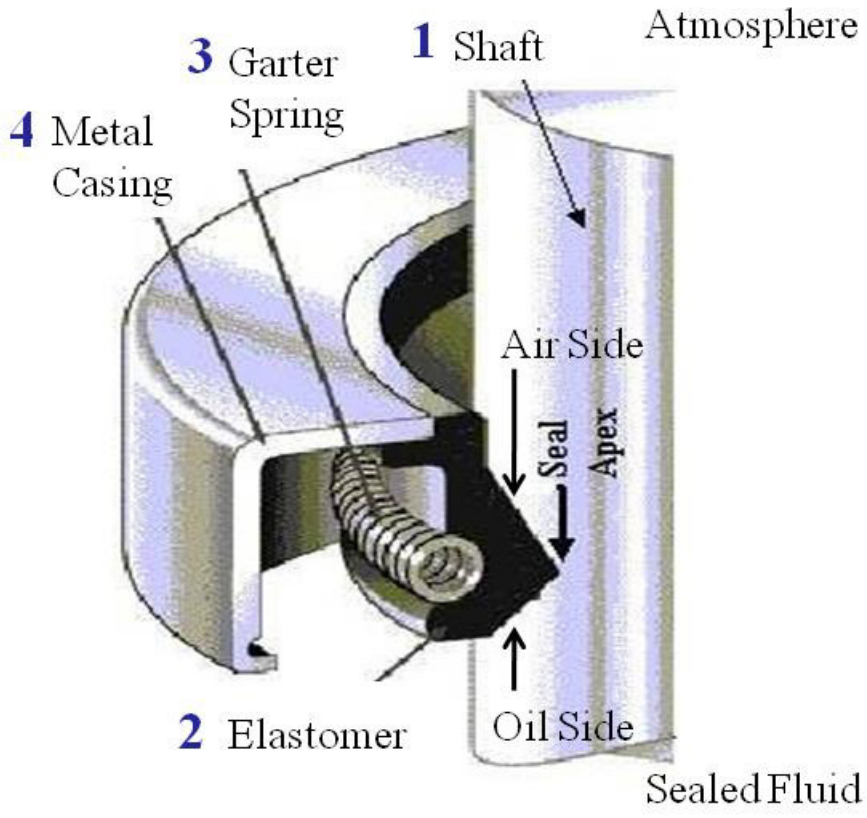

Figure 1 – Cross Sectional View of Lip Seal (Chicago Rawhide, [1])

The figure also indicates the air side, oil side and apex of the lip seal elastomer. The diameter of the shaft is larger than the diameter of the elastomer which creates an interference fit. The contact pressure created when the lip seal elastomer is mounted on the shaft is comprised of three components: force due to the interference fit, force due to the garter spring and force due to the elastomer beam effect. The air side angle also known as barrel angle and the oil side angle are indicated as α and β in the figure. Horve [2] suggested that the air side and the oil side angle should be in the range 20 – 35^{o} and 40 – 70^{o} respectively. The garter spring sits slightly towards atmosphere side of the seal. Figure 2 (a) shows the offset of the garter spring from the lip seal elastomer apex. Under static conditions, this creates an asymmetric contact pressure distribution along the axial direction at the interface between the shaft and the lip seal elastomer. After the lip seal elastomer is installed, the garter spring pushes the apex and some portion of the atmosphere side of the lip seal elastomer against the shaft.

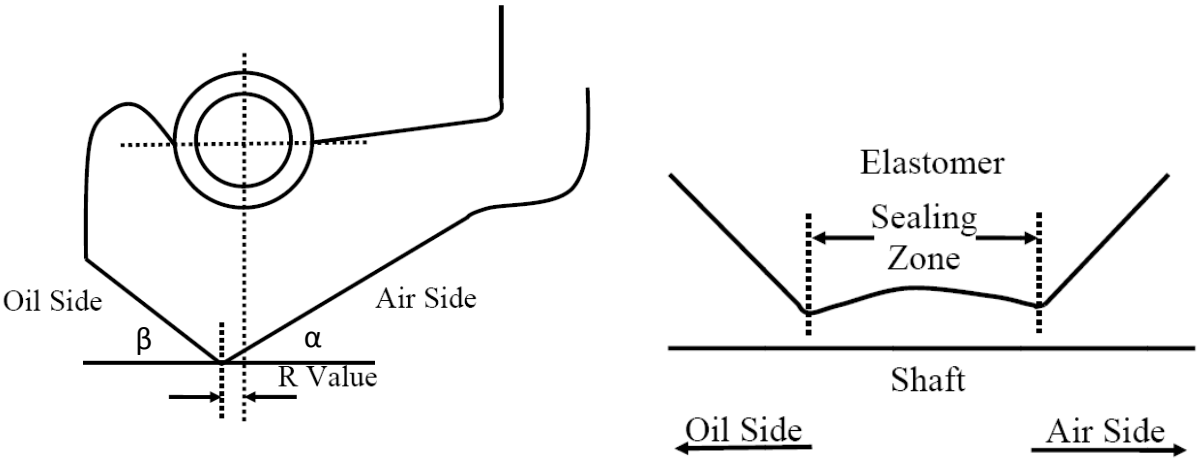

Figure 2 – Lip Seal Elastomer during (a) Static and (b) Dynamic Conditions

When the shaft starts rotating, there is boundary lubrication between the lip seal elastomer and the shaft. The shaft surface breaks through, wears away the lip seal elastomer surface and creates the sealing zone in the lip seal elastomer. Depending on the surface characteristics of the shaft, micro-asperities and micro-cavities are developed on the sealing zone of the lip seal elastomer. However in the case of plain stainless shafts, the surface finish on the shaft may influence the micro-asperities on the lip seal elastomer only during the initial period of wear. The conditions in which the lip seal operates also have a large influence on the formation of the micro-asperities and micro-cavities on the elastomer. [3] The lip seal elastomer is mainly composed of nitrile rubber and the micro-asperities are created by wearing away of the filler particles. Therefore the size and shape of the micro-asperities and micro-cavities on the elastomer surface depends on the rubber, strength of the bond between the filler particles and rubber, and roughness of the shaft.

As the shaft drags the lubricant over the micro-asperities on the elastomer, there is a pressure rise on the upstream side of the asperity and there is cavitation on the downstream side of the asperity. Because of the net pressure elevation, the sealing zone of the lip seal elastomer lifts off from the rotating shaft surface. Similarly in the case of cavities, the cavitation occurs at the leading edge and there will be pressure rise over the trailing edge. Figure 2 (b) shows the sealing zone of the lip seal elastomer during dynamic conditions. The sealing zone is not formed by equal amount of wear on the air side and oil side. The lubricant fills in the gap between the shaft and the lip seal elastomer sealing zone which reduces the wear. Hence the lip seals can operate for several hours provided appropriate micro-asperities are developed on the sealing zone of the lip seal

elastomer. The sealing zone width of the lip seal elastomer depends upon the duration of operation and the shaft surface characteristics. When the lubricant is supplied to the atmosphere side of the seal, it is pumped towards the oil side of the seal by the micro-asperities developed on the sealing zone of the elastomer. This pumping mechanism is referred to as reverse pumping which keeps the seal from leaking.

1.2 LIP SEAL DEFORMATION AND REVERSE PUMPING

Salant and Flaherty [4] considered microundulations on the lip seal elastomer surface and conducted numerical analysis of the lip seal including the structural mechanics of the lip and the fluid mechanics of the film.

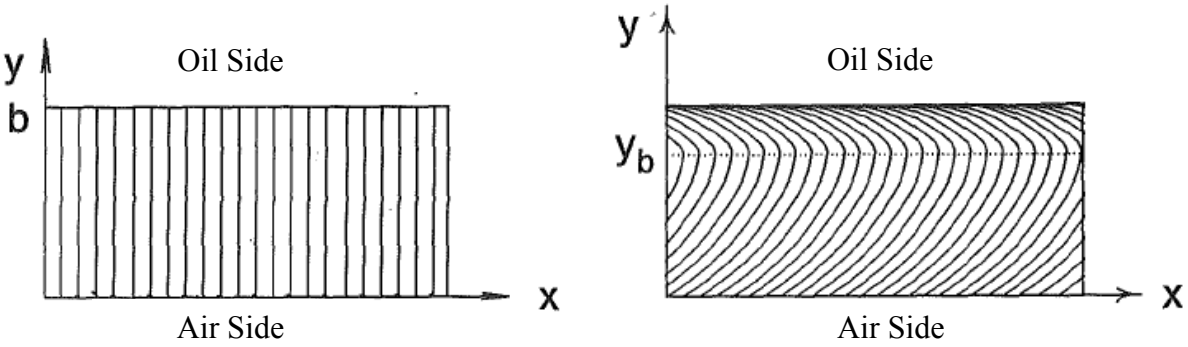

(a) (b)

Figure 3 – Microundulation Pattern on Elastomer (a) Static (b) Dynamic [4]

Figure 3 (a) shows the undulation pattern on the lip elastomer. “b” denotes the sealing zone width of the lip seal elastomer. During static conditions, the undulation patterns are

perpendicular to the circumferential direction of the seal. During dynamic conditions, the hydrodynamic pressure distribution deforms the lip seal elastomer sealing zone in the radial direction and the shear stresses in the lubricating film deform the lip surface in the circumferential direction which in turn deforms the undulation patterns. Figure 3 (b) shows the undulation pattern during dynamic condition. y_b denotes the location of maximum deformation along the circumferential direction of the lip seal. These undulation patterns act as vanes and pump the fluid from one side of the seal to the other side. The undulations patterns in the region y less than y_b pump the lubricant from the atmosphere side to the oil side and the undulations patterns in the region y greater than y_b pump the lubricant from the oil side to the atmosphere side. Salant and Flaherty [4] suggested that for a successful seal, the ratio y_b/y should be greater than 0.5. This results in a flow against the natural leakage through the seal and promotes reverse pumping. The results of that study indicate that, the microundulations deform under dynamic conditions and are responsible for reverse pumping. The results also indicated that the microundulations hydrodynamically generate high pressures with the film and provide the load support.

1.3 THESIS OVERVIEW

Most of the numerical analysis and experimental analysis that have been conducted so far in lip seals are focused to analyze parameters such as friction torque, leakage, film thickness, and shaft surface characteristics. The lip seal elastomers which ran against the modified shaft surfaces were not characterized and until now no work has been done on

characterizing lip seal elastomers run against shafts manufactured with deterministic micro-cavity patterns. In this study, a comprehensive qualitative and quantitative analysis is done on the lip seal elastomer surface using the scanning electron microscope (SEM) and Zygo optical profilometer.

Chapter 1 describes the components of the lip seal and gives an overview of the lip seal operation. It describes how the micro-asperities that are formed on the sealing zone of the lip seal elastomer and deformation of the sealing zone create the reverse pumping process. Chapter 2 presents a literature review of the theoretical and experimental analysis previously done in radial lip seals. Chapter 3 describes the manufacturing process which is used to fabricate the deterministic micro-cavities on the shaft surface. It gives an outline of the testing procedure and gives a methodology for characterizing the lip seal elastomer surface which includes sample preparation, filtering and obtaining the surface parameters for the elastomer surface. It also gives the advantages and disadvantages of using scanning electron microscope and Zygo optical profilometer. A procedure for calculating the wear rate in the lip seal elastomer from the scanning electron microscope image is also discussed. Chapter 4 defines the Birmingham 14 parameters and a through characterization of the lip seal elastomer sealing zone is done. The surface parameters were also obtained from the final shaft surface and correlation coefficients were calculated between the final shaft surface and elastomer. Chapter 5 presents the experimental results. It compares the results with the previous theoretical and experimental analysis done, shows agreement of results with the previous work, and new findings from this study. Chapter 6 presents conclusion and recommendations for the future work.

CHAPTER 2 – PREVIOUS RESEARCH

2.1 THEORETICAL ANALYSIS

Hadinata and Stephens [5] and Impellizzeri [6] have conducted numerical analysis of lip seals with micro features on shaft surface. They have found that by using asymmetric geometric features on the shaft surface, the pumping direction and pumping rate of the lip seals can be varied. Hadinata and Stephens [5] considered square, hexagonal, circular and oriented triangular geometries on the shaft surface and conducted an elastohydrodynamic analysis. The lip seal elastomer surface was assumed to be smooth. When compared to conventional lip seals, the oriented triangular asperities lowered the friction and increased the reverse pumping rate simultaneously.

Salant and Flaherty [7] considered micro-asperity patterns (circular asperities, x-oriented elliptical asperities and y-oriented elliptical asperities) on the lip seal elastomer surface and conducted a numerical analysis. Some asperity patterns exhibited reverse pumping and other patterns exhibited leakage. During dynamic conditions, the shear stress causes these micro-asperities to deform in the circumferential direction. There is cross flow between these micro-asperities and the deformed asperities act as micro vanes and produce reverse pumping. These results suggest that the sealing mechanism depends on both the presence of micro-asperities and their deformation. They found that the reverse pumping rates generated by micro-asperities are greater when compared to that of microundulations. In the numerical analysis done, the micro-asperities on the elastomer sealing zone were assumed to be of constant height and they were deterministic, which is

not in reality. They concluded that the number, density and shapes of asperities affect the reverse pumping process. Qian [8] pointed out that the locations of the maximum circumferential deformation is governed by the molecular structure of the rubber and the moulding configuration.

Salant [9] conducted elastohydrodynamic analysis of the lip seal sealing zone and meniscus formed between the lip seal and the shaft. Initially when the shaft starts rotating, the meniscus is on the air side of the seal. As the shaft speed increases, the meniscus moves closer towards the oil side of the seal. Above the critical speed, the meniscus is ingested into the sealing zone. He concluded in addition to the deformation of micro-asperities, the action of meniscus led to a non-leaking seal. Therefore the operating characteristics of the lip seal depend on the seal past history in addition to the present operating conditions and seal properties. He also found out that the seal starts leaking when the rotation of a seal operated in one direction for a long duration is reversed. This is because the deformations present in the lip seal elastomer are not completely reversed when the direction of rotation is reversed.

Hamilton, Walowit and Allen [10] conducted theoretical and experimental analysis on rotary face seals with a transparent rotor to observe the interfacial film. They observed that the film was not continuous and was interrupted by cavitation streamers. The locations at which the streamers originate or terminate corresponded to the irregularities on the stator surface. Initially there was no cavitation and torque was high. As soon as a band of cavitation appeared the torque dropped sharply. These bands where cavitation occurred were found to be grooves or scratches on the stator surface. Because of the difficulty in characterizing the asperities and cavities on the stator surface, they

conducted experiments with the stator surface photoetched with asperities. They found different kinds of micro-asperities and variation in height of the micro-asperities resulted in different load carrying capacities. Based on the experimental results and theoretical analysis, they concluded that both the micro-asperities and micro-cavities are involved in hydrodynamic lubrication.

2.2 EXPERIMENTAL ANALYSIS

Nakamura and Kawahara [11] observed micro-asperities on the lip seal elastomer sealing zone under static and dynamic conditions by running the lip seal elastomer against a hollow glass shaft. The results of the experiment indicated that the lip seals do not leak when the degree of actual contact is minimum and the micro-asperities are closer towards the oil side of the sealing zone. Kawahara [12], Nakamura [11] and Horve [13] conducted experimental studies of lip seal elastomers against plain stainless steel shafts and concluded that both the load support and the sealing mechanisms strongly depends on the micro-asperities developed on the sealing zone of the lip seal elastomer.

Jagger [14] changed loading from the radial direction to axial direction and made the friction and film thickness measurements. From these measurements he concluded that a continuous lubricant film separates the sealing zone of the lip seal elastomer and the shaft. He concluded that the sealing mechanism depends on the surface tension of the lubricating film which forms a meniscus at the interface between the shaft and elastomer. Jagger and Walker [15] compared the shaft surface and the lip seal elastomer sealing zone surface after testing. He found the shaft surface to be smooth and concluded that its

contribution to the load support is small and the micro-asperities developed on the elastomer surface make a major contribution. With the help of stylus profilometer Jagger and Walker [15] measured the height of micro-asperities and found to be in the range of 1 – 3 microns.

Paige [1] tested plain stainless steel shafts against lip seals with and without pumping aids and studied the size, shape and quantity of the asperities developed on the lip seal elastomer. She found that the micro-asperities that developed on the elastomer sealing zone to be oval and the surface roughness was not consistent across the sealing zone width. The seals which reverse pumped have the largest root mean square roughness value on the oil side of the elastomer sealing zone. Whereas the seals which did not reverse pump have the largest root mean square roughness elsewhere on the elastomer sealing zone. She found, as the roughness of the elastomer sealing zone decreased, the reverse pumping rate decreases. The pumping aids present on the lip seal elastomer control the formation of micro-asperities on the elastomer sealing zone and it increases the roughness on the oil side of the sealing zone when compared to the middle or air side.

Horve [13] pointed out the significance of the shaft surface characteristics, operating conditions and break-in period in the formation of micro-asperities on the elastomer sealing zone. The break-in period occurs approximately 20 hours of operation and during this break-in period, the shaft surface wears away the lip seal elastomer and creates the micro-asperities. Horve found out that the lip seal elastomers with rough sealing zone and greater number of micro-asperities have good reliability and high pumping rate, and the lip seal elastomers with smooth sealing zone, and lesser number of micro-asperities have poor reliability and low pumping rate. He also found that the pumping ability of a seal

with smooth wear track can be improved for a short period of time by abrading the sealing zone of the lip seal elastomer. The formulation of elastomer rubber also plays a major role in the development of the micro-asperities on elastomer sealing zone. Horve [2] said the surface finish of the shaft is important for proper operation of the lip seal. He recommended the shaft surface roughness (Ra) to be in the range between 0.25 – 0.5 μm where the lip seal elastomer will contact the shaft. If the shaft surface is very smooth, the lubricant will not be held in the sealing zone resulting in starvation and greater wear. Where as if the shaft surface is very rough the elastomer wears away quickly resulting in early seal failure. He also observed as the operation of seal progresses, the shaft surface becomes smooth and the elastomer sealing zone becomes rough. Based on this observation he concluded that the micro-asperities on the sealing zone of the lip seal elastomer support the load by acting as micro bearing pads.

Kawahara and Hirabayashi [16] investigated the lip seal surface which ran against stainless shaft using scanning electron microscope. They found that the lip seal wear track becomes smooth as the duration of operation increases and the surface roughness is not proportional to the duration of operation. Horve and Brink [17] modified the design of conventional lip seal by molding a wavy sealing edge on the elastomer along the axial direction. The wave seals led to lower operating temperature and friction torque when compared to the conventional lip seals. They found that these seals have higher pumping rates than conventional radial lip seals and the pumping rate of wave seals remained almost constant over a wide range of shaft speeds. Anno, Walowit and Allen [18] photoetched rotary shaft face seals with square asperities, circular asperities and cavities. They found that the hydrodynamic operation of face seals can be controlled effectively

by using asperities and cavities. The negative asperities result in discontinuous phase of regions of high film thickness and offer possibilities in minimizing the leakage. The load support for seals with cavities was comparable to that of asperities of all shapes but the seals with cavities have no or very low leakage.

Warren and Stephens [19] studied radial lip seal performance for seals with shaft surfaces modified with deterministic micro-cavities. They found that the deterministic micro-cavities can control the pumping direction and increase the seal performance though a large amount of variation is seen in the test data.

CHAPTER 3 – EXPERIMENT AND INSTRUMENTATION

3.1 FABRICATION OF DETERMINISTIC CAVITIES

The deterministic triangular cavities of different orientations are manufactured on the shaft surface by ultra violet (UV) photolithography which was developed at the University of Kentucky Bearings and Seals Laboratory in collaboration with the work done by Zhang [20] at the Louisiana State University.

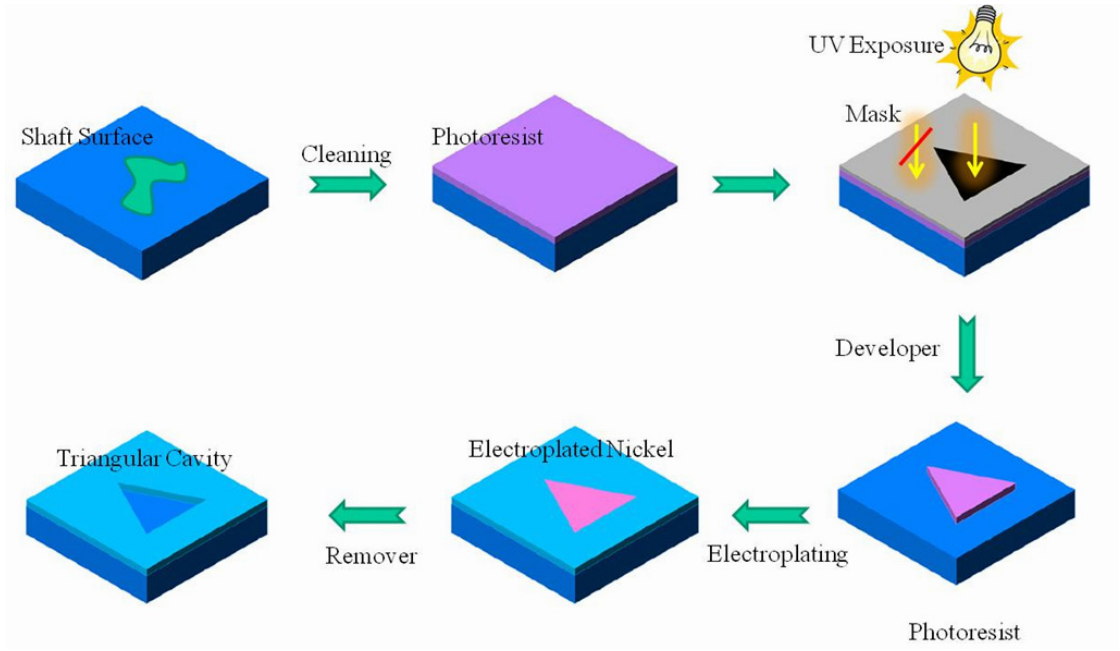

Figure 4 – Manufacturing of Deterministic Triangular Cavity Patterns

Figure 4 shows an overview of manufacturing process of the deterministic cavity patterns on the shaft surface. The deterministic nickel cavities are manufactured on stainless steel shafts. First, the shaft surface is cleaned to remove particulate matter and other impurities. After cleaning, SU-8 negative photoresist is applied. Then the shaft surface is masked with deterministic triangular patterns of desired orientation and

exposed to UV light. The UV light passes through the areas of triangles in the mask and the areas surrounding the triangles in the mask does not allow the UV light to pass through. When the surface is washed with developer solution, the photoresist areas that are not exposed are removed and the photoresist in triangular shapes are left behind. When electroplating is done, nickel will be deposited in the area surrounding the triangular photoresist asperities. After the surface is washed with the remover solution, the remaining photoresist in triangular shapes are removed and the shaft surface is left with deterministic triangular shaped electroplated nickel cavities. Different patterns of deterministic cavities are obtained on the shaft surface by using different patterns of mask.

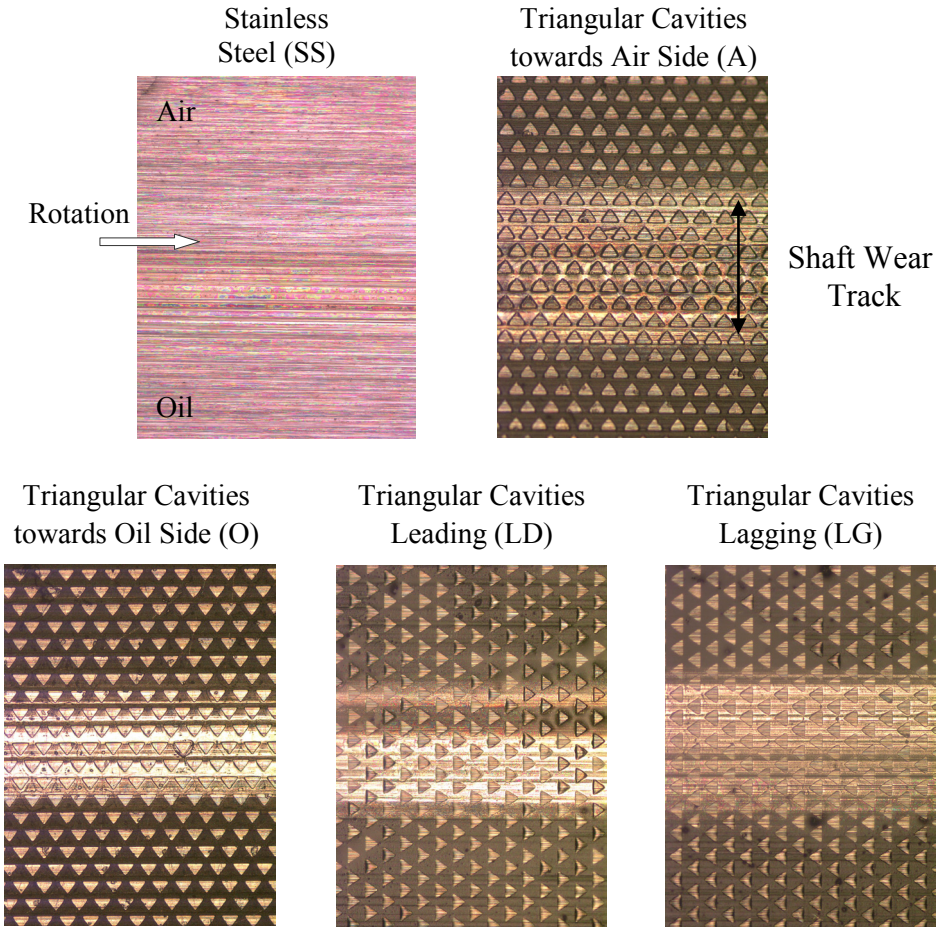

Figure 5 – Shaft Patterns Tested and Corresponding Wear Tracks [19]

Figure 5 shows the different deterministic triangular cavities manufactured on the shaft surface. The figure also displays the wear track formed on the shaft surface due to the rubbing of the lip seal elastomer. The lip seals were tested against five different patterns of shaft surface: plain stainless steel, triangular cavities oriented towards oil, triangular cavities oriented towards air, triangular cavities lagging and triangular cavities leading. The surface roughness of the stainless steel shafts fall within the range between 0.25 – 0.5 μm as suggested by Horve [2].

The following terminologies were used for denoting the different deterministic triangular cavities manufactured on the shaft surface. The triangular cavities with the apex pointing towards the oil side is referred to as "triangular cavities towards oil side (O)" and the triangular cavities with the apex pointing towards the air side is referred to as "triangular cavities towards air side (A)". The triangular cavities with the apex pointing along the direction of shaft rotation is referred to as "triangular cavities leading (LD)" and the triangular cavities with the apex pointing opposite to the direction of shaft rotation is referred to as "triangular cavities lagging (LG)". Within each pattern of the shaft, three seals were tested and within each pattern of the shaft, the surface characteristics of the shaft were kept similar.

Based on the numerical studies conducted by Hadinata and Stephens [5] and Impellizzeri [6] and manufacturing feasibilities, the triangular micro-cavities are manufactured on the shaft surface in a staggered manner. The ideal triangular cavities are

5 mm deep, have a 107 μm base and 78 μm height [19]. In the case of ideal triangular cavities oriented towards oil and air, the center to center distance is 150 μm in the circumferential direction and 114 μm in the axial direction. In the case of ideal triangular cavities lagging and leading, the center to center distance is 150 μm in the axial direction and 114 μm in the circumferential direction.

3.2 TESTING

Berens and Born [21] have stated that there is link between seal leakage and the batch of rubber compound and mold used in elastomer production. Therefore in order to ensure consistency in the material properties and geometry, the lip seal elastomers were taken from the same process batch. The lip seal elastomers which ran against stainless steel shafts are denoted as SS1, SS2 and SS3. The lip seal elastomers which ran against triangular cavities oriented towards oil and air are denoted as O1, O2, O3 and A1, A2, A3 respectively. The lip seal elastomers which ran against triangular cavities lagging and leading are denoted as LG1, LG2, LG3 and LD1, LD2, LD3 respectively.

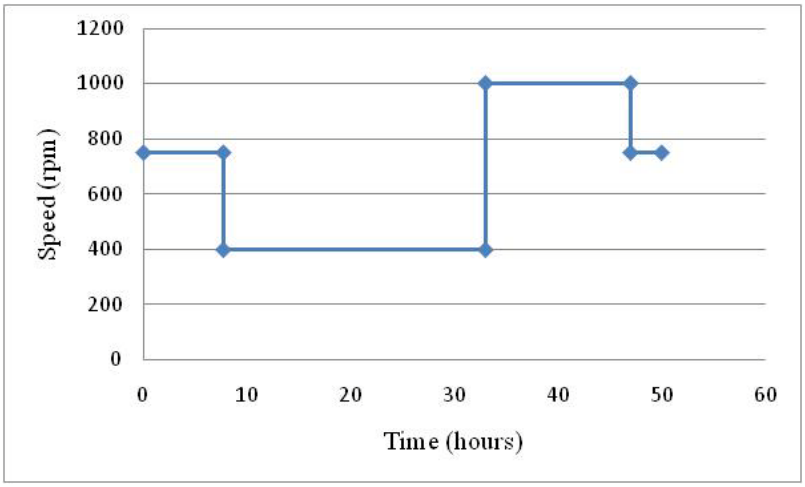

Figure 6 – Testing Done at Different Speeds

Each lip seal was tested at three different speeds: 750rpm, 400 rpm and 1000 rpm. Finally a post test is done at 750 rpm before completing the testing. Figure 6 shows the different speeds through which the tests are conducted. In each speed, the pumping rate values are recorded only after a steady state in temperature is reached. In the lip seals tested against the five different patterns of shaft, some of the seals reverse pumped and others forward pumped. For the reverse pumping seals, the pumping rate was measured by performing an oil drop test. When a known volume of the lubricant is injected at the air side of the seal there is a sudden drop in friction torque. The lubricant is pumped from the air side to the oil side of the seal. During this period, the friction remains almost constant. When all the lubricant is pumped from the air side to the oil side of the seal, there is sudden rise in friction torque. The reverse pumping rate is calculated from the volume of lubricant injected and the time taken for the transfer of lubricant. Several oil drop tests were conducted within each speed. Between two successive oil drop tests, the lip seal elastomer runs in a starved or partially starved condition for a certain period of time. Figure 7 shows the (A) drop in friction torque when the lubricant is injected at the air side, (B) the transfer of lubricant from the air side to the oil side (reverse pumping), (C) overshoot in the friction torque when all the lubricant is pumped from the air side to the oil side and (D) high wear condition for elastomer.

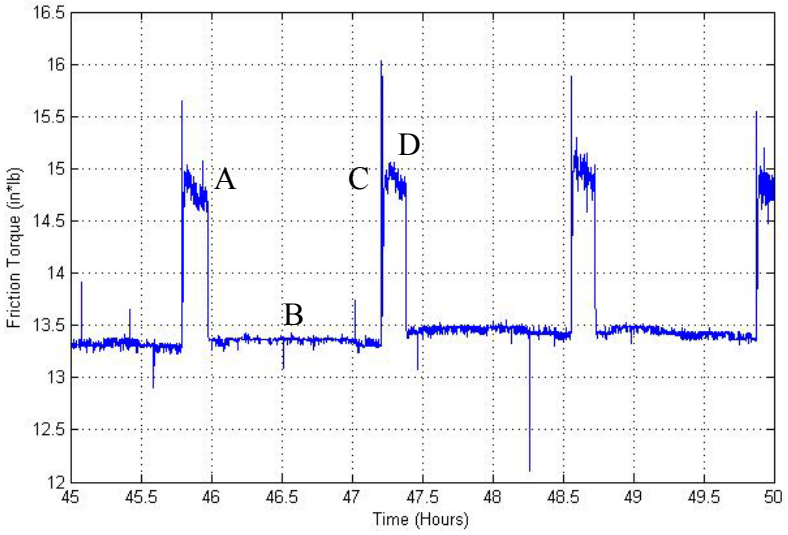

Figure 7 – Friction Torque during Oil Drop Test

For the forward pumping seals, the pumping rate was measured by maintaining a known volume of lubricant head in a graduated cylinder. When a seal is forward pumping, there is continuous transfer of lubricant from the oil side to the air side of the seal. The forward pumping rate is calculated from the change of lubricant level in the graduated cylinder and the time taken for it.

3.3 SAMPLE PREPARATION

After testing, the lip seal elastomers ran against different patterns of shaft surface were cleaned to remove any lubricant remaining on the elastomer surface. The lip seal elastomers are cleaned using all purpose cleaner in a stirrer and allowed to dry. To make sure the cleaning procedure does not affect the surface characteristics of the elastomer, two samples were prepared from an untested seal. One sample from the untested seal is

soaked in oil for 18 hours. Sample soaked in oil is cleaned using all purpose cleaner. Surfaces of both the samples are characterized and made sure that the cleaning process done does not alter any surface conditions of the lip seal elastomer.

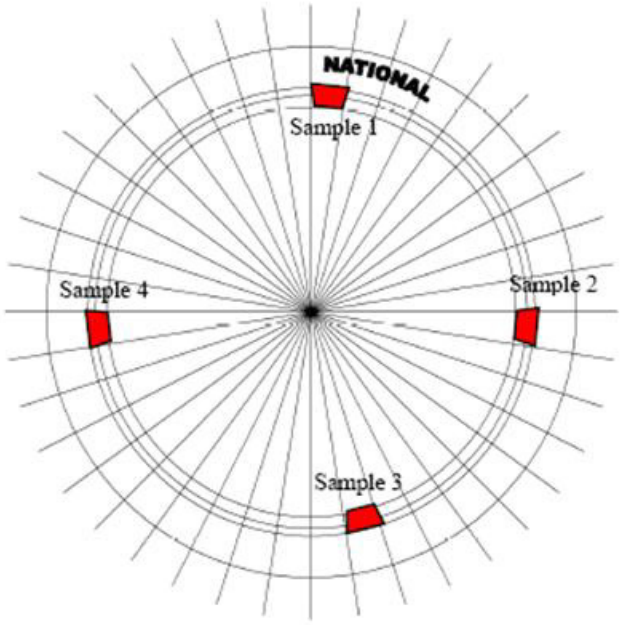

Figure 8 – Samples Cut along the Circumference of the Lip Seal Elastomer

Four samples, each of approximately 13mm in length were cut along the circumference of each seal at four different locations to check for the repeatability of the results. The cut samples were fixed on a mount using colloidal graphite. In order to view the surface topography, the surface must be reflective for an optical profilometer and electrically conductive for a scanning electron microscope (SEM). To facilitate this, after cleaning and drying, the samples were coated with gold palladium of approximately 15nm thickness [1] using sputter coater. Figure 9 shows the optical microscope image of the lip seal elastomer after coating with gold palladium.

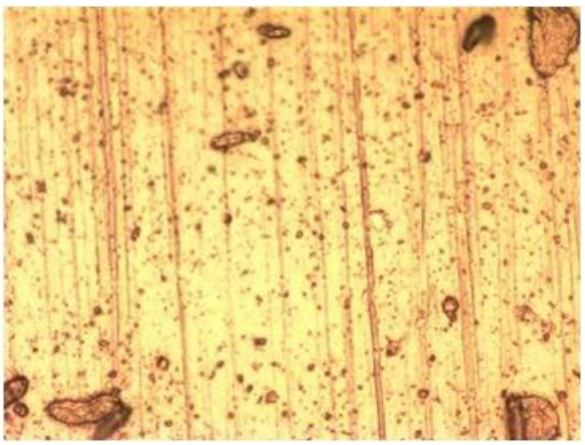

Figure 9 – Lip Seal Elastomer after Coating with Gold Palladium

Sputter coater allows the deposition of a suitable coating to provide an electrically conductive thin film over the surface topography of the specimen to be viewed. The target material (gold palladium) to be sputtered is made as cathode and the specimen to be coated is made as anode. An inert gas (argon) is admitted into the chamber. When current is applied to the target, the metal atoms separate from the target and collide with the argon atoms. The argon atoms cause the metal atoms to scatter which results in an uniform coating of gold palladium on the specimen. The thickness of coating depends on the current applied to the system and the distance between the target material and the specimen to be coated. These films also provide other advantages such as inhibit charging of the scanning electron microscope probe, reduce thermal damage to the specimen and enhance secondary electron emission.

3.4 INSTRUMENTS USED FOR SURFACE CHARACTERIZATION

Scanning Electron Microscope (SEM) and Zygo optical profilometer were used to characterize the lip seal elastomer surface. In the scanning electron microscope an electron beam is focused into a fine probe and subsequently scanned over a small rectangular area. As the electron beam interacts with the specimen, it creates various signals, such as secondary electrons, internal currents, and photon emissions, all of which are collected by appropriate detectors. With appropriate sample preparation, the SEM gives excellent depth of focus and resolution.

The scanning electron microscope has an image resolution of 3.5 nm. The specimen stage has a tilt angle of -20^{o} to $+ 90^{o}$ and rotation angle of 360^{o}. The scanning electron microscope has many advantages over other microscopes. The SEM has a large depth of field, which allows more part of a specimen to be in focus at one time. The SEM also has much higher resolution, so closely spaced features in a specimen can be magnified at much higher levels. Because the SEM uses electromagnets rather than lenses, there is more control in the degree of magnification. All of these advantages, as well as the remarkable clear images, make the scanning electron microscope one of the most useful instruments in research today. The disadvantage of the scanning electron microscope is that the size of sample that can be accommodated in the SEM chamber is limited to approximately 31mm in diameter and 10mm in height and the specimens should be vaccum compatible. The scanning electron microscope gives only qualitative information and roughness of specimen cannot be quantified. The important step in viewing the

specimen in the scanning electron microscope is how the samples are prepared. Since this is an electron scope, the electron particles must be excited and coated with certain materials in order to be seen properly. The samples should be prepared carefully or the microscope images will not view correctly.

An optical profilometer can make wide range measurements of surface heights and surface features without contact. Three dimensional topographical information can be obtained from a single scan whereas multiple parallel scans are needed for a stylus profilometer. In an optical profilometer, the light reflected from the specimen surface interferes with light from a reference optically flat surface. Deviations in the fringe pattern of bright and dark lines produced by the interference correspond to differences in surface height. The Zygo optical profilometer has a vertical resolution of 0.1 nm, Lateral resolution of 0.45 – 11.8 mm and field of view of 0.04 – 17.5 mm. The Zygo optical profilometer is capable of giving quantitative information of the surface. The surface topography measurements take short time and are done at ambient conditions.

3.5 SURFACE AND WEAR ANALYSIS

The lip seal elastomer samples were mounted with the circumferential direction of the elastomer horizontal to the objective, to analyze the surface characteristics of the wear track. Figure 10 (a) shows the scanning electron microscope image of an untested lip seal elastomer.

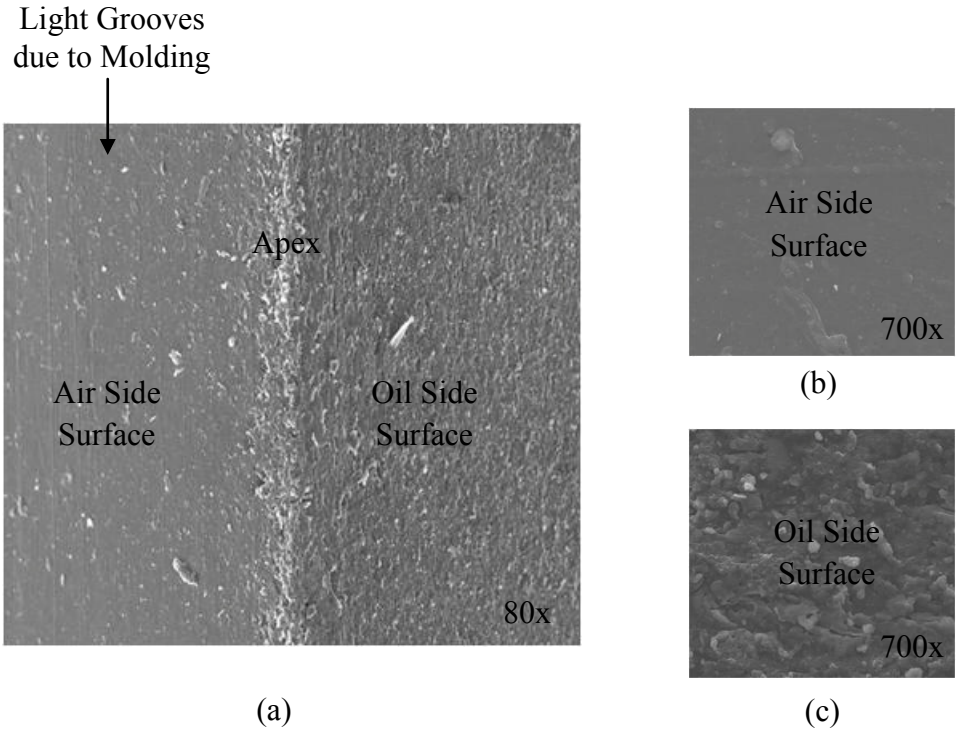

Figure 10 – SEM Image of (a) Untested Seal (b) Air Side (c) Oil Side

Figures 10 (b) and 10 (c) show the magnified image of the air side and the oil side surface of an untested elastomer. The radial lip seals are manufactured in two ways. In one method the oil side surface is a trimmed surface and the air side surface is a molded surface. In the second method, both the air side and the oil side surface are molded. In the lip seal elastomers used for testing, the molded side is on the air side and the trimmed side is on the oil side. From visual observations, the oil side surface looks rough when compared to the air side surface and contains more number of asperities. Five samples of an untested seal at different location along the circumference were analyzed. The initial rms roughness (Sq) of the air side and the oil side surface are 0.458±0.07 μm and 0.806±0.11 μm.

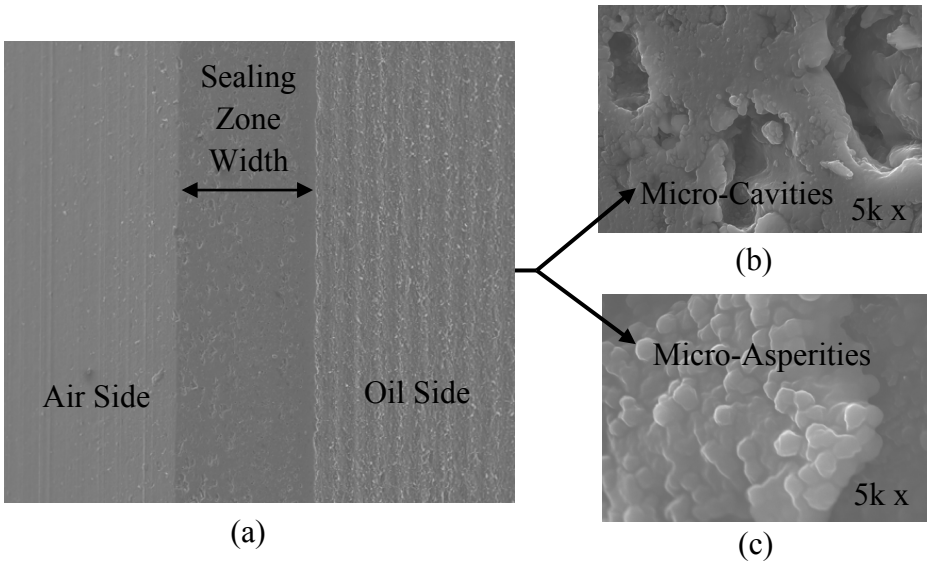

Figure 11 – SEM Image of (a) Tested Seal (b) Micro-Cavities (c) Micro-Asperities

Figure 11 (a) shows the scanning electron microscope image of a typical tested lip seal elastomer indicating the air side, oil side and sealing zone. Figures 11 (b) and 11 (c) show the micro-cavities and micro-asperities present in the sealing zone of elastomer. Comparing the scanning electron microscope image of an untested (Figure 10 (a)) and tested (Figure 11 (a)) lip seal elastomer, the tested seals have parallel grooves or ridges along the circumferential direction created on the oil side of the lip seal elastomer. These parallel grooves on the oil side of the lip seal elastomer may be due to elastomer wear particles and oil which are dragged over the elastomer surface by the shaft rotation. Every new seal starts with an apex which wears to form the sealing zone. The wearing away of the lip seal elastomer apex to form the sealing zone is clearly seen from these two figures. The sealing zone widths are measured after testing.

To estimate the amount of wear in the lip seal elastomer, two samples each of approximately 3mm in length were cut at different locations along the circumferential

direction of the seal. The lip seal elastomer samples were mounted with the circumferential direction of the elastomer vertical to the objective. Figure 12 shows the image of an untested and tested seal when the elastomer samples are mounted vertically. The wear of the apex of the lip seal elastomer resulting in the formation of sealing zone can be seen from the figures 12 (a) and 12 (b). A and B represent the reduction in the air side and oil side respectively. The amount of wear per circumferential length is estimated from the difference in area of the apex from the scanning electron microscope images of the tested and untested seals. After testing, when the lip seal elastomer is removed, the air side, oil side and sealing zone surface of the lip seal elastomer are not perfectly straight. In tests, the lip seal elastomer is installed first and then the shaft (ring) is pressed from above. This causes the lip seal apex to deflect and hence the apex and some portion of the air side surface of elastomer come in contact with the shaft. Also during the dynamic conditions, the sealing zone of the lip seal elastomer is deformed in the radial direction and circumferential direction due to the hydrodynamic pressure distribution and tangential shear stress. After testing and uninstalling the lip seal elastomer, the sealing zone forms a curvature along the axial direction. The deviation in the air side, oil side and sealing zone of the elastomer are included in the estimation of wear by measuring the curvature in the air, oil and sealing zone of the elastomer using the Zygo optical profilometer. The wear rate of the lip seal elastomer per circumferential length is calculated by dividing the wear estimate per circumferential length by the total number of hours the seal has operated.

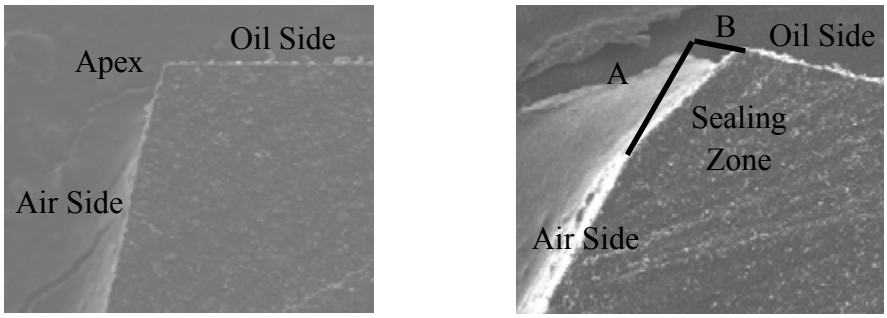

(a) (b)

Figure 12 – (a) Untested and (b) Tested Lip Seal Elastomer (Wear Measurement)

The Stitching application in Zygo was used to get the surface topography of the elastomer. In the stitching application single measurement scans are made and they are combined together. Stitching increases the field of view without increasing the lateral or vertical resolution. Figure 13 shows the stitched measurement obtained from the sealing zone of the lip seal elastomer from one of the cut-out sample.

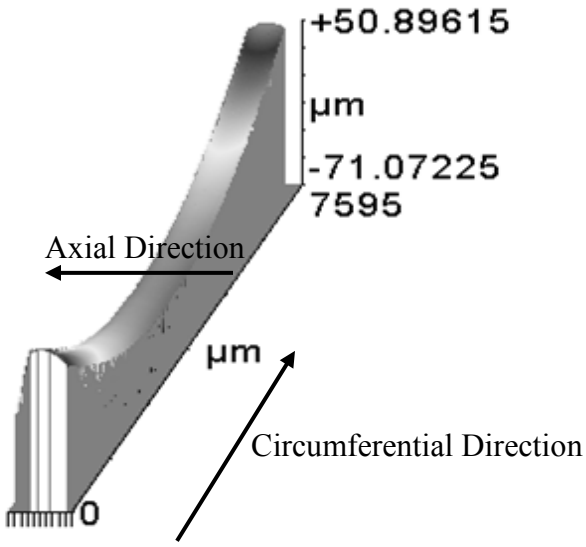

Figure 13 – Stitched Wear Track of Lip Seal Elastomer

The curvature of the lip seal along the circumferential direction can be seen from this figure. A 20 % overlap was used between two consecutive measurements and they are

averaged to minimize the amount of discontinuity and to increase the accuracy of the surface measurements.

The sealing zone surface of the lip seal elastomer is a combination of different frequency components. The two main components are the roughness and waviness. The high frequency components represent the roughness also known as micro-asperities and the low frequency components represent the waviness. A high pass Fast Fourier Transform filter (FFT) was used to filter out the roughness from the waviness data. Figure 14 shows the input profile, waviness profile and roughness profile.

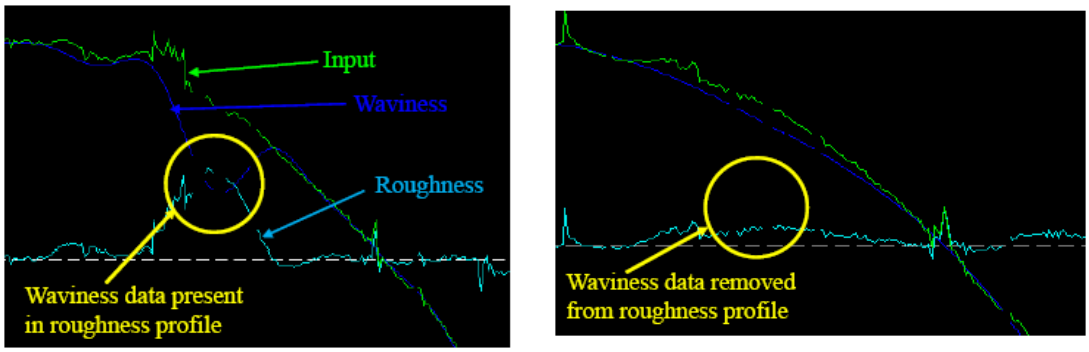

(a) (b)

Figure 14 – (a) Before and (b) After Selecting the Appropriate Cut off Frequency

When the correct cutoff frequency is not selected there is some waviness components present in the roughness components or vice versa. In Figure 14 (a) there is some roughness components still present in waviness component even after filtering has been

done. Once an appropriate cutoff frequency is selected, the roughness components are completely removed from the waviness profile as shown in figure 14 (b). Figure 15 shows how a surface is separated into roughness and waviness when filtering is applied.

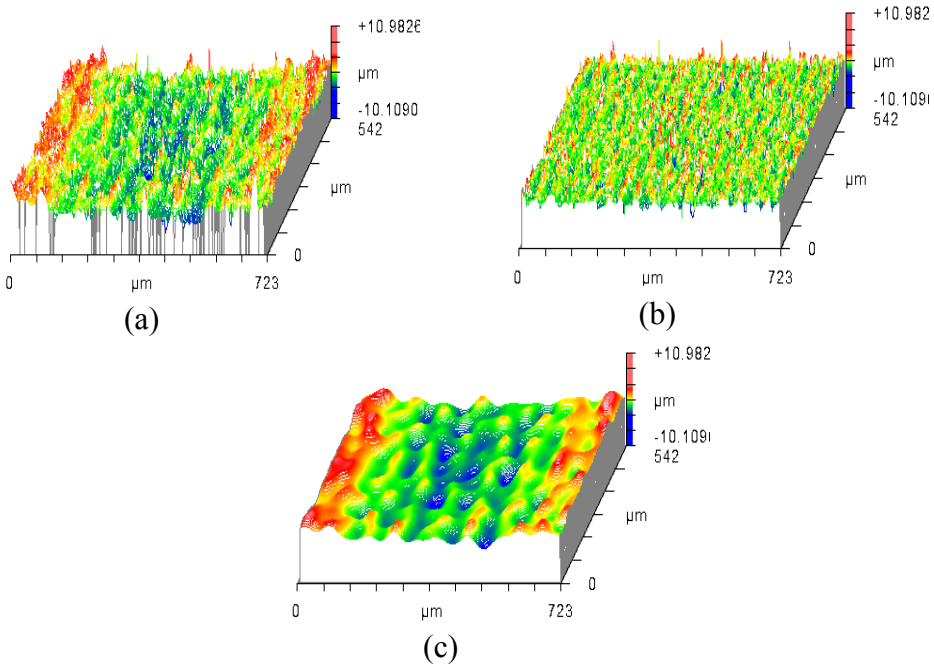

Figure 15 – (a) Input, (b) Roughness and (c) Waviness Components of a Surface

These methods are used in the following chapters to analyze the lip seal sealing zone surface and to estimate the amount of wear in the elastomer.

CHAPTER 4 – 3D SURFACE CHARACTERIZATION OF ELASTOMER

Every surface is comprised of random surface roughness with random peaks and random valleys. Deterministic surface texture consists of repeated patterns of peaks and valleys. In reality, the actual surface is also a combination of deterministic surface and random surface roughness. Three dimensional topographical analysis plays an important role in any product design and manufacturing. The performance of engineering components can be improved by selecting the appropriate three dimensional topography. The relation between the functional properties of surfaces and the characterization of surface topography is difficult to predict and it varies from application to application. The sample length and sample interval are important when characterizing a surface topography. Three dimensional topography of any surface [22] cannot be described completely by few parameters. Dong, Sullivan, Stout [22] proposed a primary parameter set called "Birmingham 14 parameters" that includes a number of parameters to describe the three dimensional topography of a surface. These parameters do not correlate with one another and they individually provide significant information about the surface.

The lip seal elastomer sealing zone is measured using a Zygo optical profilometer. After making measurements in Zygo optical profilometer, the measurements are exported to Matlab to do further calculations. The optical profilometer scans include the height measurements of the surface and are represented in the form of matrix with equal spacing of x and y. For the surface characterization of the lip seal elastomer, Birmingham 14

parameters were considered. The Birmingham 14 parameters are divided into four groups: amplitude, spatial, hybrid and functional parameters. Some of the three dimensional parameters are extended from the two dimensional parameter set.

The height of the surface is represented by $\eta(x_i, y_i)$, where $x_i=i\Delta x$, $y_i=j\Delta y$; i= 1, 2, …, M; j= 1, 2, …, N.Δx and Δy represent the sampling interval, and M and N represent the number of sampling points in the x and y directions respectively. Within each seal, samples at four different locations are considered. The surface parameters are calculated at these four sampling areas.

4.1 AMPLITUDE PARAMETERS

4.1.1 ROOT MEAN SQUARE ROUGHNESS, S_q (rms roughness)

Root mean square roughness parameter gives a measure of the roughness of a surface from the mean plane. The continuous and discrete forms of the root mean square roughness parameter are given below:

$$Sq = \sqrt{\frac{1}{l_x l_y}\int_0^{l_y}\int_0^{l_x} \eta^2(x,y)dxdy} \approx \sqrt{\frac{1}{MN}\sum_{j=1}^{N}\sum_{i=1}^{M}\eta^2(x_i,y_i)}$$

Where $\eta(x_i, y_i)$ represent the surface height measurements, l_x and l_y represent the lengths of the surface in the x and y direction respectively. Figure 16 shows the root

mean square roughness values of the lip seal elastomers after testing. The elastomers which ran against textured shafts have higher roughness when compared to the elastomers which ran against stainless steel shafts.

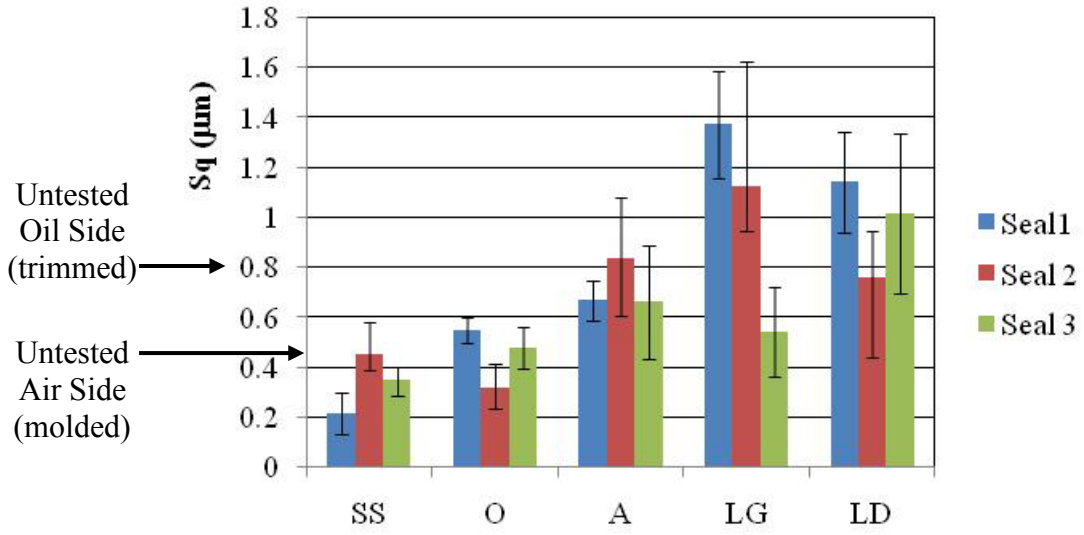

Figure 16 – Root Mean Square Roughness Values of Elastomer Surface

The lip seal elastomers O1, O2, and O3 forward pumped. These seals have significant wear only during the initial break-in period and after that there is constant film of fluid present between the shaft and elastomer which leads to lower final roughness value. The lip seal elastomers LG1, LG2, LG3 reverse pumped and between every oil drop test performed, the lip seal runs in starved or partially starved condition which leads to more wear. In addition, these seals have grooves along the circumferential direction in the sealing zone (see Figure 38 on page 75) which leads to higher roughness.

4.1.2 TEN POINT HEIGHT, S_z

Instead of maximum peak to valley height, an average of the maximum peak to valley height is considered. Ten point height of a surface topography is defined as the average value of the heights of five highest summits and the depths of five deepest valleys within the sampling area. The discrete form of the ten point height is given below:

$$S_z = \frac{1}{5}\left(\sum_{i=1}^{5}|\eta_{si}| + \sum_{j=1}^{5}|\eta_{vj}|\right)$$

Where η_{si} (i=1, 2, .., 5) represent the five highest summits and η_{vj} (j=1, 2, …, 5) represent the five deepest valleys. There are several definitions of summit height. In this study, a summit is defined by the eight nearest neighbor technique. Using different definitions of summit, affects the number of summits and the average heights of the summits. Figure 17 shows the ten point height of the elastomer sealing zone. The elastomers which ran against textured shafts contain height peaks and deepest valleys when compared to the elastomers which ran against stainless steel shafts.

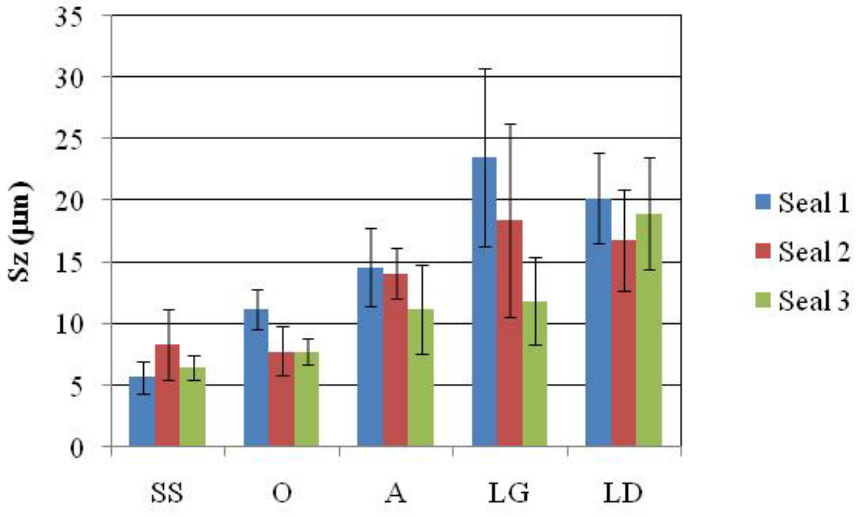

Figure 17 – Ten Point Height of Elastomer Surface

4.1.3 SKEWNESS, S_{sk}

The skewness is the measure of asymmetry of the surface heights about the mean plane. The continuous and discrete forms of skewness are given below:

$$S_{sk} = \frac{1}{S_q^3} \int_{-\infty}^{\infty} \int_{-\infty}^{\infty} \eta^3(x,y) P(\eta)\, dx\, dy \approx \frac{1}{MNS_q^3} \sum_{j=1}^{N} \sum_{i=1}^{M} \eta^3(x_i, y_i)$$

Where P(η) represent the probability distribution function of the surface η(x, y). Skewness, S_{sk} is also an extension from the two dimensional surface characterizing parameter, R_{sk}. A surface with symmetric height distribution, the skewness is zero. A surface with asymmetric height distribution, the skewness may be negative or positive. The skewness is negative if the height distribution has a longer tail at the lower side of the mean plane. The skewness is positive if the height distribution has a longer tail at the upper side of the mean plane. This parameter indicates the presence of sharp features on the surface. A large positive skewness, $S_{sk} > 1$, indicate the presence of few sharp points on the surface. These sharp points will quickly wear away when it comes in contact with another surface. Figure 18 shows the skewness values of the elastomer sealing zone.

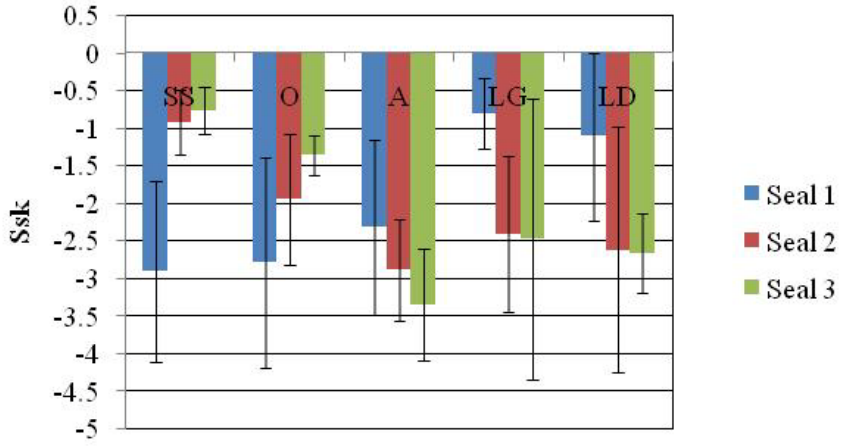

Figure 18 – Skewness of Elastomer Surface

Skewness of all the elastomer surfaces is negative. Negative skewness indicates the surface below the mean value is spread out more than above the mean plane. A large negative skewness, S_{sk} < -1, indicates the presence of significant pits and troughs and most of its highest peaks at the same level. The lip seal elastomers LG and LD have grooves in the sealing zone and the variation in the number of grooves along the circumferential direction causes significant variation of S_{sk} in the lip seal elastomers LG and LD. The variation of S_{sk} within seals which ran against similar pattern of shaft may be attributed to difference in duration of testing time.

4.1.4 KURTOSIS, S_{ku}

Kurtosis describes the shape of the surface height distribution and it is used along with skewness to identify the pits/troughs and sharpness/peakedness of a surface. Kurtosis measures the peakedness or sharpness of the height distribution. The continuous and discrete form of kurtosis is given below:

$$S_{ku} = \frac{1}{S_q^4} \int_{-\infty}^{\infty} \int_{-\infty}^{\infty} \eta^4(x,y) P(\eta)\, dx\, dy \approx \frac{1}{MNS_q^4} \sum_{j=1}^{N} \sum_{i=1}^{M} \eta^4(x_i, y_i)$$

The three dimensional kurtosis is also extended from the two dimensional one. A Gaussian surface has a kurtosis value of 3. A centrally distributed surface height distribution has a kurtosis value larger than 3. A wide spread surface height distribution

has a kurtosis value less than 3. There is significant variation of kurtosis within the seals which ran against Stainless steel shafts. This may be due to the presence of outliers in surface heights which results in large value of kurtosis. Hence by analyzing both skewness and kurtosis it may be possible to identify the flat tops and deep valleys. Figure 19 shows the kurtosis values of the elastomers.

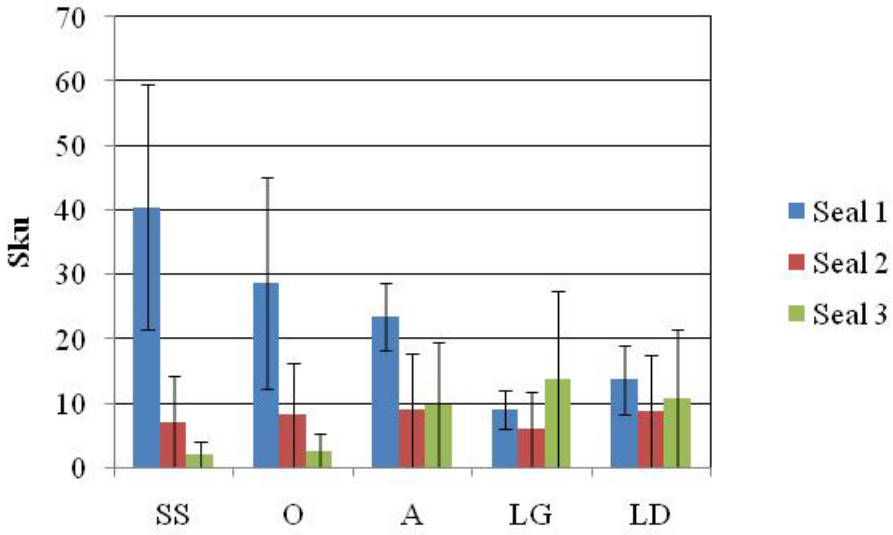

Figure 19 – Kurtosis Value of Elastomer Surface

The kurtosis value of all the elastomers is greater than 3. Negative skewness and large kurtosis indicate the lip seal elastomer surface to be of flat top with deep valleys in it.

4.2 FUNCTIONAL PARAMETERS

Engineering surfaces are used in many applications such as sealing, fluid retention, wear, friction and bearing. Based on application requirements, the surfaces are designed with appropriate topographical features. The functional parameters are used to describe the bearing and fluid retention properties of a surface. These functional parameters are

obtained from a curve called Abbott-Firestone curve also known as bearing area ratio curve. The Abbott-Firestone curve is divided into different regions and is classified into different functional zones. In addition to the bearing and fluid retention information, the Abbott-Firestone curve contains information about the material volume and void volume of a surface. Figure 20 shows a sample bearing area ratio curve.

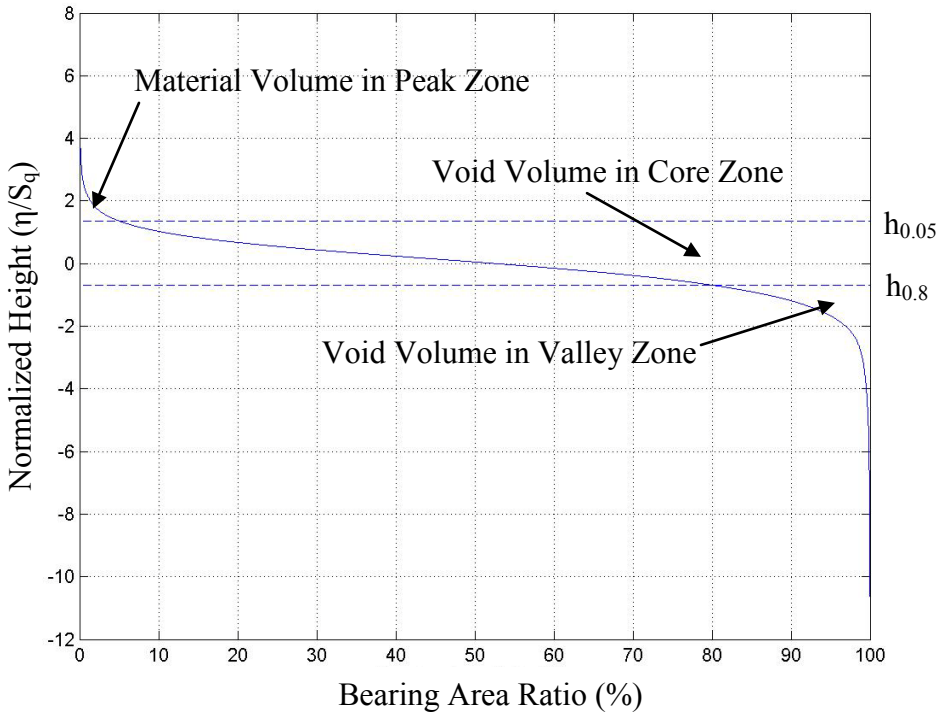

Figure 20 – Bearing Area Ratio Curve

Two horizontal lines are drawn: one line intersects at 5% of bearing area which is denoted by $h_{0.05}$ and other intersects at 80 % of bearing area which is denoted by $h_{0.8}$. Now the bearing area ratio curve is classified into three zones: peak zone, core zone and valley zone. The area enclosed below the bearing area ratio curve and the top horizontal line represents the material volume in the peak zone. The area enclosed above the bearing

area ratio curve, the top horizontal line and the bottom horizontal line represents the void volume in the core zone. The area enclosed above the bearing area ratio curve and the bottom horizontal line represents the void volume in the valley zone.

4.2.1 SURFACE BEARING INDEX, S_{bi}

The surface bearing index indicates the bearing property of a surface. The surface bearing index is defined as the ratio of root mean square roughness over the surface height at 5% bearing area ratio.

$$S_{bi} = \frac{S_q}{\eta_{0.05}} = \frac{1}{h_{0.05}}$$

Where $\eta_{0.05}$ is the surface height at 5% bearing area. The larger the surface bearing index, better the bearing properties of the surface. For a Gaussian surface, the surface bearing index is 0.608μm. The surface bearing index increases correspondingly when a surface transforms from an unworn to worn stage [23].

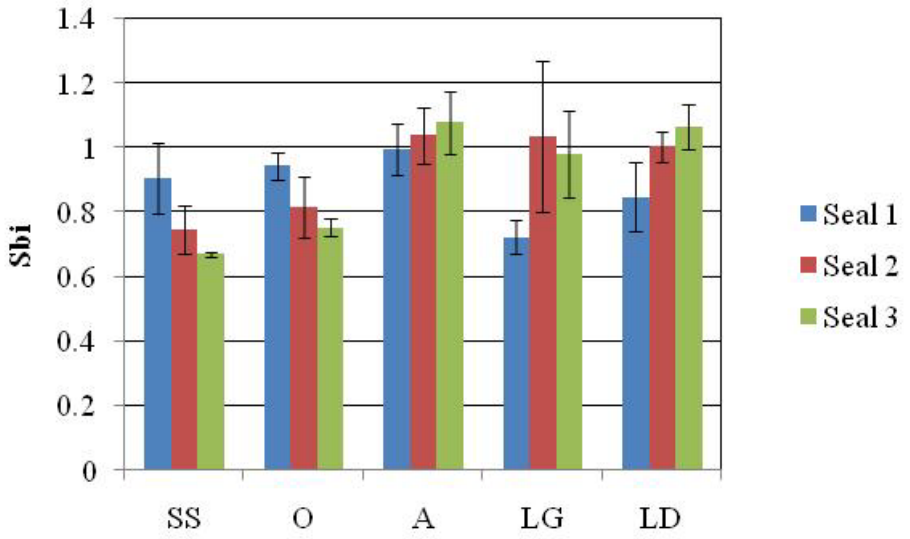

Figure 21 – Surface Bearing Index of Elastomer Surface

Figure 21 shows the surface bearing index of the elastomers. The surface bearing index values of the elastomers were between 0.7 and 1.1. Surface bearing index larger than 0.608 indicates that sealing zone surface is having almost a flat top. The surface bearing index values of the elastomers fall within the range between 0.3 and 2 as suggested by Dong, Sullivan, Stout [22] for engineered surfaces.

4.2.2 CORE FLUID RETENTION INDEX, S_{ci}

The core fluid retention index indicates the fluid retention property of a surface in the core zone. The core fluid retention index is defined as the ratio of the void volume per unit sampling area in the core zone over the root mean square roughness. The core fluid retention index is given by the expression:

$$S_{ci} = \frac{1}{S_q} \frac{V_v(h_{0.05}) - V_v(h_{0.08})}{(M-1)(N-1)\Delta x \Delta y}$$

Larger value of S_{ci} indicates good fluid retention property of a surface in the core zone. Figure 22 shows the core fluid retention index of the elastomer sealing zone and the value of S_{ci} remains almost the same for all the elastomers.

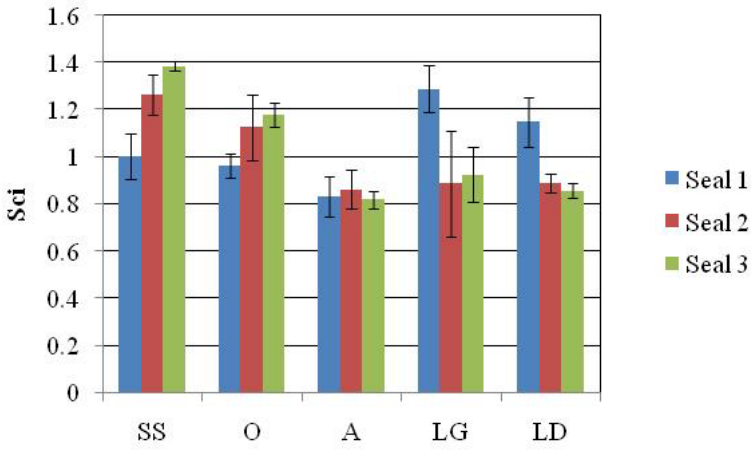

Figure 22 – Core Fluid Retention Index of Elastomer Surface

The core fluid retention index for a Gaussian surface is 1.56. When a surface progresses from an unworn to a worn surface the core fluid retention index decreases correspondingly [23]. When the lip seal elastomer runs against the shaft, the top asperities are reduced this ultimately decreases the void volume in the core zone. The core fluid retention index values of the elastomers were between 0.67 and 1.41. Dong, Sullivan, Stout [22] suggested the core fluid retention index of all surfaces fall within the range between 0 and $0.95(h_{0.05} - h_{0.8})$. The maximum value calculated from the height measurements of bearing area ratio curve is 2.99. Sci values obtained from the elastomer surfaces fall within the suggested range.

4.2.3 VALLEY FLUID RETENTION INDEX, S_{vi}

The valley fluid retention index indicates the fluid retention property of a surface in the valley zone. The valley fluid retention index is defined as the ratio of void volume per unit sampling area in the valley zone over the root mean square roughness. The expression for valley fluid retention index is given by:

$$S_{vi} = \frac{1}{S_q} \frac{V_v(h_{0.08})}{(M-1)(N-1)\Delta x \Delta y}$$

Figure 23 shows the valley fluid retention index of the elastomers.

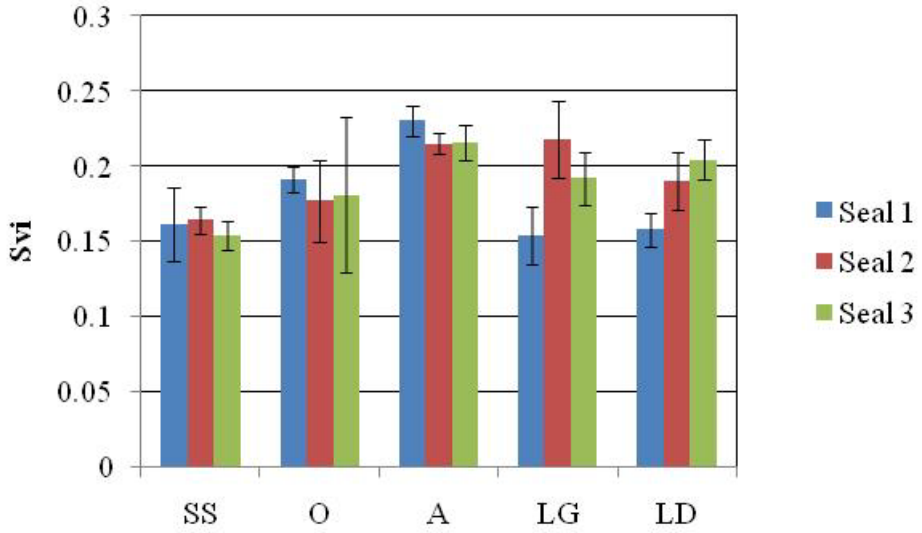

Figure 23 – Valley Fluid Retention Index of Elastomer Surface

Larger value of S_{vi} indicates good fluid retention property in the valley zone. The valley fluid retention index for a Gaussian surface is 0.11. The valley fluid retention index remains relatively constant when a surface progresses from an unworn to a worn surface [23]. The valley fluid retention index values of the elastomers were between 0.14 and 1.24. Dong, Sullivan, Stout [22] suggested the valley fluid retention index of all surfaces should fall within the range between 0 and $0.02(h_{0.8} - h_{min})$. The maximum value of the range calculated from the height measurements of bearing area ratio curve is 3.71. S_{vi} values obtained from elastomer surfaces fall within the suggested range.

4.3 AREAL AUTOCORRELATION FUNCTION, AACF

Areal Autocorrelation function indicates the dependence of the data values at one location on the data values at another location. The continuous and discrete forms of Areal Autocorrelation Function are given below:

$$R(\tau_x, \tau_y) = E[\eta(x,y)\eta(x+\tau_x, y+\tau_y)]$$

$$= \lim_{l_x, l_y \to \infty} \frac{1}{4 l_x l_y} \int_{-l_y}^{l_y} \int_{-l_x}^{l_x} \eta(x,y)\, \eta(x+\tau_x, y+\tau_y)\, dx\, dy$$

Where η(x,y) represent the surface heights.

$$R(\tau_i, \tau_j) = \frac{1}{(M-i)(N-j)} \sum_{l=1}^{N-j} \sum_{k=1}^{M-i} \eta(x_k, y_l)\eta(x_{k+i}, y_{l+j})$$

Where i=0, 1,…., m<M; j=0, 1,…, n<N;

$\tau_x = i\Delta x$, $\tau_y = j\Delta y$

m and n are the maximum numbers of autocorrelation lengths in the x and y directions respectively. Calculation of areal autocorrelation function using the discrete form consumes lot of time. Hence, the areal autocorrelation function was calculated using the Fast Fourier Transform (FFT) algorithm. The Areal Autocorrelation function decays fast in a direction indicating less correlation of the surface data in that direction. The slow decay of Areal Autocorrelation function indicates high correlation of surface data in that direction. Based on these information isotropy and anisotropy of the surfaces can be identified. If a surface is periodic in either one or two directions, then the Areal Autocorrelation function is also periodic in the respective directions. Any engineered surface contains both deterministic components and random components. The decay of Areal Autocorrelation function mainly depends upon the major frequency components. The dependence of surface height data may or may not be same in different directions. Therefore the decay of Areal Autocorrelation function may be different in different

directions. For isotropic surfaces, the decay of Areal Autocorrelation function along all directions will be similar. For anisotropic surfaces, the decay of Areal Autocorrelation function will be faster along one direction and slower along other direction. Refer to Figures 29 to 33 for results.

4.4 AREAL SPECTRAL DENSITY, APSD

Areal spectral analysis condenses the information available in space domain into frequency domain. It indicates the contributions of different wavelength components present in surface heights. Areal spectral analysis is also used to find and separate the "roughness" and "waviness" components. Fourier transform is used in the calculation of Areal Spectral Density. The continuous and discrete forms of Fourier transforms are given by

$$F(\omega_x, \omega_y) = \int_{-\infty}^{\infty} \int_{-\infty}^{\infty} \eta(x, y)\, exp\left[-j2\pi(\omega_x x + \omega_y y)\right] dx\, dy$$

$$F(\omega_p, \omega_q) = \sum_{l=0}^{N-1} \sum_{k=0}^{M-1} \eta(x_{k+1}, y_{l+1})\, exp\left[-j2\pi\left(\frac{p}{M}k + \frac{q}{N}l\right)\right]$$

$p = 0,1, \dots, M-1; q = 0,1, \dots, N-1$

$$\omega_p = \frac{p}{\Delta x M}, \omega_q = \frac{q}{\Delta y N}$$

Where ω_p and ω_q are the angular frequencies in the orthogonal directions. The Areal Spectral Density is obtained by

$$G(\omega_p, \omega_q) = F(\omega_p, \omega_q) * F^*(\omega_p, \omega_q)$$

$F^*(\omega_p, \omega_q)$ represent the complex conjugate of $F(\omega_p, \omega_q)$. The low frequency components present in the areal spectral density graph provide useful information. The areal spectral density energy is almost evenly distributed for an isotropic random surface. When a surface has significant periodicity along one or two directions, the energy of areal spectral density is concentrated on the specific frequency of periodicity and along the direction of periodicity. When the surface is directional, the areal spectral density is also directional. Calculations are further made in the areal spectral density to obtain angular spectrum which reveals additional information. The angular spectrum is obtained by integrating the spectral density. The angular spectrum is given by

$$G_a(\theta) = \int_0^{R(\theta)} G(\theta, r)\, dr$$

$$R(\theta) = \frac{1}{2}[(\Delta x\ \cos\theta)^2 + (\Delta y\ \sin\theta)^2]^{-\frac{1}{2}}$$

$$0 \leq \theta \leq 179$$

where $G(\theta, r)$ is the power spectrum in polar coordinates. The angular spectrum display individual peaks at the angles where the powers are concentrated for anisotropic surface. The angular spectrum is used to identify the texture direction of a surface. Refer to Figures 29 to 33 for results.

4.5 SPATIAL PARAMETERS

Figure 24 shows the relation between the x and y coordinates and the directionality of the surface. The positive and negative surface directions are withrespect to the y axis.

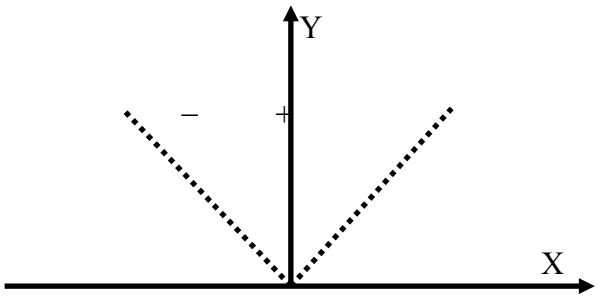

Figure 24 – Surface Texture Direction

The four spatial parameters considered are the fastest decay autocorrelation length, density of summits, texture aspect ratio and texture direction of the surface.

4.5.1 FASTEST DECAY AUTOCORRELATION LENGTH, S_{al}

The fastest decay autocorrelation length is defined as the shortest distance in which the value of normalized areal autocorrelation function decays to a value of 0.2 in any direction.

$$S_{al} = \min\left(\sqrt{\tau_x^2 + \tau_y^2}\right), \mathrm{R}(\tau_x + \tau_y) \leq 0.2$$

The decay rate of areal autocorrelation function is dominated by the major frequency components. A large value of autocorrelation length denotes that the surface is dominated

by the longer wavelength low frequency components. While a small value of autocorrelation length denotes that the surface is dominated by the shorter wavelength high frequency components. Refer to table 1 for results.

4.5.2 DENSITY OF SUMMITS, S_{ds}

The density of summits indicates the number of summits present in a unit sampling area. The density of summits is given by

$$S_{ds} = \frac{Number\ of\ Summits}{(M-1)(N-1)\Delta x \Delta y}$$

The number and density of summits vary based on the definition of summit. In this study eight nearest neighbor technique was used to identify a summit. Figure 25 shows the density of summits for the elastomers. The elastomers which ran against stainless steel shafts were found to have more number of summits per unit sampling area.

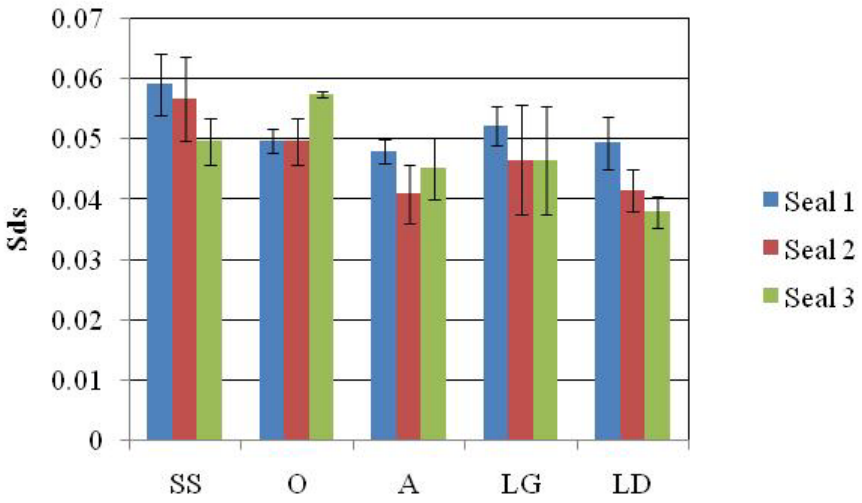

Figure 25 – Density of Summits of Elastomer Surface

4.5.3 TEXTURE ASPECT RATIO, S_{tr}

Texture aspect ratio is used to indicate the texture pattern of a surface. The texture aspect ratio is defined by

$$S_{tr} = \frac{Fastest\ decay\ distance\ of\ the\ \ AACF\ to\ 0.2\ in\ any\ possible\ direction}{Slowest\ decay\ distance\ of\ the\ \ AACF\ to\ 0.2\ in\ any\ possible\ direction}$$

The value of texture aspect ratio varies between 0 and 1. Larger values of the texture aspect ratio indicate more uniform surface texture in different directions. Smaller values of texture aspect ratio indicate more anisotropy of the surface.

Table 1 – Fastest Decay Autocorrelation Length & Texture Aspect Ratio of Elastomer

Elastomer No.	Sal (μm)	Str
3	4.53	0.03
15	4.54	1.00
38	2.26	1.00
4	22.69	2.83
9	5.80	0.51
41a	5.77	1.41
5	5.78	0.64
8	11.33	1.00
13	8.58	1.00
11a	9.17	0.08
14	15.89	0.16
18	5.67	0.62
12a	4.68	0.30
17	12.52	0.20
39	17.04	0.32

Table 1 gives the fastest decay autocorrelation length and texture aspect ratio of the elastomer sealing zone surface. Smaller value of fastest decay autocorrelation length indicates the surface is more isotropic. Larger value of S_{al} denotes that the surface is dominated by longer wavelength low frequency components. Value of Str greater than 0.5 indicates the surface is more isotropic. Elastomers ran against triangular cavities lagging and leading have low value of texture aspect ratio which indicates the surfaces are strongly anisotropic. Elastomers which ran against stainless steel shafts, triangular cavities oriented towards oil and air have texture aspect ratio greater than 0.5 indicating these surfaces are strongly isotropic.

4.5.4 TEXTURE DIRECTION, S_{td}

Texture direction indicates the prominent direction of the surface withrespect to y axis. The texture direction of the surface is determined by

$$S_{td} = \begin{cases} -\beta, \beta \leq {}^{\pi}/_{2} \\ \pi - \beta, \pi/2 < \beta \leq \pi, \\ \beta = value\ of\ \theta\ at\ which\ G_a(\theta) is\ maximum \end{cases}$$

When the surface has uniform texture the value of S_{td} is greater than 0.5. Therefore the texture direction is not applicable to surfaces which have S_{td} greater than 0.5.

4.6 HYBRID PARAMETERS

The hybrid parameters indicate the changes in both the amplitude and spacing of surface heights.

4.6.1 ROOT MEAN SQUARE SLOPE, $S_{\Delta q}$

The root mean square slope is calculated from the surface slope at a point. For a surface with discrete surface height data, the root mean square slope is given by

$$S_{\Delta q} = \sqrt{\frac{1}{(M-1)(N-1)} \sum_{j=2}^{N} \sum_{i=2}^{M} \rho_{ij}^2}$$

Where ρ_{ij} represent the slope with two data points in each direction and is given by

$$\rho_{ij} = \left[\left(\frac{\eta(x_i, y_i) - \eta(x_{i-1} - y_j)}{\Delta x} \right)^2 + \left(\frac{\eta(x_i, y_i) - \eta(x_i - y_{j-1})}{\Delta y} \right)^2 \right]^{1/2}$$

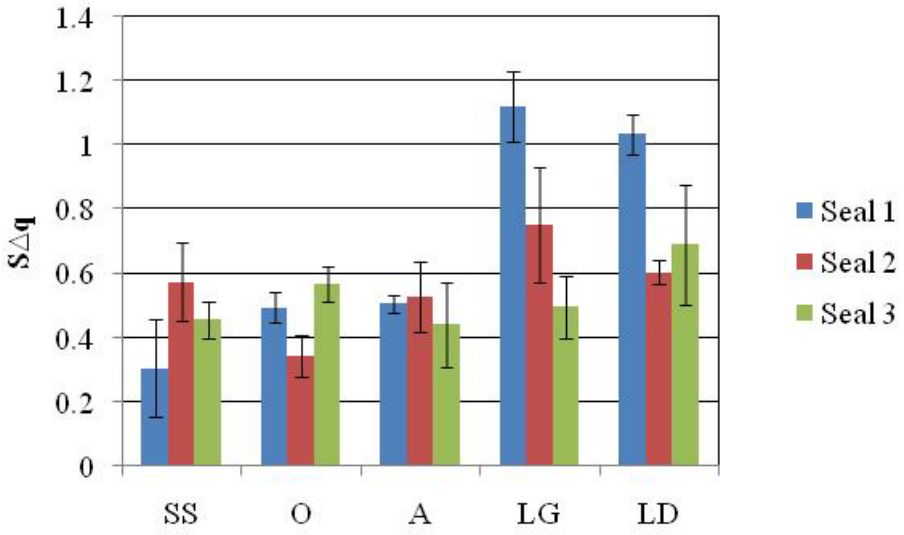

Figure 26 – Root Mean Square Slope of Elastomer Surface

Figure 26 shows the root mean square slope of the elastomer surface. The elastomer which ran against shafts manufactured with triangular cavities lagging and leading were found to have more root mean square slope when compared to the other surfaces.

4.6.2 ARITHMETIC MEAN SUMMIT CURVATURE, S_{sc}

The arithmetic mean summit curvature of a surface is defined as the average of the principle curvature of the summits within the sampling area considered. The arithmetic mean summit curvature of the surface with three data points in each direction is given by

$$S_{sc} = -\frac{1}{2n}\sum_{k=1}^{n}\left(\frac{\eta(x_{p+1}, y_q) + \eta(x_{p-1}, y_q) - 2\eta(x_p, y_q)}{\Delta x^2} + \frac{\eta(x_p, y_{q+1}) + \eta(x_p, y_{q-1}) - 2\eta(x_p, y_q)}{\Delta y^2}\right)$$

This denotes that the sum of the curvatures of a surface at a point along any two orthogonal directions is equal to the sum of the principle curvatures. Figure 27 shows the arithmetic mean summit curvature of the elastomer sealing zone surface.

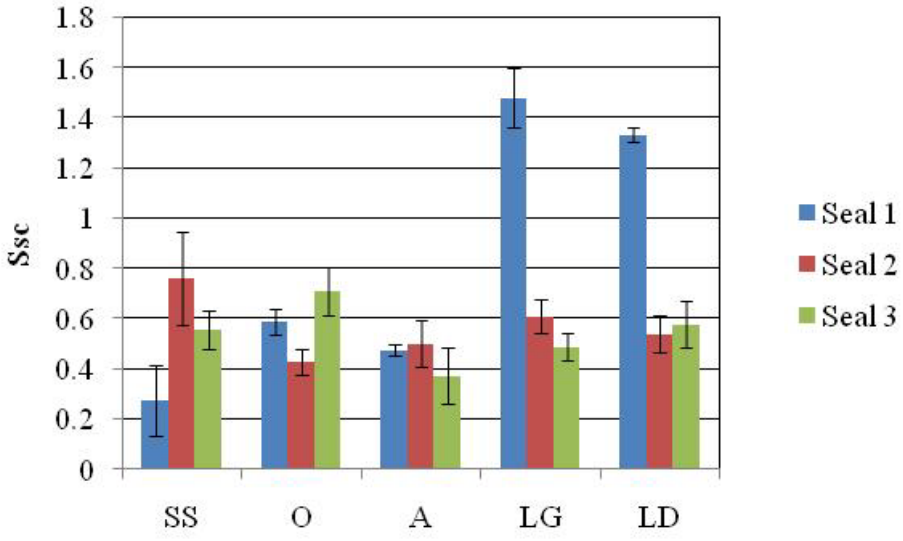

Figure 27 – Arithmetic Mean Summit Curvature of Elastomer Surface

The arithmetic mean summit curvature of all the elastomers remains almost the same expect for the sample 1 of triangular cavities lagging and leading.

4.6.3 DEVELOPED INTERFACIAL AREA RATIO, S_{dr}

The developed interfacial area ratio is the ratio of interfacial area of the surface over the sampling area. The developed interfacial area ratio is given by

$$S_{dr} = \frac{\sum_{j=1}^{N-1}\sum_{i=1}^{M-1} A_{ij} - (M-1)(N-1)\Delta x\,\Delta y}{(M-1)(N-1)\Delta x\,\Delta y} \times 100\%$$

Where $A_{ij} \approx \sqrt{1 + \left(\frac{\eta(x_{i+1},y_j)-\eta(x_i,y_j)}{\Delta x}\right)^2 + \left(\frac{\eta(x_i,y_{j+1})-\eta(x_i,y_j)}{\Delta y}\right)^2}\,\Delta x\,\Delta y$

Larger value of developed interfacial area ratio indicates significant change is either amplitude or spacing of the surface heights or both. The developed interfacial area ratio also indicates the progress of surface from an unworn condition to a worn condition.

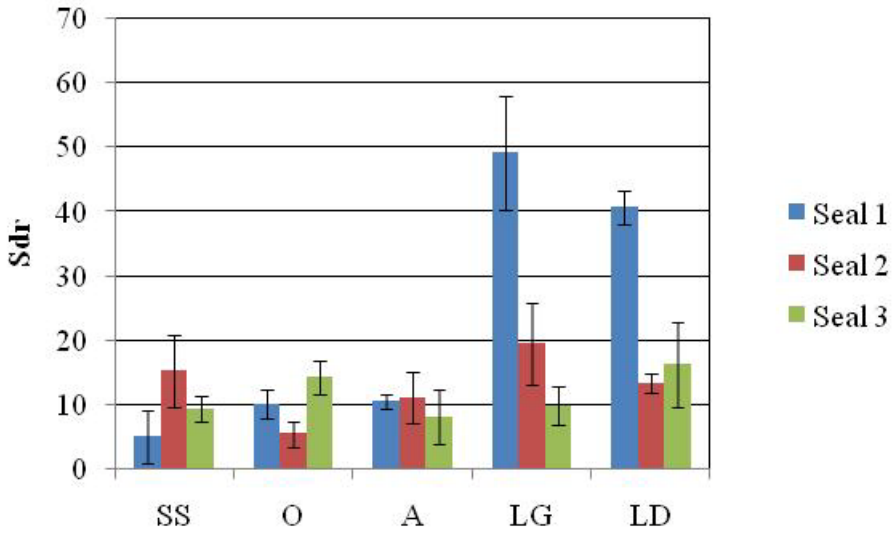

Figure 28 – Developed Interfacial Area Ratio of Elastomer Surface

Figure 28 shows the developed interfacial area ratio of the elastomer sealing zone. The developed interfacial area ratio remains almost the same except for the elastomers which ran against triangular cavities lagging and leading. This is due to the grooves created on the elastomer sealing zone by the triangular wedges formed between the triangular cavities on the shaft. The seals LG1 and LD1 ran for less duration of hours when compared to other LG and LD seals. The surfaces of LG1 and LD1 have more peaks and valleys which results in high value of developed interfacial area ratio and arithmetic mean summit curvature

4.7 AACF, APSD, ANGULAR SPECTRUM OF ELASTOMER SEALING ZONE

4.7.1 Elastomers Ran Against Stainless Steel Shafts

AACF

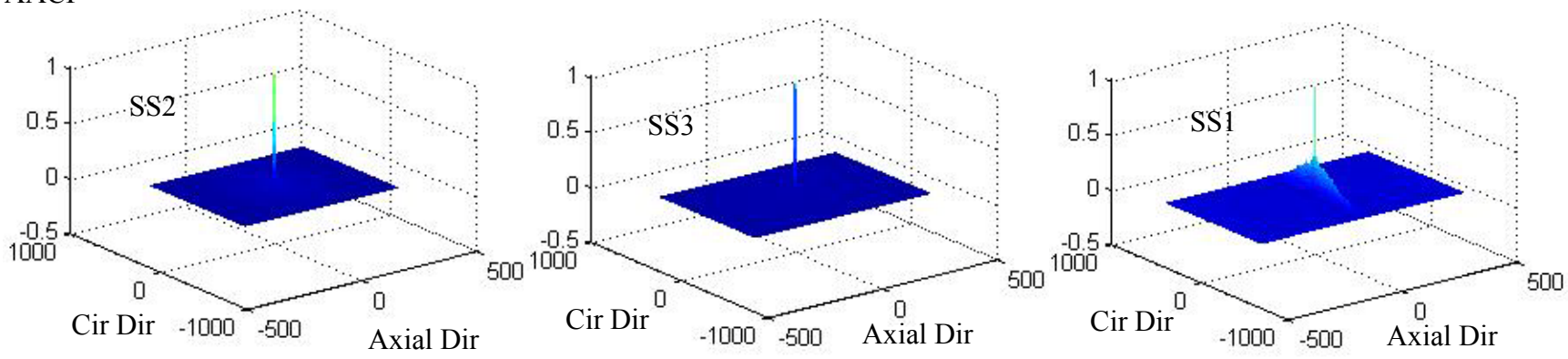

APSD

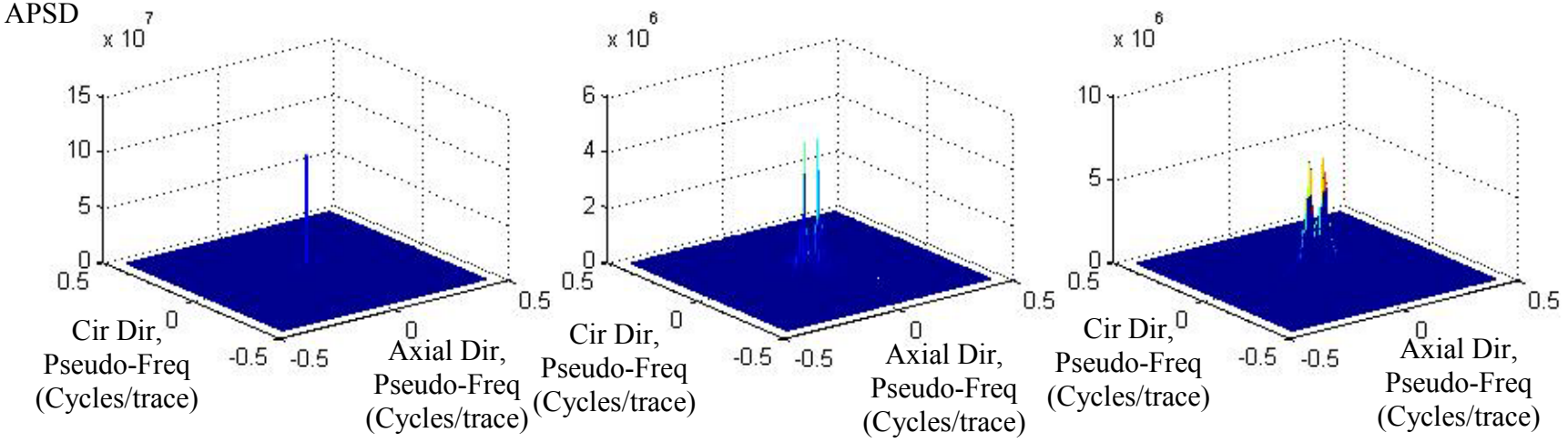

Angular Spectrum

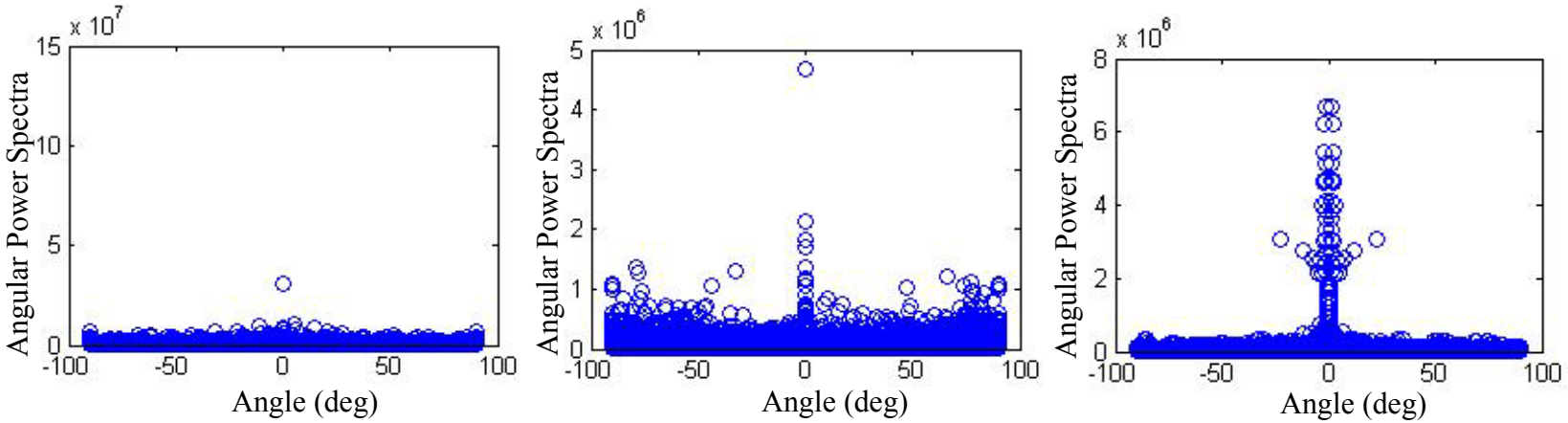

Figure 29 – AACF, APSD, Angular Spectrum of Elastomers

Ran Against Stainless Steel Shaft

Figure 29 shows the AACF, APSD and Angular Spectrum of elastomers ran against stainless steel shafts. The Areal auto correlation functions of elastomer SS2 and SS3 decays rapidly in all the directions. This suggests that there is no correlation of the surface height data in all directions and the elastomer sealing zone surface is isotropic. The AACF of elastomer SS1 decays rapidly along the axial direction and decays slowly along the circumferential direction which indicates less correlation of data along the axial direction and high correlation of data along the circumferential direction.

Low frequency components play an important role in APSD of surfaces and energy of APSD is very low at high frequencies. For the elastomer SS2, the APSD energy is evenly distributed in a circular manner around the origin which indicates the elastomer sealing zone is isotropic. In the elastomers SS3 and SS1, the main energy of APSD is concentrated on frequency of periodicity. These suggest the sealing zone surface becomes directional as the duration of operation increases. The angular spectrum plots of elastomers SS3 and SS1 show distinctive peaks at 0^o i.e. along circumferential direction.

4.7.2 Elastomers Ran Against Triangular Cavities Oriented Towards Oil

AACF

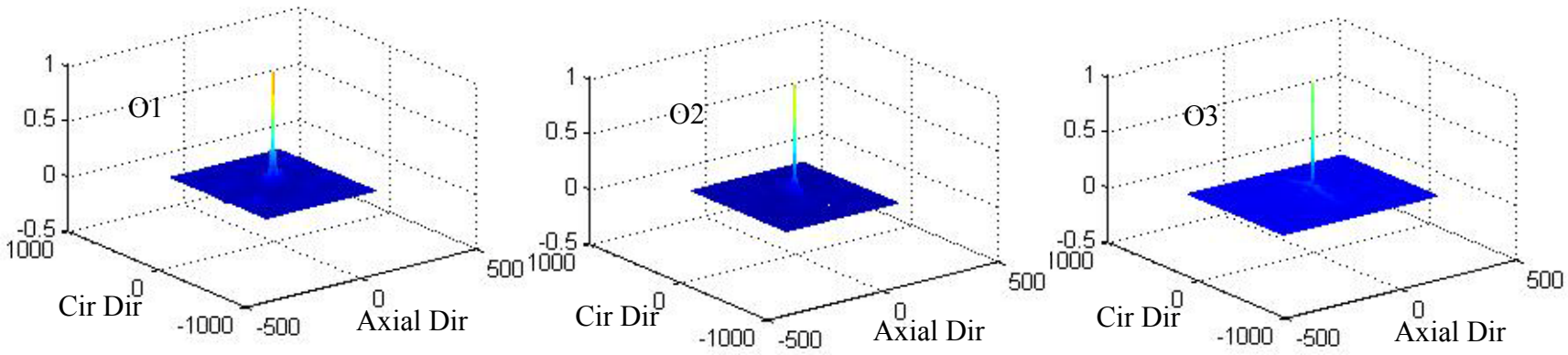

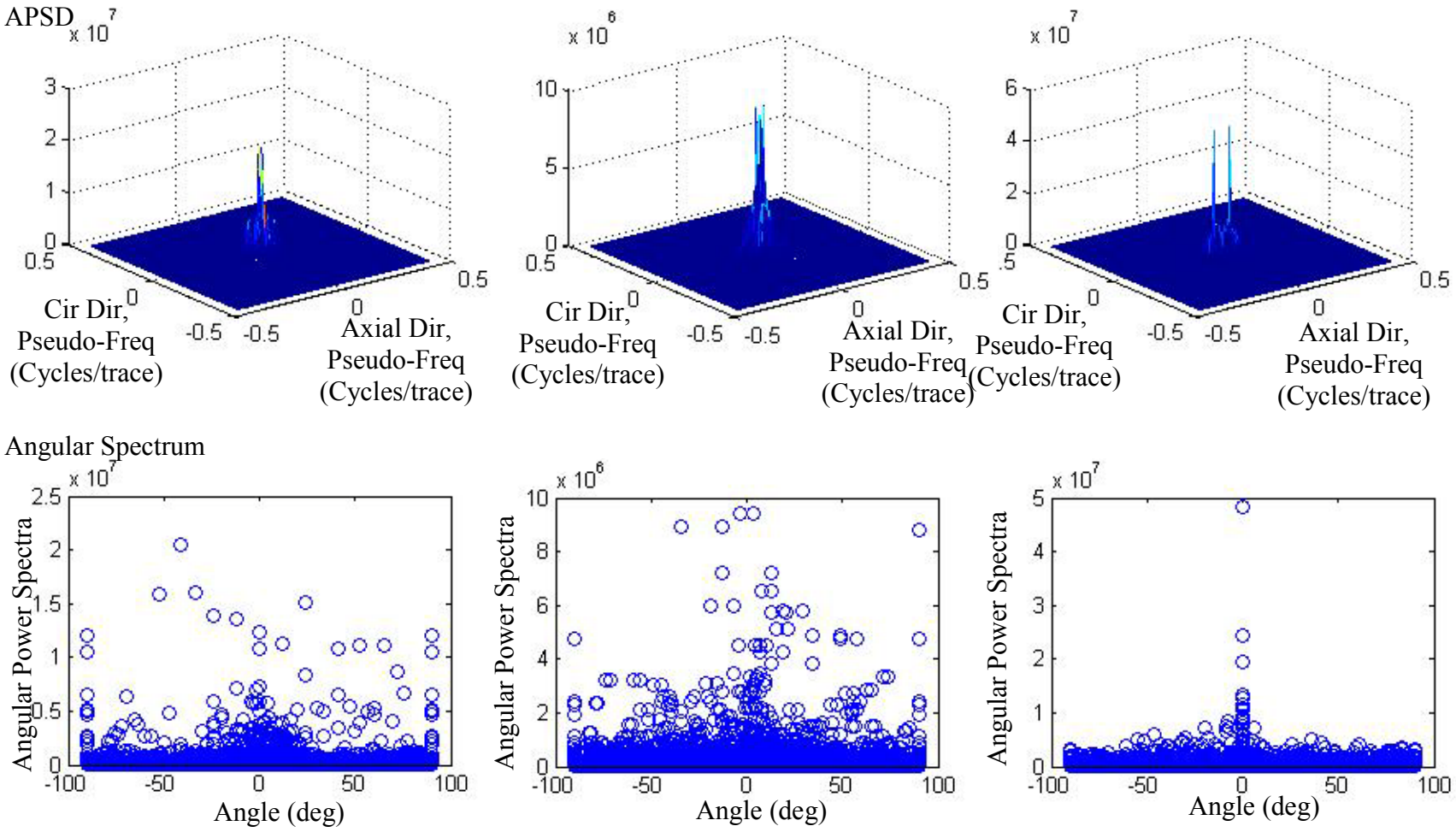

Figure 30 – AACF, APSD, Angular Spectrum of Elastomers

Ran Against Triangular Cavities Oriented Towards Oil

Figure 30 shows the AACF, APSD and Angular Spectrum of elastomers ran against triangular cavities oriented towards oil. AACF of elastomers O1 and O2 decays rapidly along all direction. The AACF of elastomer O3 decays faster along the axial direction and decays slower, indicating a slight correlation along the circumferential direction. The APSD energy of the elastomers O2 and O3 are grouped together around the origin in a circular fashion indicating the surface is isotropic. The APSD of elastomer O3 shows the sealing zone is directional and the angular spectrum indicates the surface texture direction is along the circumferential direction.

4.7.3 Elastomers Ran Against Triangular Cavities Oriented Towards Air

AACF

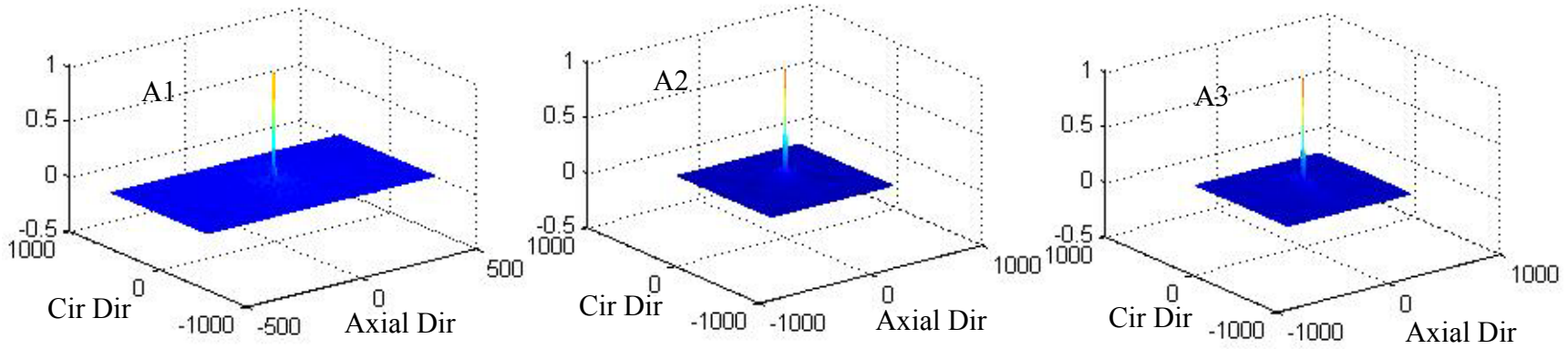

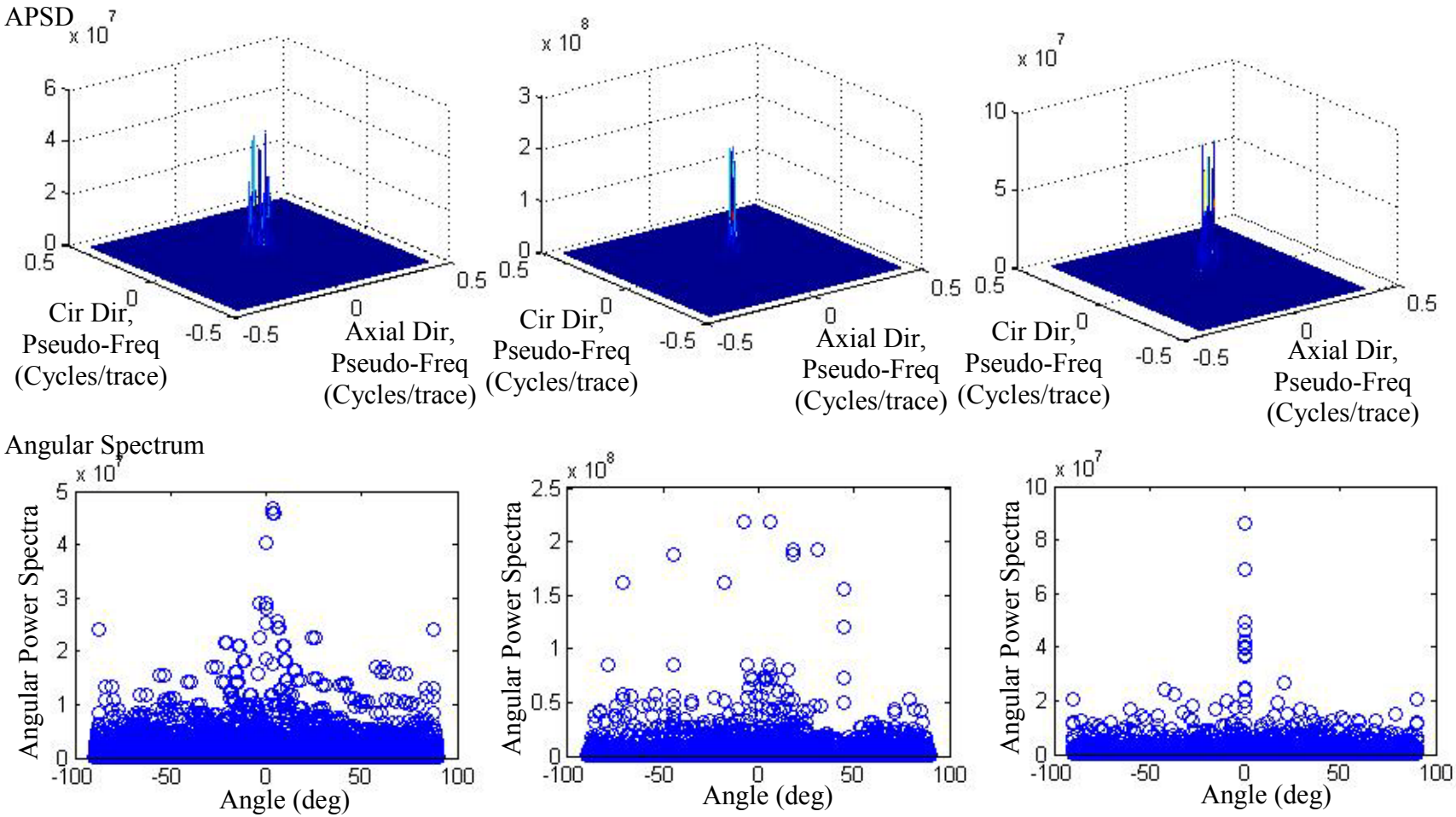

Figure 31 – AACF, APSD, Angular Spectrum of Elastomers

Ran Against Triangular Cavities Oriented Towards Air

Figure 31 shows the AACF, APSD and Angular Spectrum of elastomers ran against triangular cavities oriented towards air. The AACF of the elastomers A1, A2 and A3 are similar to that of O1, O2 and O3. There is no correlation of the data along the axial direction and the correlation along the circumferential direction increases as the duration of operation increases. Even though the AACF of lip seals O1, O2, O3 and A1, A2, A3 are similar, the lip seals O1, O2, O3 forward pumped and lip seals A1, A2, A3 reverse pumped. This clearly shows the deterministic triangular micro-cavities manufactured on the shaft surface play a significant role in the lip seal pumping direction.

From APSD and angular spectrum plots, the sealing zone of the lip seal elastomer becomes directional along the circumferential direction as the operation time progresses.

4.7.4 Elastomers Ran Against Triangular Cavities Lagging

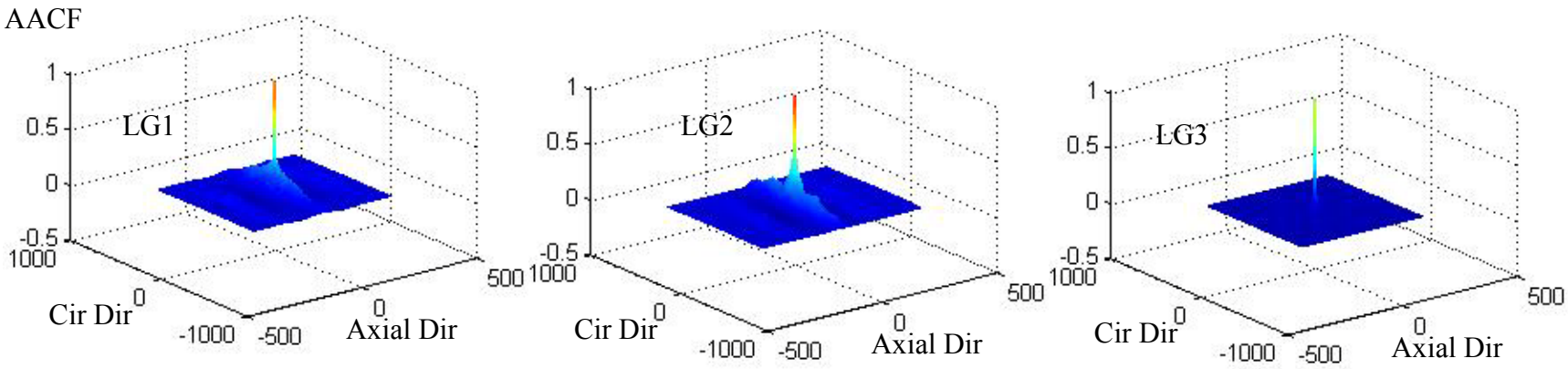

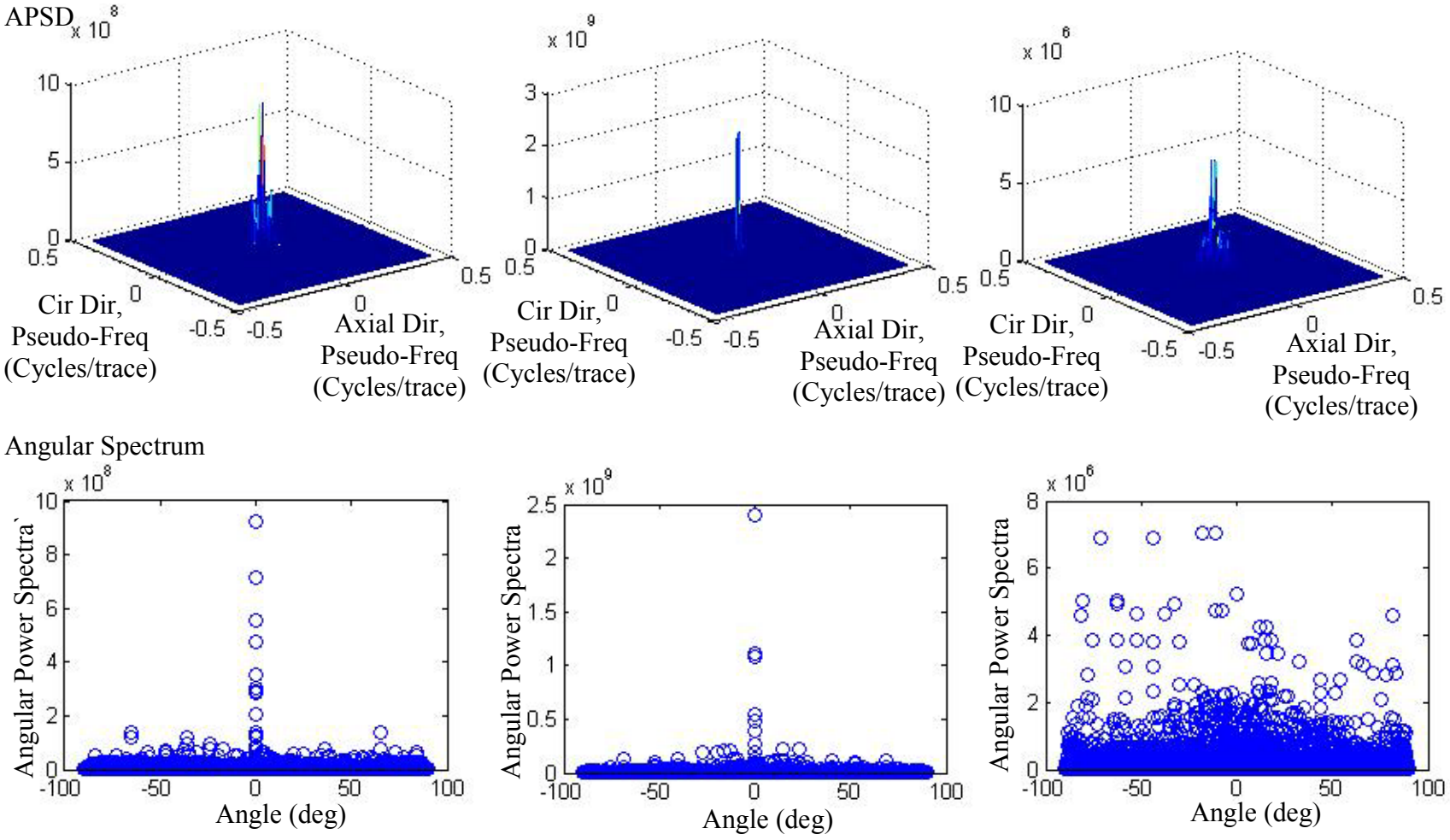

Figure 32 – AACF, APSD, Angular Spectrum of Elastomers

Ran Against Triangular Cavities Lagging

Figure 32 shows the AACF, APSD and Angular Spectrum of elastomers ran against triangular cavities lagging. The AACF decays slowly along the circumferential direction indicating correlation of data along the axial direction. The AACF decays rapidly along the axial direction but it oscillates about the mean plane before it completely dies out. This is due to the grooves (microundulation) present in the elastomer sealing zone along the circumferential direction.

4.7.5 Elastomers Ran Against Triangular Cavities Leading

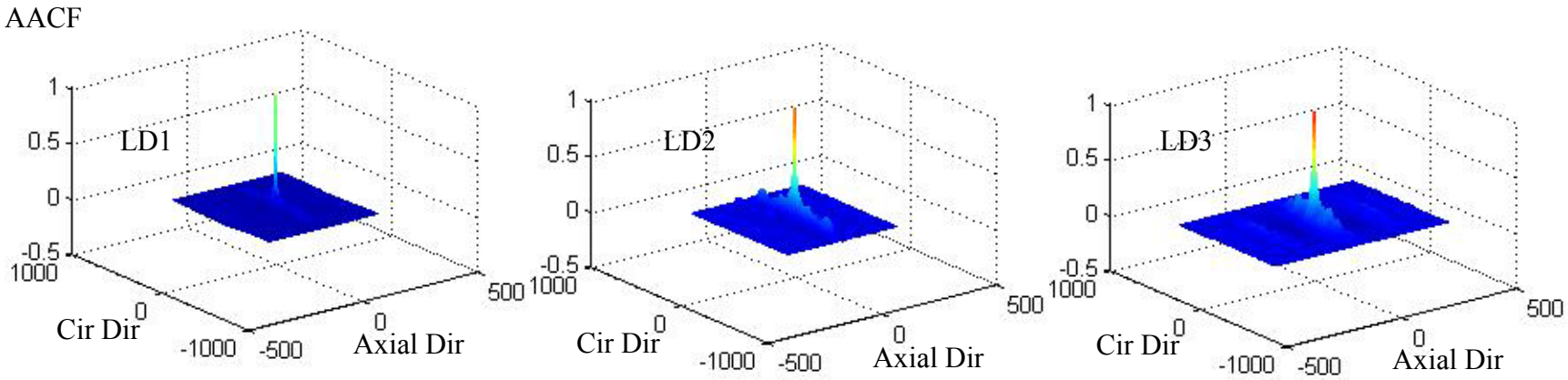

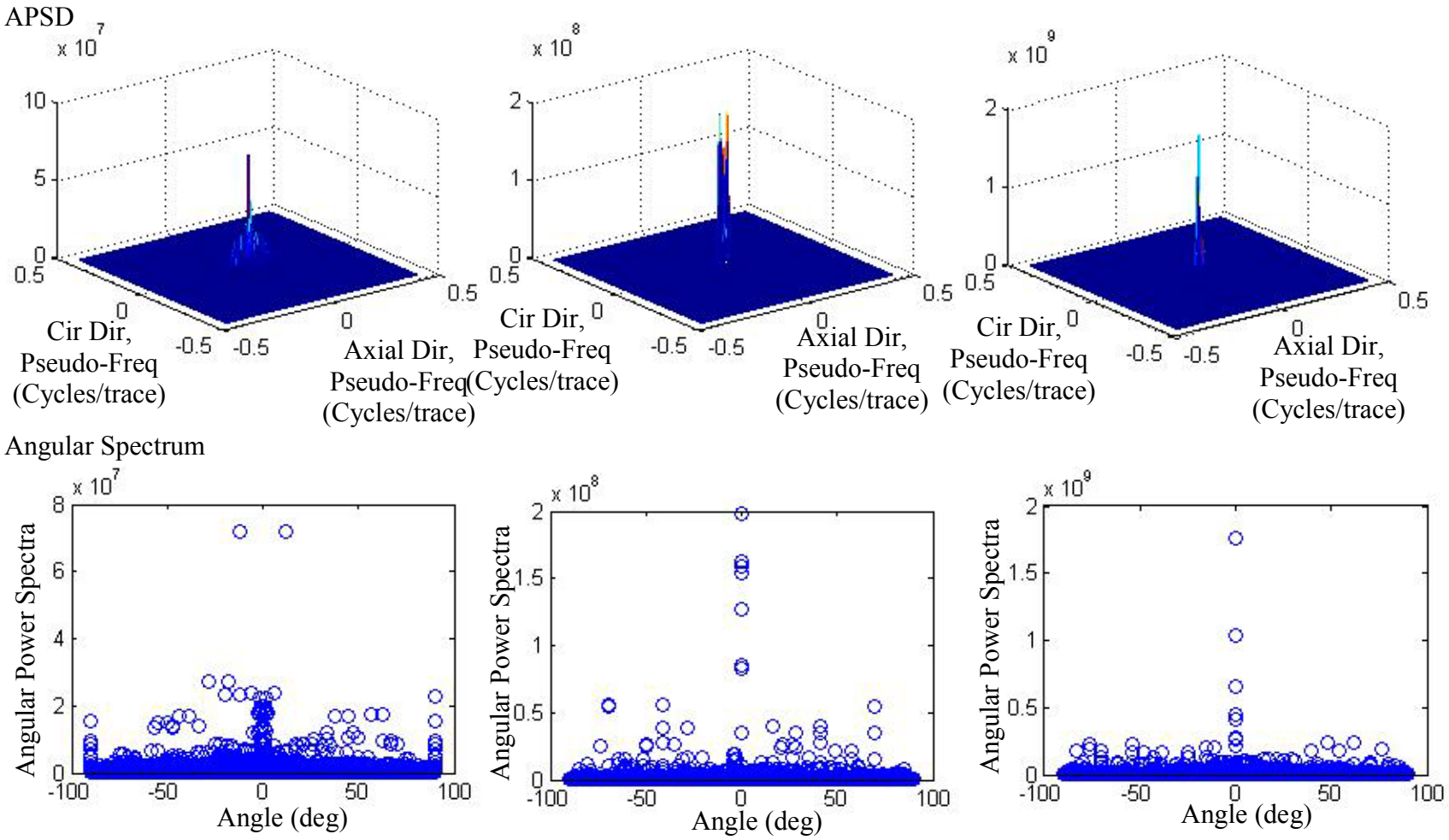

Figure 33 – AACF, APSD, Angular Spectrum of Elastomers

Ran Against Triangular Cavities Leading

Figure 33 shows the AACF, APSD and Angular Spectrum of elastomers ran against triangular cavities leading. The AACF of the elastomers 12a, 17 and 39 are similar to that of 11a, 14, 18. These lip seal elastomers ran against different patterns of deterministic triangular cavities manufactured on the shaft surface and they reverse pumped. Even though they have similar AACF, these lip seals have different pumping rates. This indicates the deterministic triangular cavities lagging and leading manufactured on shaft surface does not result in complete change in the pumping direction but the orientation of the triangular cavities lead to different pumping rates.

The elastomers which ran against shafts manufactured with triangular cavities lagging and leading, the main energy of APSD is concentrated along the direction perpendicular to the circumferential direction. There are several frequency components present which indicates the surface is directional along the circumference and it is not periodic. From the discussion of Birmingham 14 parameters in this chapter, the surface parameters: root mean square roughness, skewness, kurtosis, areal auto correlation function, areal power spectral density and angular spectrum were particularly useful in desscribing the elastomer surface topography.

4.8 CORRELATION – SHAFT AND ELASTOMER SURFACE PARAMETERS

The surface parameters for both the lip seal elastomer and shaft are calculated after testing. The lip seal elastomers were ran against 5 different patterns of shaft. Within each pattern, three shafts were tested. Within each shaft, the surface parameters are computed on the shaft wear track at four different locations around the circumference of the shaft. These surface parameters are obtained from Birmingham 14 parameters. The average and standard deviation values of the surface parameters on shaft wear track are given in Appendix 1. Table 2 shows the correlation coefficient between the shaft surface parameters and elastomer surface parameters.

Table 2 – Correlation between elastomer and shaft surface parameters

ELASTOMER

SHAFT FINAL WEAR TRACK

	Sq	**Ssk**	**Sku**	**Svi**	**Sbi**	**Sci**	**Sdq**	**Sds**	**Ssc**	**Sz**	**Sdr**
Sq	0.55	-0.12	-0.05	-0.02	0.34	-0.35	0.40	-0.46	0.25	0.57	0.32
Ssk	-0.18	-0.02	-0.03	-0.20	0.01	-0.02	-0.27	-0.20	-0.22	-0.18	-0.27
Sku	-0.28	0.10	0.07	-0.01	-0.24	0.26	-0.16	0.40	-0.08	-0.30	-0.10
Svi	-0.17	0.03	0.02	0.20	-0.15	0.16	-0.08	0.23	-0.11	-0.21	-0.09
Sbi	0.64	-0.01	-0.12	0.16	0.20	-0.21	0.61	-0.22	0.47	0.64	0.55
Sci	-0.51	0.12	0.02	-0.24	-0.27	0.31	-0.47	0.16	-0.32	-0.52	-0.40
Sdq	0.46	-0.15	0.00	0.15	0.27	-0.31	0.34	-0.33	0.23	0.52	0.28
Sds	-0.07	0.02	0.20	0.19	-0.05	0.04	0.04	0.28	0.04	-0.01	0.06
Ssc	0.23	-0.03	-0.01	0.25	0.11	-0.12	0.23	-0.12	0.19	0.28	0.20
Sz	0.25	-0.20	0.06	0.05	0.23	-0.26	0.17	-0.24	0.11	0.28	0.14
Sdr	0.48	-0.11	0.01	0.09	0.24	-0.27	0.37	-0.31	0.27	0.56	0.32

Even though the shaft surface characteristics play an important role in the formation of micro-asperities on the lip seal elastomer and in the operation of lip seal, there is not significant correlation between the final surface parameters of the shaft and elastomer. This indicates that there are other phenomenon's and parameters such as the thin lubricating film that exists between the elastomer and shaft, temperature at the shaft and seal interface, deformation of the elastomer sealing zone in axial and circumferential direction, properties of elastomer which are simultaneously involved in the development of lip seal elastomer sealing zone rather than the shaft surface characteristics alone.

CHAPTER 5 – RESULTS AND DISCUSSION

The lip seals were tested against five different patterns on the shaft. Previously research has been conducted in lip seal elastomers running against stainless steel shafts. Horve [2] conducted experiments of lip seal elastomers running against plain stainless steel shafts. He has given a range of lip seal sealing zone widths when lip seal operated for certain duration of time. Figure 34 shows the sealing zone width of the lip seal elastomers which ran against plain stainless steel shafts. These sealing zone widths fall under the range suggested by Horve. In the lip seal elastomers tested in this study, the sealing zone width increases as the duration of operation increases. It also seen that the width of the sealing zone varies over the circumferential direction of the lip seal elastomer.

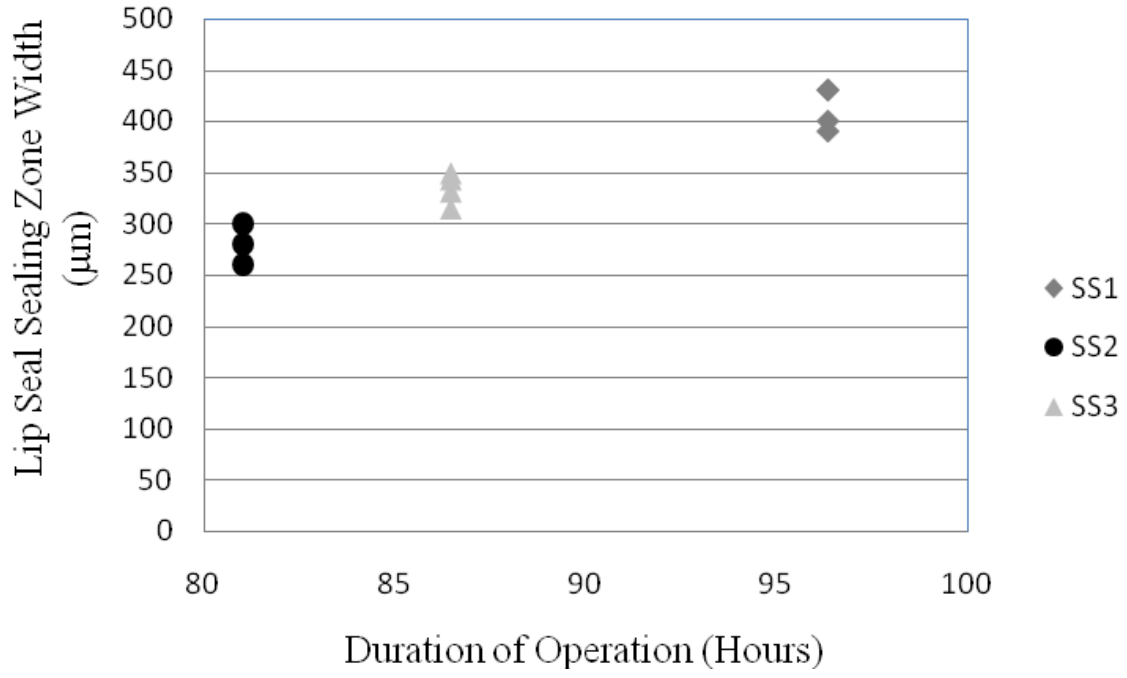

Figure 34 – Sealing Zone Width of Elastomers which ran against Stainless Steel Shafts

The sealing zone width gives an estimation of the width of the lubricant film present between the lip seal elastomer and shaft. The sealing zone width of the lip seal elastomers which ran against shafts manufactured with deterministic triangular micro-cavities are shown in Figure 35.

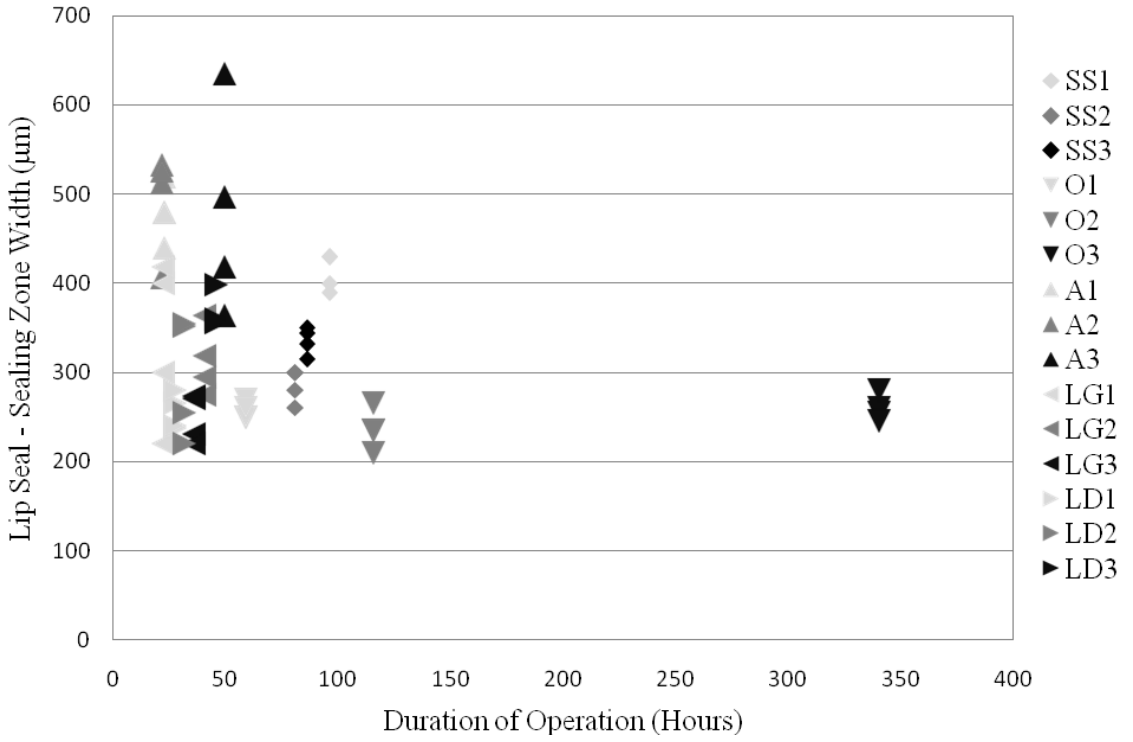

Figure 35 – Sealing Zone Width of Lip Seal Elastomer

From each lip seal elastomer four samples were analyzed at four different locations along the circumference of the seal. The width of the elastomer sealing zone does not remain constant along the circumference. Gawlinski and Kasprzyk [24] studied the influence of shaft surface roughness on the wear of the lip seal sealing zone. They found that the relative position of contact region along the sealing edge can vary over the lip

circumference within two or three contact widths. This variation in contact position along the sealing edge can change the contact pressure distribution and there by altering the lip seal elastomer wear rate. Hence the wear rate of the elastomer does not remain constant along the circumference of the seal.

The lip seal elastomers which ran against plain stainless steel shafts and against shafts manufactured with deterministic triangular cavities oriented towards the oil side had little variation of the sealing zone width among the four samples with a standard deviation of 18.34 μm and 15.6 μm respectively. Whereas the lip seal elastomers which ran against deterministic triangular cavities oriented towards the air side, triangular cavities lagging and triangular cavities leading, the sealing zone width of the lip seal elastomers varied more among the four samples analyzed with standard deviations of 69.82 μm, 52.64 μm, and 36.34 μm respectively.

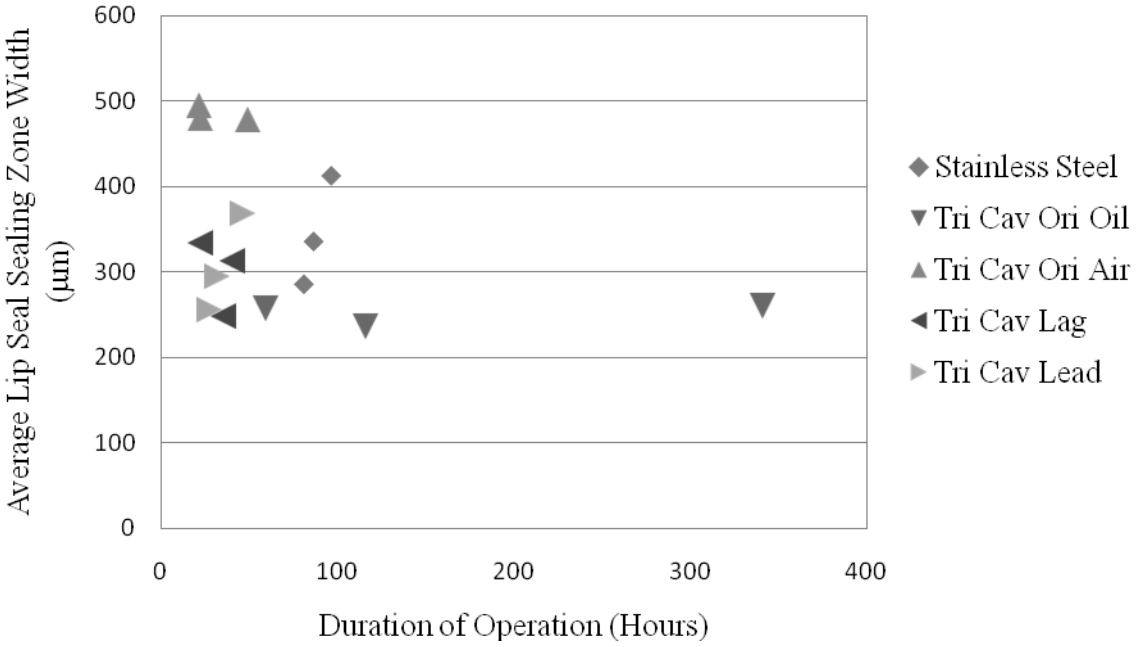

Figure 36 – Average Sealing Zone Width of Lip Seal Elastomer

Figure 36 shows the average sealing zone width of the four samples obtained from each lip seal elastomer. The lip seal elastomers which ran against deterministic triangular cavities oriented towards the oil side have almost constant sealing zone widths even though these lip seal elastomers ran for different hours of operation. These seals forward pumped and during forward pumping there is a constant film of lubricant present between the lip seal elastomer and the shaft. This reduces the wear to minimum. The sealing zone width of the lip seal elastomers which ran against shafts manufactured with deterministic triangular cavities leading have the same slope as the lip seal elastomers which ran against stainless steel shafts. The sealing zone width of the lip seal elastomers which ran against triangular cavities lagging are grouped together without any significant variation. The sealing zone width of the lip seal elastomers which ran against shafts manufactured with triangular cavities oriented towards the air side remained almost constant as the direction of operation increases, even though these lip seals reverse pumped. On the whole, the elastomer sealing zone width is lowest for the lip seals which forward pumped and highest for the lip seals which reverse pumped.

Table 3 shows the wear track width of the surface textured shafts. After testing and uninstalling, relaxation occurs in the lip seal elastomers. This is inferred by comparing the wear track widths of the shaft and the seal. For all the elastomers ran against different surface textured shafts, the wear track width of the shaft is always greater than that of elastomer.

Table 3 – Shaft Wear Track Widths [19]

Shaft Surface	Wear Track Width (μm)
Triangular Cavities Oriented towards Oil	674±200
Triangular Cavities Oriented towards Air	1024±31
Triangular Cavities Lagging	811±124
Triangular Cavities Leading	829±158

Table 4 shows the average sealing pressure and scaled sealing pressure. Scaled sealing pressure is calculated excluding the area formed by the triangular cavities assuming the elastomer sealing zone comes in contact with the area surrounding the triangular cavities. The asperity area fraction, which is defined as the ratio of area of asperity to that of unit cell is 0.24 and the force of spring is 83.21 N/m.

Table 4 – Average Sealing Pressure

Seal	Average Sealing Pressure (kPa)	Scaled Average Sealing Pressure (kPa)
SS	247.3	325.4
O	331.8	436.6
A	171.9	226.1
LG	282.9	372.2
LD	277.8	365.5

During dynamic conditions when the lip seal elastomer is running against the shaft there is hydrodynamic pressure distribution which deforms the elastomer in the radial direction and there is tangential deformation along the circumferential direction caused by the shear stresses. When the lip seal elastomer is uninstalled after testing, there is a curvature along the axial direction of the elastomer sealing zone in a direction opposite to the deformation of the elastomer sealing zone during dynamic conditions. A Fast Fourier Transform filter was used to remove the longer wavelength in the elastomer sealing zone

leaving behind the roughness measurements alone. The tested elastomers have a mean wavelength of 34.84 μm with a standard deviation of 8.88 μm. The sealing zone width of the lip seal elastomer and the corresponding filter cutoff wavelength is shown in Figure 37.

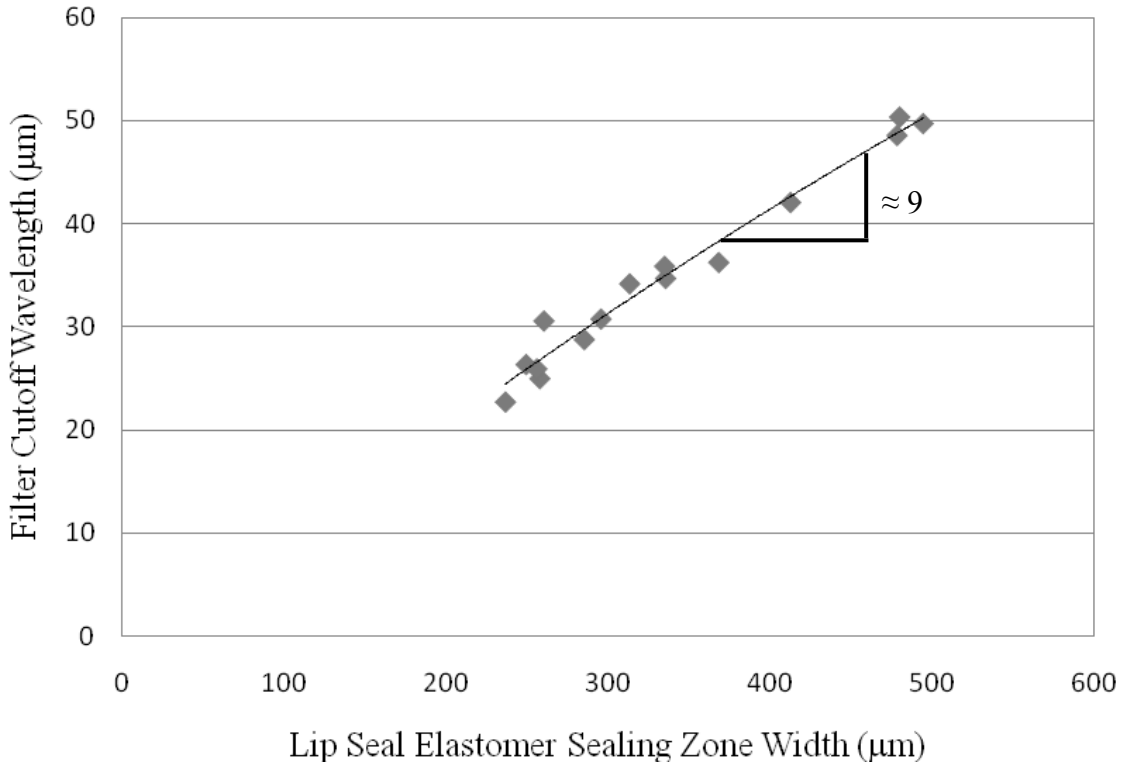

Figure 37 – Sealing Zone Filter Cutoff Wavelength of Elastomers

It can be seen that the sealing zone width of the lip seal elastomer is approximately 9 times the filter cutoff wavelength. From this study and from the previous research conducted by Horve [13], the sealing zone width of the elastomer increases as the duration of operation increases. As seen in Figure 37, as the sealing zone width of the elastomer increases, the filter cutoff wavelength increases. It can be inferred that as the lip seal elastomer sealing zone width increases, the curvature of the elastomer sealing

zone along the axial direction decreases. It is known that [9] the hydrodynamic pressure distribution on the edges of the elastomer sealing zone is low compared to the middle. Therefore under dynamic conditions, there is more radial deformation in the middle portion of the elastomer sealing zone when compared to the edges. The greater interaction between the shaft and the elastomer on the edges of the sealing zone results in greater wear at the edges. Loss of lip seal elastomer due to wear leads to changes in contact width of the elastomer and the pressure distribution. This wearing away of the edges without changing much of the middle portion of the elastomer sealing zone causes the middle portion of the sealing zone to form a curvature when it is uninstalled. In brief it can be concluded from the filter cutoff wavelength and the variation of roughness along the axial direction, as the time progresses, the shaft wears the elastomer sealing zone at the edges and causes the sealing zone of the elastomer to deform more along the radial direction. The root mean square roughness values along the axial direction of the lip seal may be used to predict the deformation of lip seal elastomer sealing zone in the radial direction.

Figures 38 shows the scanning electron microscope images of the lip seal elastomer sealing zone which ran against different patterns of shaft surface. The air and oil sides of the sealing zone are shown in the figure. The seal label and corresponding hours of operation are indicated on the bottom right corner of each image. From visual observations, in the case of the lip seal elastomer which ran against stainless steel shafts, the number of micro-asperities and micro-cavities are higher for seal SS2 and lower for seal SS1. It can be seen that as the duration of operation increases, the sealing zone becomes relatively smooth.

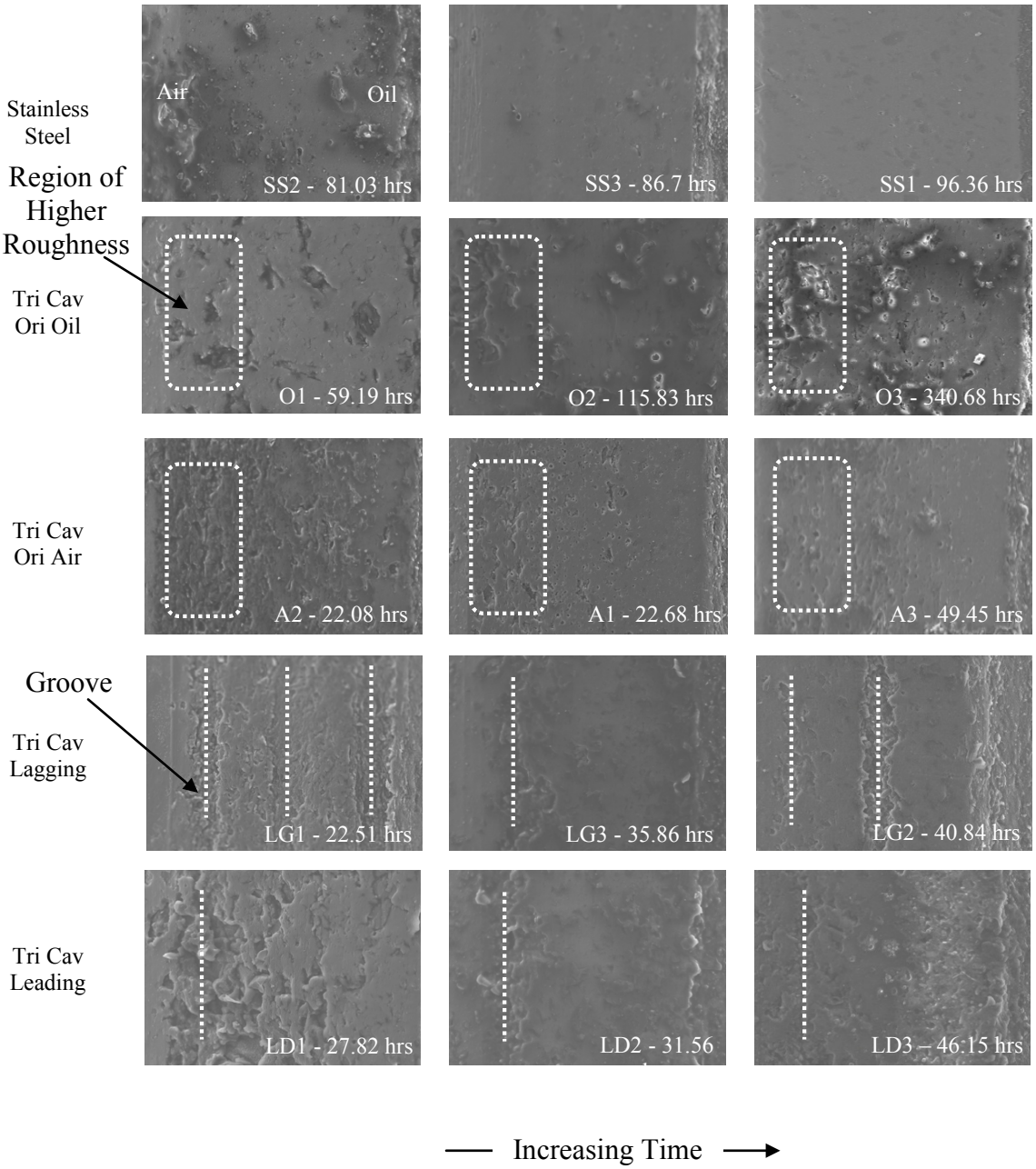

Figure 38 – Scanning Electron Microscope Images of Lip Seal Elastomer Wear Track

Horve [2] conducted experiments of lip seals against stainless steel shafts and has given the scanning electron microscope images of the lip seal elastomer sealing zone. Qualitatively the lip seal wear track images from the present study agree with the work done by Horve. The lip seal elastomer which ran against triangular cavities oriented

towards the oil side and those which ran against triangular cavities oriented towards the air side have their air side rough when compared to the oil side of the sealing zone as indicated by the dashed boxes. In other words, the air side of the sealing zone has greater number micro-asperities and micro-cavities when compared to the oil side. In the lip seal elastomer which ran against triangular cavities lagging and leading, the samples have grooves / microundulations in the sealing zone along the circumferential direction as indicated by dashed lines. These grooves / microundulations have micro-asperities and micro-cavities in addition to the micro-asperities and micro-cavities present on the ridges of the sealing zone. The number of grooves present in the sealing zone varies along the circumferential direction.

After making measurements in zygo and exporting to Matlab, the profile plots of the sealing zone along the axial direction are obtained by averaging the measurements along the circumferential direction. The profile plots of the lip seal elastomer sealing zone are shown in Figure 39. In the lip seal elastomers which ran against stainless steel shafts, the sealing zone is found to be smooth in the middle and rough on the edges which indicated by circles in the figure. All the tested lip seal elastomers (which ran against stainless steel shaft, triangular cavities oriented towards the oil side and air side) exhibit the largest micro-asperities along the air side and oil side edges of the sealing zone with relatively small asperities distributed evenly in the middle of the sealing zone. Whereas the lip seal elastomers which ran against triangular cavities lagging and leading exhibited largest micro-asperities along the edges and grooves of the sealing zone. Overall within all the

tested lip seal elastomers, the height of the asperities varies between 0 to 0.5 μm with the largest on the edges.

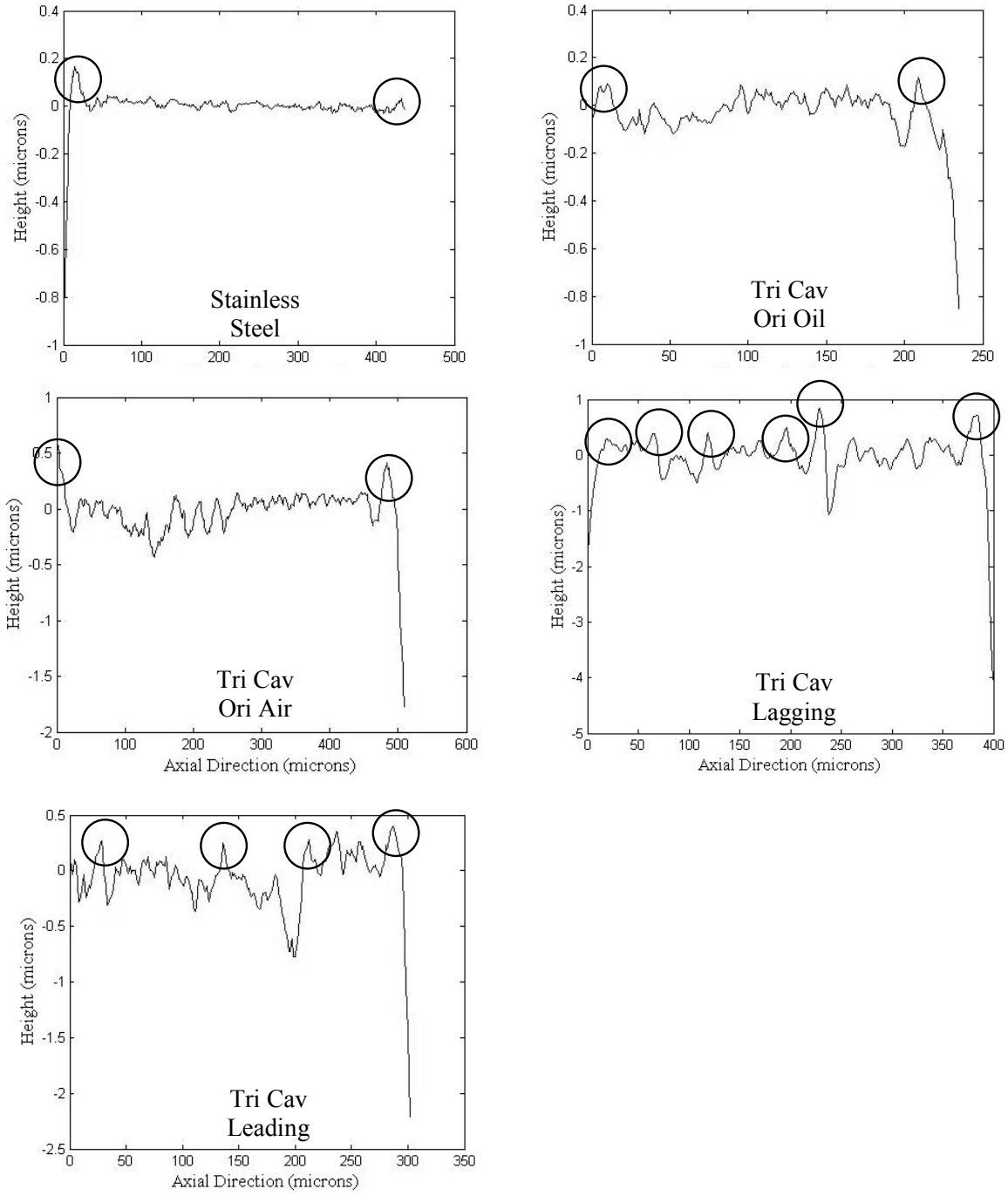

Figure 39 – Profile Plots of Lip Seal Elastomer Sealing Zone

This may be because the hydrodynamic pressure distribution along the axial direction of the sealing zone is lowest at the edges, causing lower film thickness and more contact between the elastomer and shaft. Before applying the Fast Fourier Transform (FFT) filter to the sealing zone of the lip seal elastomer, the average roughness (Ra) is 1.03 μm. This value agrees with the previous work done by Paige [1] and it is close to 1.27 μm obtained by Jagger and Walker [15].

The sealing zone of the lip seal elastomer is divided along the axial direction into a number of thins strips along the circumferential direction. The root mean square roughness is measured along the axial direction by moving the strip from the air side to the oil side. Figure 40 shows the root mean square roughness along the axial direction for four samples from the seals which ran against stainless steel shafts.

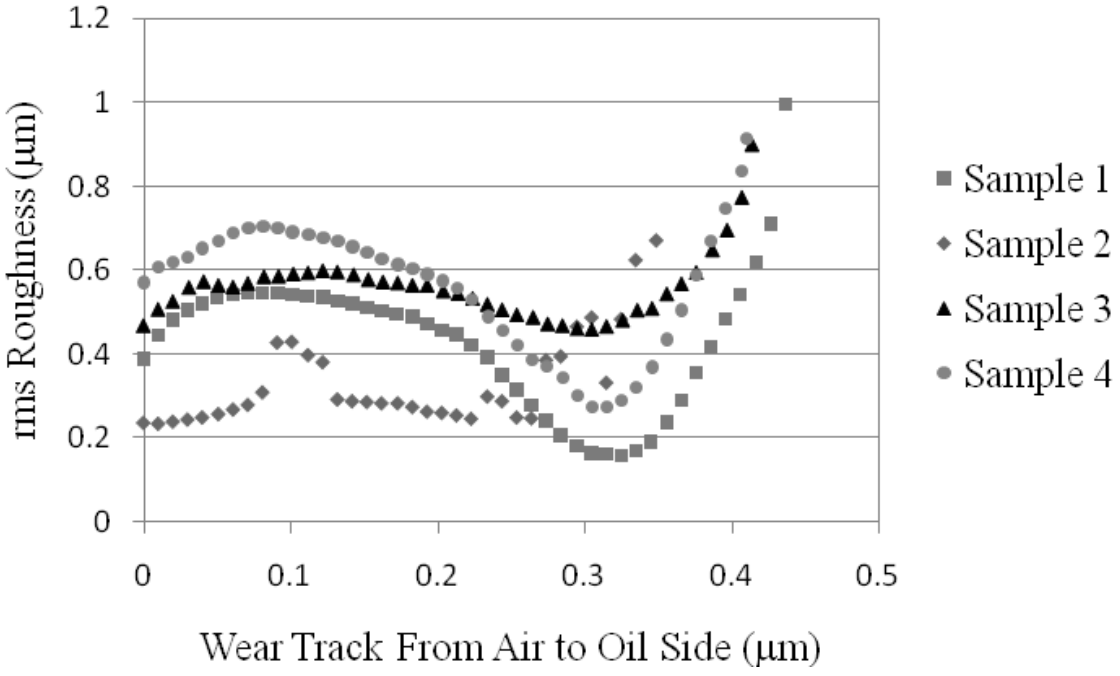

Figure 40 – Roughness Variation from Air to Oil Side of Elastomer Sealing Zone

The continuous variation of root mean square roughness along the axial direction indicates that the thickness of the liquid film which separates the lip seal elastomer from the shaft varies along the axial direction during lip seal operation. In the seals which reverse pumped, there is a drop in the root mean square roughness of the elastomer sealing zone closer towards the oil side. This may be due to the high pressure distribution and shear deformation near the oil side of the elastomer sealing zone for the seals which reverse pumped. Figure 41 shows the axial location in the lip seal sealing zone where the root mean square roughness is minimum. 0 % and 100 % represents the location of the air and oil side edge of the elastomer sealing zone respectively.

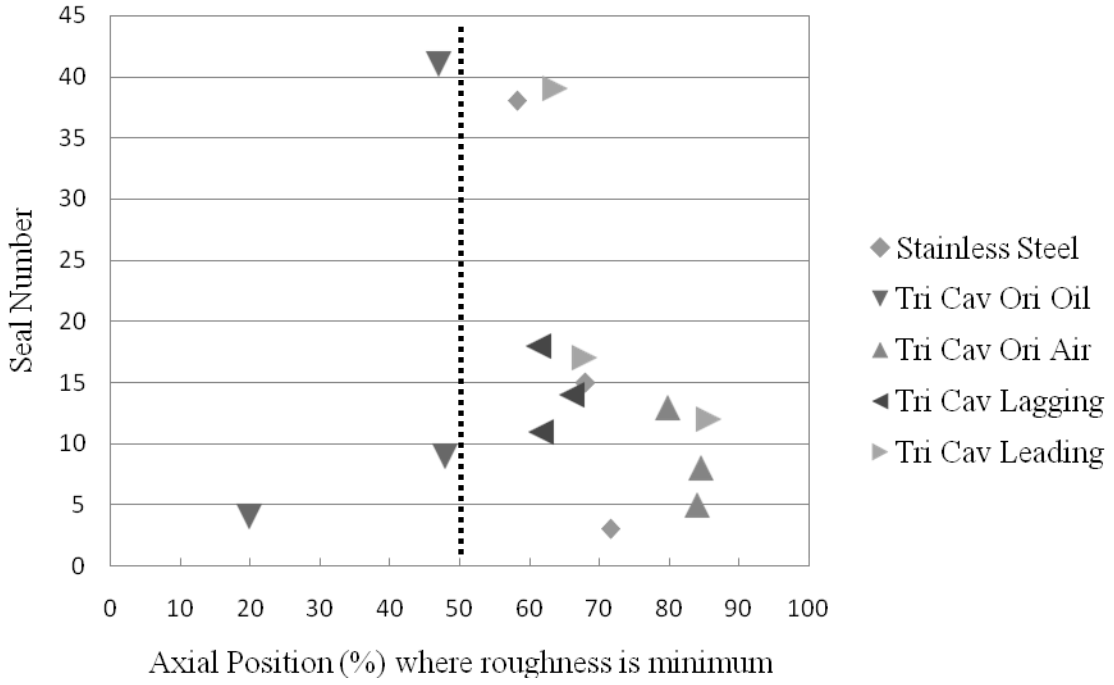

Figure 41 – Axial Position of Minimum Roughness in the Elastomer Sealing Zone

The lip seals which forward pumped (seals ran against triangular cavities towards the oil side) have minimum root mean square roughness at an axial location of less than 50 % which is closer to the air side of the seal. All other lip seals which reverse pumped have

minimum roughness at an axial location greater than 50 % which is closer to the oil side. The lip seal elastomers which ran against different patterns of shaft have minimum roughness at different locations in the sealing zone. The deterministic triangular micro-cavities and their orientation may deform the sealing zone of the lip seal elastomer differently under dynamic conditions.

The axial location on the sealing zone of the lip seal elastomer where the roughness is minimum and the corresponding pumping rates are given in Table 5.

Table 5 – Elastomer Axial Position of Minimum Roughness and Pumping Rates

Description	Axial Position of Minimum Roughness (%) ± Std. Dev.	Minimum Roughness 95% Confidence (%)	Pumping Rate (mL/hr) ± Std. Dev. (1000 rpm) @ $T = T_{final}$	Pumping Rate 95% Confidence (mL/hr)	Correlation Coefficient
Stainless Steel	71.6±5.1	63.5-79.7	-7.3±1.9	-8.5 – -6.1	- 0.98
	68.1±3.3	62.8-73.4	6.6±0.5	-6.9 – -6.3	
	58.2±4.6	50.9-65.5	5.6±0.9	-6.1 – -5.1	
Triangular Cavities Oriented Oil	19.9±12.4	0.2-39.6	4.5±0.4	0.9 – 8.1	- 0.99
	46.9±4.1	40.4-53.4	1.4±0.6	0.4 – 2.4	
	47.8±12.4	28.1-67.5	1.2±0.3	-1.5 – 3.9	
			Pumping Rate (mL/hr) (750 rpm) @ $T = T_{final}$		
Triangular Cavities Oriented Air	84.5±8.1	71.6-97.4	14.3±1.1	-16.1 – -12.5	- 0.66
	84.0±8.1	71.1-96.9	6.8±1.9	-11.5 – -2.1	
	79.7±8.1	66.8-92.6	5.8±0.2	-6.1 – -5.5	
Triangular Cavities Lagging	66.0±11.2	48.2-83.8	11.3±0.3	-11.8 – -10.8	0.69
	61.7±11	44.2-79.2	14.3±3.0	-19.1 – -9.5	
	61.3±15.3	37.0-85.6	28.3±5.2	-36.6 – -20	
Triangular Cavities Leading	85.7±10.6	68.8-100.0	6.0±0.7	-7.1 – -4.9	0.99
	67.9±7.1	56.6-79.2	10.3±0.6	-11.3 – -9.3	
	63.7±10.2	47.5-79.9	10.7±0.5	-11.5 – -9.9	

Three seals were tested against each pattern of shaft and four samples were analyzed within each seal. The axial position of minimum roughness measurements given in Table 5 were averages obtained from the four samples. This is a small sample size so the 95% confidence interval is computed and given in Table 5. The 95% confidence interval for a small sample size is given by the formula:

$$x = x \pm \frac{t_{\nu,P} \times S}{\sqrt{n}}$$

Where S is the standard deviation, n is the number of samples, ν is the degrees of freedom = n-1. The value of tν, P is obtained from the Student-t distribution based on the degrees of freedom and probability, P%. The seals which ran against stainless steel shafts have minimum roughness near the oil side of the seal. As the axial location of minimum roughness moves closer towards the oil side of the seal, the lip seals pump more amount of lubricant from the air side to the oil side, in other words the reverse pumping rate increases. For the reverse pumping SS seals, the correlation coefficient between the axial location of minimum roughness and pumping rate is -0.98. Seals which ran against triangular cavities oriented towards the oil side forward pumped. As the location of minimum roughness moves closer towards the air side of the seal, the lip seals pump more amount of lubricant from the oil side to the air side, in other words the forward pumping rate increases. The correlation coefficient is negative because the pumping rate of these seals increases as the axial position of minimum roughness decreases. The observations for the seals which ran against stainless steel shafts were also seen for the seals which ran against shafts fabricated with triangular cavities oriented towards the air side. Seals ran against triangular cavities lagging and triangular cavities leading reverse

pumped and they have minimum roughness at an axial location greater than 50 % of the sealing zone. The reverse pumping rates of these seals were high when the axial location of minimum roughness is closer to 60% of the sealing zone from the air side.

The variation of roughness along the axial direction of the sealing zone is shown in Figure 40. Salant [9] conducted numerical analysis of lip seals and concluded that in a reverse pumping seal, the maximum circumferential displacement occurs at an axial location closer to the oil side of the elastomer. Similarly the position of minimum roughness is closer towards the oil side for the seals which reverse pumped. When the position of minimum roughness is closer to the oil side, the amount of lubricant pumped from the air side to the oil side is greater than the amount of lubricant pumped from the oil side to the air side. This results in flow of lubricant against the leakage through the seal. Hence, the seals which have minimum roughness closer towards the oil side of the seal reverse pumped. When the position of minimum roughness is closer towards the air side, the amount of lubricant pumped from the oil side to the air side is greater than the amount of lubricant pumped from the air side to the oil side. This results in the leakage of lubricant. Hence, the seals which have minimum roughness closer towards the air side of the seal forward pumped.

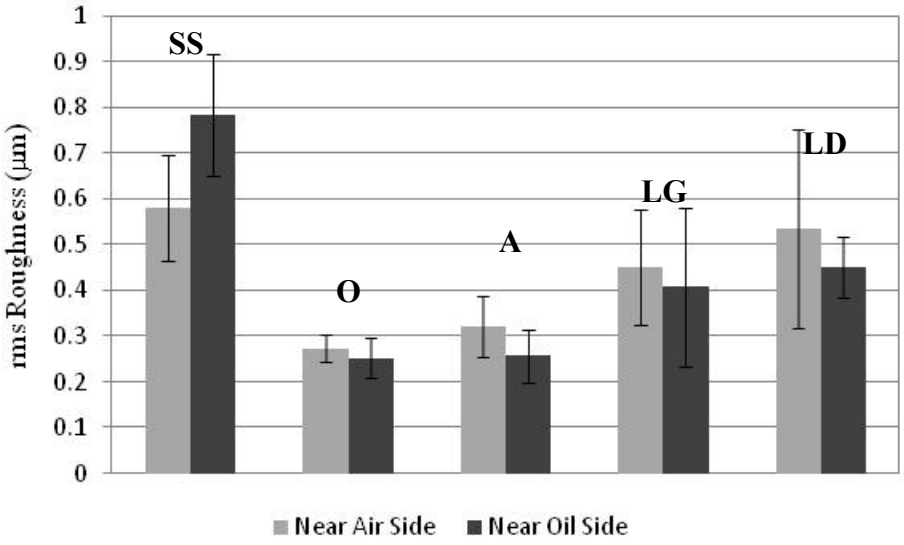

Figure 42 – rms Roughness near Air and Oil Side of the Elastomer

Figure 42 shows the roughness at the air side and oil side of the elastomer sealing zone. Seals which ran against stainless steel shafts have high roughness near the oil side the sealing zone and these seals reverse pumped. This indicates high density of contact between the seal and the shaft near the oil side of the sealing zone. Previously Nakamura and Kawahara [11] and Paige [1] conducted experiments of lip seals running against stainless steel shafts. They observed that the lip seal elastomers which reverse pumped exhibited higher rms roughness value near the oil side of the sealing zone and those lip seal elastomers which forward pumped had higher rms roughness value in the sealing zone other than the oil side. These results agree with those of stainless steel seals in this work and support the statement that reverse pumping depends on the size and location of micro-asperities within the sealing zone of the elastomer [11]. The lip seal elastomers (O, A, LG, LD) which ran against shafts manufactured with deterministic micro-cavities have higher rms roughness near the air side of the sealing zone as shown in Figure 26. Based upon the results from previous research done by Nakamura and Kawahara and Paige, the

seals O, A, LG and LD should forward pump. This agrees with the lip seal elastomers which ran against shafts manufactured with deterministic triangular micro-cavities oriented towards the oil side. However, the elastomers which ran against shafts manufactured with triangular micro-cavities oriented to air side, micro-cavities lagging and leading, were found to reverse pump despite exhibiting higher rms roughness values near the air side of the elastomer sealing zone. This demonstrates that shaft surface features, if present, control how the elastomer sealing zone develops and dominates the pumping direction of the seal. Even with surface features present on the shaft surface, the pumping rate of the lip seal is significantly influenced by the surface features of both the shaft and the lip seal elastomer.

The apex of the lip seal elastomer wears to almost a flat surface of finite width after testing. In the tests conducted, the width of the elastomer sealing zone varied between 210 μm and 635 μm. Table 6 shows the reduction in length of the air side (A) and the oil side (B) measured from the scanning electron microscope (SEM) image. The ratio of reduction in length of the air side over the oil side is lowest for the lip seals which forward pumped (O1, O2 and O3). In these seals, there is almost equal amount of wear in both the air side and oil side of the lip seal elastomer. As the duration of operation increases, the ratio of reduction in the air side over the oil side decreases. This is because, initially when the seal is installed, the air side of the elastomer is in contact with the shaft surface. When the shaft starts rotating there is wear in the air side of the seal and the lubricant is pumped from the oil side to the air side. As the time progresses there is wear on the oil side of the elastomer. The correlation coefficient between the ratio of reduction length and the duration of operations for the forward pumping seals is -0.99. In the case

of all other seals which reverse pumped, the lubricant is pumped from the air side to the oil side and there is greater amount of wear on the air side of the seal when compared to the oil side. The seal LD2 has a high ratio of reduction length because the wear on the oil side of lip seal elastomer is very small when compared to the wear on the air side.

Table 6 – Air and Oil Side Wear of the Elastomer

Seal No.	Air Side Reduction (μm) – A	Oil Side Reduction (μm) – B	Ratio A/B	Duration of Operation (hours)
O3	0.30±0	0.209±0.06	1.45	340.78
O2	0.31±0.03	0.12±0.13	2.59	115.9
O1	0.41±0.24	0.159±0.04	2.64	59.2
LG3	0.4±0.07	0.129±0	3.14	35.9
LD3	0.32±0.04	0.098±0.13	3.30	46.2
SS3	0.35±0.01	0.097±0.11	3.59	86.5
SS1	0.81±0.07	0.136±0.06	5.95	96.4
LG2	0.54±0.07	0.081±0.01	6.70	40.9
A3	0.88±0.24	0.125±0.15	7.05	49.5
A2	0.79±0.03	0.089±0.06	8.94	22.1
LG1	0.79±0.07	0.087±0.09	9.06	22.5
LD1	0.61±0.04	0.061±0.06	10.15	27.8
SS2	0.70±0.04	0.045±0.02	15.58	81.0
A1	0.66±0.12	0.023±0.01	29.51	22.7
LD2	0.70±0.09	0.002±0.04	468.67	31.6

It is important to study the lip seal elastomer wear in order to improve the lip seal design and performance. The deterministic triangular micro-cavities manufactured on shaft surface may store lubricant during static conditions and make it available during startup. This may lead to reduction in wear of the lip seal elastomer during startup. Figure 43 shows the lip seal elastomer wear rate per circumferential length.

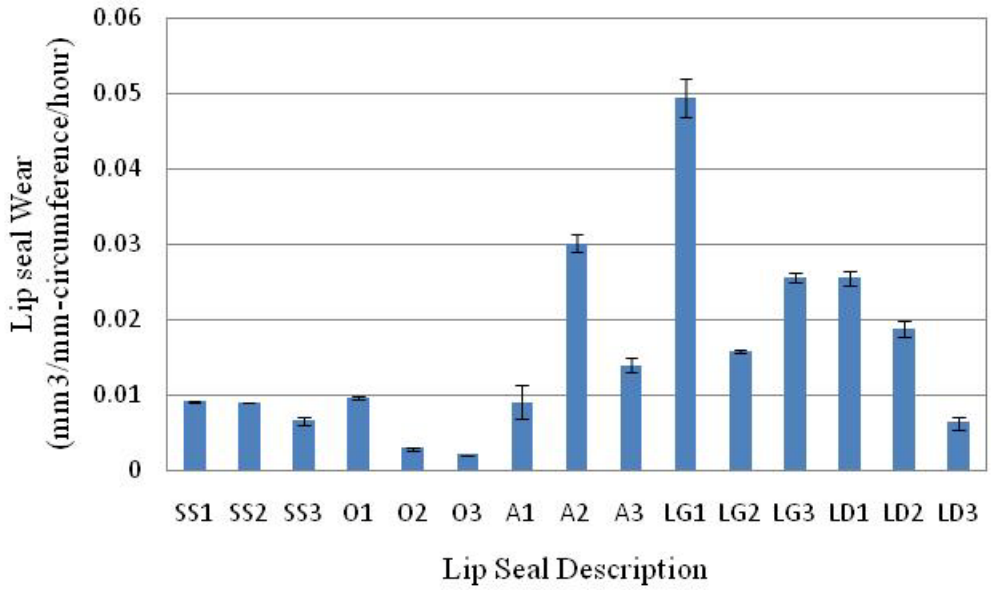

Figure 43 – Lip Seal Elastomer Wear

The wear rate of the elastomers which ran against shafts manufactured with triangular micro-cavities varies from the elastomers which ran against stainless steel shafts. Seals O2 and O3 which forward pumped have the lowest wear rate when compared to the other seals which reverse pumped. In the case of seals which forward pumped, there is constant film of lubricant present between the shaft and the elastomer sealing zone. This prevents the shaft from rubbing against the elastomer thereby reducing the wear. The seals A, LG and LD which reverse pumped have greater wear when compared to other seals because these seals are lubricated for certain amount of time while performing oil drop test and are partially lubricated or starved during rest of its operation. Even though the operating conditions, shaft surface characteristics within each pattern and production batch of elastomer used for testing were kept the same, there is variation in the wear of the elastomer within each pattern of the shaft surface. Every lip seal elastomer is mated with

the shaft running against it and results in the deviation of wear as seen by Warren and Stephens[19]. Further the different orientation of triangular micro-cavities manufactured on shaft surface causes difference in wear rate, ultimately affecting the lip seal performance.

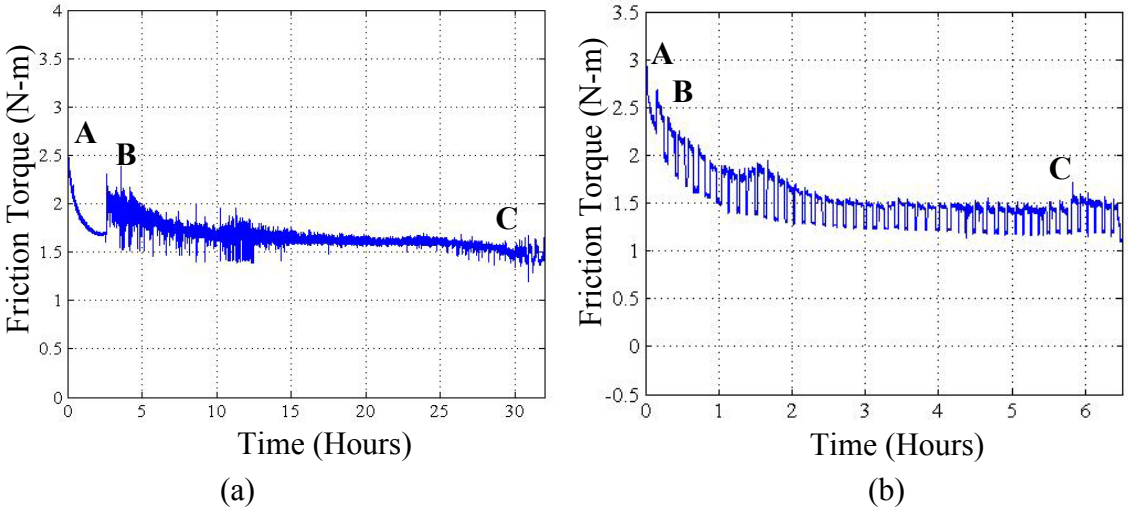

Figure 44 – Friction Torque (a) Stainless Steel (b) Textured Shaft

Figure 44 (a) and (b) shows the friction torque for the elastomer ran against stainless steel shaft and surface textured shaft respectively. Initially when the shaft starts to rotate, there is sudden increase in friction torque (A). (B) represent the point at which the friction torque increases again. During the period between (A) and (B), the oil present between the elastomer and shaft surface is pumped to the oil side. After the point (B), the seal runs in starved condition and the shaft surface continues to wear the elastomer. After temperature has reached equilibrium (C), the change in friction torque is very small. The

time between the points (B) and (C) indicate the initial wear-in time. The wear-in time calculated for the stainless steel case is approximately 28.7 hours where as the wear-in time for the "A", "LG" and "LD" surface textured case are approximately 7, 6.5 and 7.8 hours respectively. The wear-in time for the lip seal elastomers ran against textured shafts is less compared to the lip seal elastomers ran against stainless steel shafts.

For proper performance of the lip seals, Horve[2] recommended the surface roughness (Ra) of the shafts be between 0.25 – 0.5 μm. In the experiments conducted, only the surface roughness of the stainless steel shafts (SS1 and SS2) fall within that range. The surface roughness of the textured shafts (O, A, LG, and LD) before testing excluding the triangular micro-cavities has an average of 0.4 μm. The surface roughness of the shafts manufactured with deterministic triangular micro-cavities has an average of approximately 2.5 μm. Shafts even with high roughness away from the suggested range, the lip seals reverse pumped. This suggests along with the surface roughness of the shaft, the surface texture on the shaft plays a role in the operation of lip seals. Figure 45 shows the final surface roughness of the lip seal elastomers.

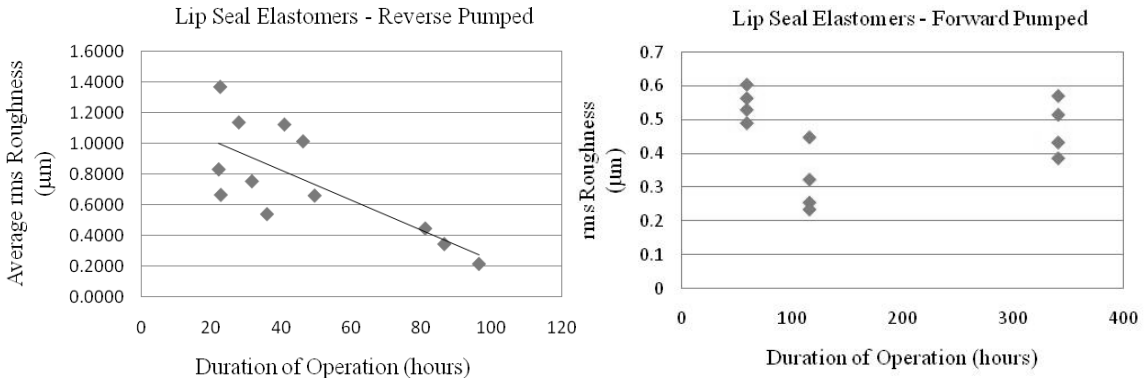

Figure 45 – rms Roughness of the Lip Seal Elastomers

As the duration of operation increases, the lip seal wear track roughness decreases for the seals which reverse pumped. For the seals which forward pumped, the lip seal wear track roughness remains almost constant or the shaft surface characteristics may change the lip seal roughness within a range along the operation. Figure 46 shows the shaft surface roughness before testing (bt) and after testing (at) for all the patterns which ran against the lip seals.

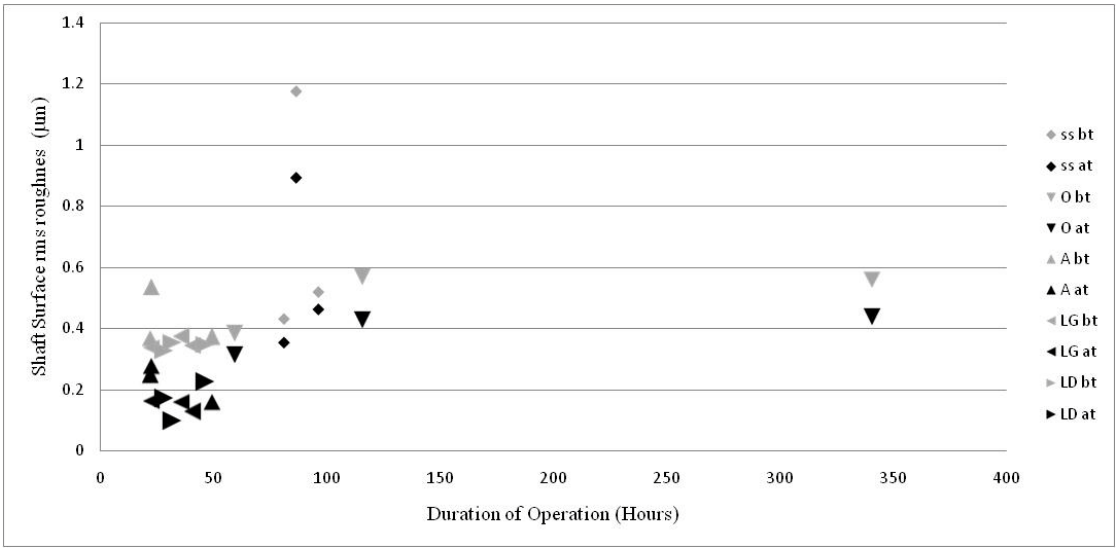

Figure 46 – Average rms Roughness of Shaft Surface

The width of the wear track on the shaft surface varies depending on the width of the elastomer sealing zone and the amount of elastomer deformation. The root mean square roughness is strongly affected by the size of the sampling points. In order to make a comparison between the untested and tested shaft surface roughness, the sampling points for the surface measurements were kept the same depending on the wear track width of the shaft. The roughness values are obtained only from the area surrounding the triangular cavities since only these portions come in contact with the elastomer while

running. The roughness of the shaft surface decreases which indicates the shaft surface is becomes smooth as the duration of operation increases. In the case of seals which ran against stainless steel shafts, the micro-asperities developed on the elastomer sealing zone were believed to create the reverse pumping action. In the case of seals running against shafts manufactured with deterministic triangular cavities, since there is not much change in the surface characteristics of the shaft, both the shaft and the elastomer surface contribute to the lip seal operation.

Grooves were found on the sealing zone of the lip seal elastomers which ran against shafts manufactured with triangular cavities lagging and leading. These grooves, also known as microundulations, were along the circumferential direction of the seal. This may due to the triangular wedges present in the shaft surface which is formed by the area surrounding the deterministic triangular cavities with apex pointing along and against the direction of rotation. The width of the grooves fall within the range between A and B as described in Figure 47.

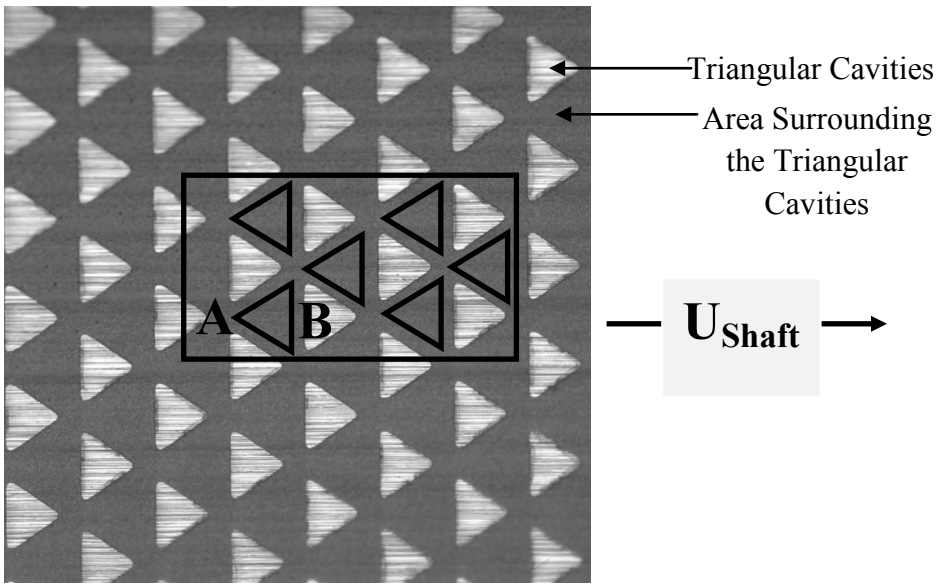

Figure 47 – Shaft Surface Manufactured with Triangular Cavities Leading

Under static conditions, an average of two rows of triangular cavities manufactured on shaft surface come in contact with the sealing zone of the lip seal elastomer. The number of grooves is not constant and varies along the circumferential direction of the seal. This is because the relative position of sealing zone contact region varies along the circumferential direction. Nakamura and Kawahara [11] conducted experiments with lip seals against a hollow glass shaft and observed the formation of micro-cavitation in the valleys of the micro-asperities. The lip seal elastomers with the grooves in the sealing zone have high pumping rates when compared to other seals. The areas surrounding the micro-cavities on the shaft surface and the micro-cavities on the shaft surface run against the grooves and ridges present on the elastomer sealing zone. Along with the deterministic triangular micro-cavities manufactured on the shaft surface, the additional cavitation caused by the grooves on the elastomer sealing zone may aid the pumping rate of the seals. Salant and Flaherty [7] considered microundulations on the lip seal elastomer and conducted a numerical analysis. These microundulations were perpendicular to the circumferential direction of the seal. The results of that study indicate these microundulations deform under dynamic conditions and are responsible for reverse pumping. The results also indicate that the microundulations hydrodynamically generate high pressure within the film and provide load support.

CHAPTER 6 – SUMMARY, CONCLUSION AND FUTURE WORK

6.1 SUMMARY

This work utilizes scanning electron microscope and Zygo optical profilometer to analyze the micro-asperities and micro-cavities present in the sealing zone of the lip seal elastomer and compare them to the deterministic triangular cavities manufactured on the shaft surface and the pumping rate of the lip seal. Triangular cavities of different orientations were considered on the shaft surface. The results of this study indicate that the deterministic triangular cavities manufactured on the shaft surface and their orientation play an important role in the wear of the lip seal elastomer and therefore formation of the lip seal elastomer sealing zone. Even though similar operating conditions, lip seal elastomer and shaft were used for testing, every lip seal elastomer is mated with the shaft running against it.

6.2 CONCLUSION

The results from the experimental study of lip seal elastomer running against plain stainless steel shaft agree with the previous numerical and experimental analysis. From this study, the following conclusions are drawn:

1. There is both qualitative and quantitative agreement with the previous work done by Horve and Paige with respect to the width, roughness and scanning electron microscope images of the elastomer sealing zone.

2. The width and the roughness of the elastomer sealing zone remains constant over time for the seals which forward pumped because of the constant film of oil between the elastomer sealing zone and the shaft.

3. The lip seal ran against “O” texture leaks as it is designed and this type of design is used in applications to seal dirt from housing such as a wheel bearing.

4. There is high correlation between the filter cutoff wavelength and the sealing zone width of the lip seal elastomer by factor of 9. The increase in filter cutoff wavelength as the sealing zone width increases and the variation of roughness along the axial direction of the sealing zone can be further analyzed to predict the deformation of the elastomer sealing zone.

5. The seals which ran against triangular cavities lagging and leading had grooves in the sealing zone along the circumferential direction. These seals have higher pumping rates when compared to those without grooves.

6. Larger asperities congregate on either edge of the elastomer sealing zone. This is due to a lower hydrodynamic pressure distribution on the edges of the sealing zone and more interaction between the lip seal elastomer and the shaft.

7. There is significant correlation between the axial position of minimum roughness in the elastomer sealing zone and the pumping rate.

8. The lip seals which ran against shafts manufactured with deterministic triangular cavities have higher roughness near the air side irrespective of whether seals reverse or forward pumped.

9. There is more wear on the air side of the elastomers which reverse pumped and equal wear on both the air and oil side of the elastomers which forward pumped.

10. The pumping rate for seals with textured shafts is influenced by both the micro-features on the shaft and those on the elastomer while the pumping direction of the seals is dominated by the features found on the shaft surface.

6.3 FUTURE WORK

1. The lip seal elastomers could be ran for same hours of operation against the shaft manufactured with different patterns and comparison could be made between them.
2. The effect of only cavities on the shaft surface on the elastomer was analyzed in this study. The effect of asperities on the shaft surface on the elastomer could be studied.
3. Instead of considering the sealing zone of the lip seal elastomer to be of regular periodic surface textures, numerical analysis could be done taking into account of the random isotropic nature of the micro-asperities and micro-cavities in the sealing zone of the elastomer.

4. All the numerical models done so far considered the sealing zone surface of the elastomer to remain constant as the duration of operation increases which is not in reality. The numerical model should also incorporate the wear of the lip seal elastomer. This is because, due to the wear of the elastomer, there is change in the micro-asperities and micro-cavities on the elastomer sealing zone, the elastomer sealing zone width, the deformation of the elastomer sealing zone, film thickness of lubricant present between the elastomer and the shaft, the pumping rate of the lubricant. Hence the performance of lip seal changes as the time progresses.
5. Comparison should be made between the roughness in the sealing zone of the elastomer and the deformation of the sealing zone during dynamic conditions by running the lip seal elastomers against hollow glass shaft. By running against a hollow glass shaft, the break-in period, where the micro-asperities are developed can also be indentified clearly.
6. The lip seal elastomers with grooves also known as microundulation along the circumferential direction were found to have high pumping rates. Parallel grooves could be created on the air and oil side surface of the lip seal elastomer and their effects on reverse pumping could be studied.

APPENDIX

A. Surface Parameters of Final Shaft Wear Track

SS		
	Average	**Standard Deviation**
Sq	0.69	0.26
Ssk	-1.02	0.67
Sku	6.40	4.08
Svi	0.15	0.03
Sbi	0.76	0.11
Sci	1.22	0.22
Sdq	0.25	0.04
Sds	0.01	0.00
Ssc	0.13	0.03
Sz	7.24	1.11
Sdr	2.74	0.82

O		
	Average	**Standard Deviation**
Sq	2.36	0.36
Ssk	-0.95	0.34
Sku	2.52	0.97
Svi	0.09	0.05
Sbi	1.05	0.11
Sci	0.89	0.11
Sdq	0.50	0.05
Sds	0.01	0.00
Ssc	0.19	0.02
Sz	14.61	6.95
Sdr	9.32	1.60

A		
	Average	**Standard Deviation**
Sq	2.30	0.45
Ssk	-0.66	0.18
Sku	1.88	0.41
Svi	0.06	0.03
Sbi	0.97	0.05
Sci	0.99	0.06
Sdq	0.42	0.04
Sds	0.01	0.00
Ssc	0.15	0.03
Sz	11.55	1.73
Sdr	7.00	1.22

LG		
	Average	**Standard Deviation**
Sq	3.08	0.23
Ssk	-1.13	0.22
Sku	2.53	0.44
Svi	0.07	0.02
Sbi	1.23	0.11
Sci	0.82	0.07
Sdq	0.52	0.07
Sds	0.01	0.00
Ssc	0.18	0.01
Sz	14.81	0.93
Sdr	10.95	2.62

LD		
	Average	**Standard Deviation**
Sq	2.65	0.18
Ssk	-1.19	0.20
Sku	2.81	0.66
Svi	0.10	0.07
Sbi	1.16	0.07
Sci	0.82	0.07
Sdq	0.47	0.03
Sds	0.01	0.00
Ssc	0.18	0.01
Sz	13.92	2.42
Sdr	8.93	0.91

B. MATLAB PROGRAM

```
% ========================================================== %
% Program 1 - export "XYZ" data from ZYGO optical profilometer to MATLAB
% ========================================================== %

fid = fopen('XYZ.txt'); % opening the text file named "XYZ"
c = textscan(fid,'%f %f %s %s');
fclose(fid);
y=c{1};
x=c{2};
z1=c{3};

i=size(z1);
j=i(1,1);
clear i
for i=1:1:j
    str=strcmp(z1{i},'No');
    if (str==1)
        z1{i}=NaN;
    else
        z1{i}=str2double(z1{i});
    end
end
z=cell2mat(z1);
save('weartrack','x','y','z');

clear
clc
load weartrack.mat;
a=size(x);
b=a(1,1);
k(1)=0;
n=2;

for i=1:1:b-1
    c=x(i+1)-x(i);
    if c==1
    k(n)=i;
    n=n+1;
    end
end
k(n)=b;

b=1;
c=size(k);
```

```
for n=1:1:c(1,2)-1
   a=1;
   for i=k(n)+1:1:k(n+1)
      x1(a,b)=x(i);
      y1(a,b)=y(i);
      z1(a,b)=z(i);
      a=a+1;
   end
   b=b+1;
end
save('xyz','z1')


%  ========================================================== %
% Program 2 – Calculation of Sa, Sq, St, Ssk, Sku
%  ========================================================== %

clear
clc
load xyz.mat
eta=z1;
[m,n]=size(eta);

% replacing the NaN with zero, because when a couple of numbers are added
% with NaN, the result the matlab displays is NaN

eta(isnan(eta))=0; % isnan(chi) is function which detects NaN in a matrix
% chi(isnan(chi)) replaces all those NaN locations with zero

lx=331;ly=535;
dx=lx/(m-1);
dy=ly/(n-1);

for i=1:m
   for j=1:n
      x(i,j)=(i-1)*dx;
      y(i,j)=(j-1)*dy;
   end
end

sa=(sum(sum(abs(eta))))/(m*n);
sq=sqrt((sum(sum((eta.^2))))/(m*n));% the dot after eta is kept so that every element in
the matrix is squared rather than matrix squaring
% A^5 vs A.^5: A^5 multiplies A with itself 5 times (matrix product;
% possible only when A is square) whereas A.^5 raises every element of A to the 5th
power.
```

```
st=max(max(eta))-min(min(eta)); % peak to valley height
ssk=(sum(sum(eta.^3)))/(m*n*(sq^3));
sku=(sum(sum(eta.^4)))/(m*n*(sq^4));

figure;surf(x,y,eta)
xlabel('Axial Direction'),ylabel('Circumferential Direction')

figure;mesh(x,y,eta)
xlabel('Axial Direction'),ylabel('Circumferential Direction')
hgsave('surf_mesh')

figure;contour(x,y,eta)
xlabel('Axial Direction'),ylabel('Circumferential Direction')
hgsave('surf_contour')

save('eta','eta')
save('xy','x','y','dx','dy','lx','ly')
save('result2','sa','sq','st','ssk','sku')
save('dim','lx','ly')


% ========================================================== %
% Program 3 – Calculation of Sds, Ssc, Sz
% ========================================================== %

clear
clc
load eta.mat
load xy.mat

[m,n]=size(eta);
eta1=[eta(m,:);eta;eta(1,:)]; % added the first and last row initially instead of
% column because the seal extends on the top and bottom instead of the
% sides
etaf=[eta1(:,n) eta1 eta1(:,1)];

% calculation of number of summits and valleys
sum=0; % for calculating the arithmrtic mean curvature of a surface Ssc
ns=0; %ns represent the counter for number of summits
for i=2:m+1
   for j=2:n+1
      % neig represents the height of the neighbouring points, neighs for
      % summits and neigv is for valleys
      neigs=[etaf(i-1,j+1),etaf(i-1,j),etaf(i-1,j-1),etaf(i,j+1),etaf(i,j-1),
             etaf(i+1,j+1),etaf(i+1,j),etaf(i+1,j-1)];
      nmax=max(neigs);
```

```
        if etaf(i,j)>nmax
            ns=ns+1;
            etas(i-1,j-1)=etaf(i,j); % i-1 and j-1 because the new matrix
            %  is same as the dimesion of eta
            t1=((etaf(i+1,j)+etaf(i-1,j)-(2*etaf(i,j)))/(dx^2));
            t2=((etaf(i,j+1)+etaf(i,j-1)-(2*etaf(i,j)))/(dy^2));
            a(i-1,j-1)=t1+t2; % a represent the summation term and stores
            % in the corresponding summit location
            sum=sum+a(i-1,j-1);
        else
            etas(i-1,j-1)=0;
        end
    end
end

Sds=ns/((m-1)*(n-1)*dx*dy);
Ssc=(-1/2)*(1/ns)*(sum);

figure;contour(x,y,etas)
xlabel('Axial Direction'),ylabel('Circumferential Direction')
hgsave('summits')

% for valleys
sum=0; % for calculating the arithmrtic mean curvature of a surface Ssc
nv=0; %ns represent the counter for number of summits
for i=2:m+1
    for j=2:n+1
        % neig represents the height of the neighbouring points, neighs for
        % summits and neigv is for valleys
        neigv=[etaf(i-1,j+1),etaf(i-1,j),etaf(i-1,j-1),etaf(i,j+1),etaf(i,j-
1),etaf(i+1,j+1),etaf(i+1,j),etaf(i+1,j-1)];
        nmin=min(neigv);
        if etaf(i,j)<nmin
            nv=nv+1;
            etav(i-1,j-1)=etaf(i,j); % i-1 and j-1 because the new matrix
            % is same as the dimesion of eta
        else
            etav(i-1,j-1)=0;
        end
    end
end
figure;contour(x,y,etav)
xlabel('Axial Direction'),ylabel('Circumferential Direction')
hgsave('valleys')
```

```
% calculation of Sz (maximum peak to valley height)

etas=reshape(etas,1,[]); % converting the matrix into an array
etas=sort(etas,'descend'); % sorting in descending to find 5 highest peaks
etas=abs(etas); % finding the absolute value

etav=reshape(etav,1,[]); % converting the matrix into an array
etav=sort(etav); % sorting in ascending, to find 5 lowest valleys
etav=abs(etav); % finding the absolute value

shp=0; %sum of height peak
slv=0; %sum of lowest valley
for i=1:5
   shp=shp+etas(i);
   slv=slv+etav(i);
end
Sz=(shp+slv)/5;

save('result3','ns','etas','Sds','Ssc','nv','etav','Sz')


% ========================================================== %
% Program 4 – Calculation of Sbi
% ========================================================== %

clear
clc
load eta
load xy.mat

[a,b]=size(eta); % getting the size of thr given data
aa=lx*ly;
load result2.mat
etabar=eta/sq;
dmat=sort((reshape(etabar,a*b,1)),'descend'); % different d values
c=a*b;
baratio=1:1:c;
baratio=(baratio/(a*b))*100;
plot(baratio,dmat),grid,xlabel('Bearing Area Ratio (%)'),ylabel('Normalised Height
etabar=(eta/Sq)')
hold on

% Plotting of BAC
a=ceil(baratio);
b=find(a==5);
b=max(b);
```

```
x1=[0 100];
y1=[dmat(b) dmat(b)];
sbi=1/y1(1,1) % y1(1,1) is eta at 0.05
plot(x1,y1,'--')
hold on

c=ceil(baratio);
d=find(c==80);
d=max(d);
x2=[0 100];
y2=[dmat(d) dmat(d)]; % y2(1,1) is eta at 0.8
plot(x2,y2,'--')

e=ceil(baratio);
f=find(e==100);
f=max(f);
x3=[baratio(f) 100];
y3=[dmat(f) dmat(f)];

p=y1(1);
q=y2(1);
r=min(min(eta));
s=max(max(eta));

print -djpeg bac
save('values2','baratio','dmat','a','b','c','d','e','f','p','q','r','s')
save('bac1','sbi')


% ========================================================== %
% Program 5 – Calculation of Sci, Svi
% ========================================================== %

% Getting the area for calculating the core fluid retention index

clear
clc
load values2
xvalues=baratio(b:d);
xvalues=[100 xvalues 100];
yvalues=(dmat(b:d))';
n=size(yvalues);
yvalues=[yvalues(1) yvalues yvalues(n(1,2))];
ans1=polyarea(xvalues,yvalues);
figure(1),plot(xvalues,yvalues);
sci=ans1/(100)
```

```
% Getting the area for calculating the valley fluid retention index

load values2
xvalues=baratio(d:f);
xvalues=[100 xvalues];

yvalues=(dmat(d:f))';
yvalues=[yvalues(1) yvalues];
ans2=polyarea(xvalues,yvalues);
figure(2),plot(xvalues,yvalues);
svi=ans2/(100)
save('bac2','sci','svi')


%  ========================================================== %
% Program 6 – Calculation of Sdr
%  ========================================================== %

clear
clc
load eta.mat
load xy.mat

[m,n]=size(eta);

for i=1:m-1
   for j=1:n-1
      t1=sqrt(((dy)^2)+(((eta(i,j))-(eta(i,j+1)))^2));
      t2=sqrt(((dy)^2)+(((eta(i+1,j+1))-(eta(i+1,j)))^2));
      t3=sqrt(((dx)^2)+(((eta(i,j))-(eta(i+1,j)))^2));
      t4=sqrt(((dx)^2)+(((eta(i,j+1))-(eta(i+1,j+1)))^2));
      A(i,j)=((t1+t2)*(t3+t4))/4;
   end
end
Ad=sum(sum(A)); %Af is the total developed area on the surface
As=(m-1)*(n-1)*dx*dy; % sampling area
Sdr=((Ad-As)*100)/As; % Sdr is in percentage

save('result6','Ad','As','Sdr')
```

```
% ================================================================ %
% Program 7 – Calculation of Sdq
% ================================================================ %

clear
clc
load eta.mat
load xy.mat
[m,n]=size(eta);
eta1=[eta(m,:);eta;eta(1,:)]; % added the first and last row initially instead of
% column because the seal extends on the top and bottom instead of the
% sides
etaf=[eta1(:,n) eta1 eta1(:,1)];

for i=2:m+1
   for j=2:n+1
      rhoq(i-1,j-1)=(((etaf(i,j)-etaf(i-1,j))/dx)^2)+(((etaf(i,j)-etaf(i,j-1))/dy)^2);
   end
end

rhoqf=sum(sum(rhoq));
Sdq=sqrt(rhoqf/((m-1)*(n-1)));
save('result7','Sdq')


% ================================================================ %
% Program 8 – Calculation of AACF
% ================================================================ %

clear
clc
load eta

% creating the AACF plot

[r_corr1]=xcorr2(eta);
r_corr=r_corr1/(max(max(abs(r_corr1))));
save('r_corr','r_corr')
load('r_corr','r_corr')
% creating the spacing for the eta values based on the total number of eta
% values available and total length in x direction and y direction
[m,n]=size(r_corr);

load dim
dx=(2*lx)/(m-1);
dy=(2*ly)/(n-1);
```

```
for i=1:m
   for j=1:n
      x(i,j)=-lx+(i-1)*dx;
      y(i,j)=-ly+(j-1)*dy;
   end
end

figure;surf(x,y,r_corr)
xlabel('Axial Direction');ylabel('Circumferential Direction');

figure;mesh(x,y,r_corr)
xlabel('Axial Direction');ylabel('Circumferential Direction');
hgsave('aacf_mesh')
figure;contour(x,y,r_corr)
xlabel('Axial Direction');ylabel('Circumferential Direction');
hgsave('aacf_contour')


% ========================================================== %
% Program 9 – Calculation of APSD
% ========================================================== %

clear
clc
load eta
xx=fft2(eta);
G=xx.*(conj(xx)); % taking complex conjugate

[M,N]=size(G);
Gfin=fftshift(G);

load dim
dx=(2*lx)/(M-1);
dy=(2*ly)/(N-1);

for i=1:M
   for j=1:N
      x(i,j)=((-lx-dx/2)+(i-1)*dx)/dx;
      y(i,j)=((-ly-dy/2)+(j-1)*dy)/dy;
   end
end

x=x/lx;
y=y/ly;

figure;mesh(x,y,Gfin)
```

```
xlabel('Axial Direction, Pseudo-Freq (cycles/trace)');ylabel('Circumferential Direction,
Pseudo-Freq (cycles/trace)');
hgsave('apsd_mesh')

figure;contour(x,y,Gfin)
xlabel('Axial Direction, Pseudo-Freq (cycles/trace)');ylabel('Circumferential Direction,
Pseudo-Freq (cycles/trace)');
print -djpeg apsd_contour

% angular spectrum

for i=1:M
   for j=1:N
      angle(i,j)=(180/pi)*atan(y(i,j)/x(i,j));
   end
end
figure;plot(angle,Gfin,'bo')
xlabel('Angle (deg)'),ylabel('Angular Power Spectra')
print -djpeg ang_spec
```

REFERENCES

1. Jenny, Paige., *"Experimental and Theoretical Comparison of Radial Lip Seal Operation"*. 2005, Master's Thesis: University of Kentucky, Department of Mechanical Engineering, Lexington, Kentucky, USA.
2. Horve, L., *"Shaft Seals for Dynamic Applications"*. 1996: Marcel Dekker, Inc., New York, ISBN 0-8247-9716-7.
3. Johnston, D. E., *"Using the Frictional Torque of Rotary Shaft Seals to Estimate the Film Parameters and the Elastomer Surface Characteristics".* Proceedings of the 8th BHRA International Conference on Fluid Sealing, Durham, Cranfield, Bedfordshire, 1978. **Paper C1**.
4. Salant , Richard F. and Flaherty, Andrew L. (1994) *"Elastohydrodynamic Analysis of Reverse Pumping in Rotary Lip Seals with Microundulations"*. Journal of Tribology **116**, 56-62.
5. Hadinata, P. C. and Stephens, L. S., *"Soft Elastohydrodynamic Analysis of Radial Lip Seals with Deterministic Microasperities on the Shaft".* Journal of Tribology, 2007. **129**(4).
6. Impellizzeri, D. M., *"Model Development and Investigation of Micro-Deterministic Asperity Feastures/Textures Using the Jakobsson-Floberg-Olsson (JFO) Cavitation Condition Modified Reynolds Equation".* Master's Thesis: University of Kentucky, Department of Mechanical Engineering, Lexington, Kentucky, USA., 2006.
7. Salant , Richard F. and Flaherty, Andrew L. (1995) *"Elastohydrodynamic Analysis of Reverse Pumping in Rotary Lip Seals with Microasperities"*. Journal of Tribology **117**, 53-59.
8. Qian, D. S., *"The Sealing Mechanism and Design Factors of Radial Lip Seals for Crankshafts".* Neiranji Gongsheng (Chin. Internal Combustion Engine Engng), 1984. **5**: p. 10-13.
9. Salant , Richard F., *"Modeling Rotary Lip Seals".* Wear, Elsevier, New York, 1997: p. 92-99.
10. Hamilton, D. B., Walowit, J. A., and Allen, C. M., *"A Theory of Lubrication by Microirregularities".* Transactions of ASME, Journal of Basic Engineering, 1966. **88**: p. 177-185.
11. Nakamura, K. and Kawahara, Y. (1984) *"An Investigation on Sealing Properties of Lip Seals through Observation of Sealing Surfaces under Dynamic Conditions"*. Proceedings of the BHRA 10th International Conference on Fluid Sealing, Innsbruck, Austria, 87-105.
12. Kawahara, Y., Abe, M., and Hirabayashi, H., *"An Analysis of Sealing Charateristics of Oil Seals".* ASLE Trans., 1980. **23**: p. 93-102.
13. Horve, L., *"The Correlation of Rotary Shaft Radial Lip Seal Service Reliability and Pumping Ability to Wear Track Roughness and Microasperity Formation".* CR Industries, Elgin, IL SAE 910530, February, 1991: p. 620-627.
14. Jagger, E. T., *"Rotary Shaft Seals: The Sealing Mechanism of Synthetic Rubber Seals Running at Atmospheric Pressure".* Proc. Inst. Mech. Eng., 1957. **171**: p. 597-616.

15. Jagger, E. T. and Walker, P. S. (1966) *"Further Studies of the Lubrication of Synthetic Rubber Rotary Shaft Seals"*. Proc. Inst. Mech. Eng. **181, Part 1**, 191-204.
16. Kawahara, Y. and Hirabayashi, H., *"Effect of Surface Condition of Lip on Sealing Phenomena of Oil Seals"*. SAE Paper 780405, 1978: p. 1-10.
17. Horve, L. A. and Brink, R. V., *"Wave Seals (A Solution to the Hydrodynamic Compromise)"*. ASLE Lubrication Eng., 1973. **29**(6): p. 265-270.
18. Anno, J. N., Walowit, J. A., and Allen, C. M., *"Load Support and Leakage from Microasperity Lubricated Face Seal"*. Journal of Basic Engineering, Transactions of ASME, Ser. F, 1969: p. 726-731.
19. Warren, K. H. and Stephens, L. S., *Effect of Shaft Microcavity Patterns for Flow and Friction Control on Radial Lip Seal Performance - A Feasibility Study.* Tribology Transactions (accepted for publication), 2009.
20. Zhang, Jian, *LIGA Mold Insert Fabrication Using SU-8 Photoresist.* 2002.
21. Berens, A. S. and Born, J. H., *"The Effect of Surface Microstructure on the Performance of Rotary Lip type Oil Seals"*. Proceedings of the 4th European Rubber abd Plastic Conference, 1974. **June**: p. 4 - 7.
22. Dong, W. P., Sullivan, P. J. , and Stout, K. J. , *"Comprehensive study of parameters for characterizing three dimensional surface topography III: Parameters for characterizing amplitude and some functional properties"*. Wear, 1994: p. 29-43.
23. Stout, K. J., *"Development of Methos for the Characterization of Roughness in Three Dimension"*. 2000.
24. Gawlinski, M and Kasprzyk, Z., *"Shaft Surface Roughness and its Influence on the Wear of the Lip sealing Edge"*. Material Science, 2003. **9**(1): p. 58-61.

VITA

Vetrivel Kanakasabai

Born June 20, 1985 in Mayiladuthurai, Tamil Nadu, India

Education:

Bachelor of Engineering in Mechanical Engineering, 2006

College of Engineering, Anna University, India

Scholastic Awards and Professional Membership:

Kentucky Graduate Scholarship (2006 - 2008)

Member of National Scholars Honor Society

Professional Publication:

Surface Analysis of the Elastomer in Lip Seals Ran against Shafts Manufactured with Micro Cavity Patterns. IMechE, Proceedings of the Institution of Mechanical Engineers, Journal of Engineering Tribology (Submitted Jun09)